

# *Functional Inorganic Oxide Layers*

by

**Mohammed Bouzbib**

Ph.D. Program of Environmental Chemistry, Doctoral School of Environmental  
Sciences,

Faculty of Science, Eötvös Loránd University

**Ph.D. Thesis**

Submitted to the Doctoral School of Environmental Sciences

Faculty of Science, Eötvös Loránd University



**Supervisor: Dr. Katalin Sinkó, DSc**

Eötvös Loránd University, Institute of Chemistry  
Department of Analytical Chemistry, Environmental Sciences  
Sol-gel Laboratory

Doctoral School of Environmental Sciences  
Head of School and Program: Dr. Tamás Turányi, DSc

Budapest

2023

## Acknowledgments

I would like to express my heartfelt gratitude to Professor Katalin Sinkó. Her guidance, support, and encouragement have been instrumental in helping me reach my goals. The value of her advice and constructive suggestions cannot be overstated, and I am deeply appreciative of her dedication and expertise. Without her assistance, completing my thesis to the high standard it is today would not have been possible.

I would like to extend my deepest gratitude to LightTech Company for its invaluable support and contributions to this research. Their commitment to advancing technology and their generous assistance have been instrumental in the success of this thesis.

Special thanks to Tamás Turányi Head of the Doctoral School for his help finding my supervisor in the same way as Professor Imre M. Jánosi.

I am grateful to Professor János Rohonczy from the Institute of Chemistry, for his great collaboration with laboratory nuclear magnetic resonance (NMR) analysis.

I would like to express my sincere gratitude to the members of my defense jury for their time and effort in evaluating my research work. Their expertise and insights have been invaluable in helping me to improve my thesis and reach my goals. I deeply appreciate their commitment to this process and the constructive feedback they have provided.

My thanks also go to all the personnel of the common electron microscopy service. I would like to thank all my colleagues at Sol-gel Laboratory, especially Ádám Péter for helping me during those years concerning the administration process and the time we shared.

I am grateful for the support provided by the Stipendium Hungaricum Scholarship Program 2017-2022. I also appreciate the Ministry of Higher Education and Scientific Research (Morocco) for their contributions.

During this journey far from home, I was so blessed to meet such incredible people with warm hearts who helped me during the hardest time, for whom I am sincerely thankful.

I would like to thank all my friends and I cannot close these acknowledgments without thanking and expressing my eternal love to my beautiful and dearest mother and father for their encouragement, patience, inspiration, motivation, and thanks to all my family who supported me morally throughout my studies from the beginning of my first steps.

## Table of Contents

<b>List of abbreviations</b> .....	<b>5</b>
<b>List of figures</b> .....	<b>6</b>
<b>Introduction and objectives</b> .....	<b>9</b>
<b>Motivation</b> .....	<b>10</b>
<b>I. Literature review</b> .....	<b>11</b>
I.1. Thin films .....	11
I.2. Overview of aluminum oxide .....	12
I.2.1. Preparation of aluminum oxide .....	14
I.3. Overview of vanadium oxides .....	15
I.3.1. Structural and electrical properties of V <sub>2</sub> O <sub>5</sub> .....	17
<b>II. Methods of synthesis and characterization</b> .....	<b>20</b>
II.1. Synthesis methods .....	20
II.1.1. Sol-gel technique .....	20
II.1.1.1. Hydrolysis .....	21
II.1.1.2. Condensation .....	21
II.1.1.3. Aging.....	22
II.1.1.4. Drying .....	22
II.1.1.5. Thermal treatment.....	22
II.1.1.6. Structural influential parameters.....	22
II.2. Deposition methods .....	23
II.2.1. Dip-coating (DP) .....	23
II.2.2. Atomic layer deposition (ALD).....	24
II.2.3. Chemical vapor deposition (CVD).....	24
II.2.4. Spray pyrolysis (SP).....	25
<b>III. Experimental details</b> .....	<b>26</b>
III.1. Synthesis of aluminum oxide thin films .....	26
III.1.1. Layer from Al <sub>2</sub> O <sub>3</sub> suspension .....	26
III.1.2. Layer from boehmite suspension.....	26
III.1.3. Layer by sol-gel method starting from basic Al acetate .....	26
III.1.4. Layer by sol-gel method starting from Al nitrate .....	27
III.1.5. Layer by sol-gel method starting from Al isopropoxide .....	27
III.2. Synthesis of vanadium oxide thin films.....	28
III.2.1. Sol-gel synthesis starting from NH <sub>4</sub> VO <sub>3</sub> .....	28
III.2.2. Synthesis starting from VO <sub>2</sub> .....	29

III.2.3. Synthesis starting from vanadyl acetylacetonate, VO(ac) <sub>2</sub> .....	29
III.2.4. Synthesis starting from ammonium decavanadate .....	29
III.3. Investigation Methods .....	30
III.3.1. Scanning electron microscopy (SEM) .....	30
III.3.2. Reflection optical microscopy (ROM).....	30
III.3.3. Grazing incidence X-ray diffraction (GIXRD).....	30
III.3.4. UV–Visible spectroscopy .....	30
III.3.5. FTIR spectroscopy.....	31
III.3.6. <sup>51</sup> V nuclear magnetic resonance spectroscopy (NMR) .....	31
III.3.7. pH meter.....	31
III.3.8. Dip Coater Machine.....	31
<b>IV. Results and discussion .....</b>	<b>32</b>
IV.1. Synthesis of gamma-aluminum oxide thin films .....	32
IV.1.1. Layer from boehmite suspension.....	32
IV.1.2. Layer by sol-gel method starting from basic Al acetate (AlAc) salt .....	38
IV.1.3. Layer by sol-gel method starting from Al nitrate .....	44
IV.1.4. Layer by sol-gel method starting from Al isopropoxide .....	46
IV.2. Comparison of Al <sub>2</sub> O <sub>3</sub> layers prepared by various synthesis routes.....	48
IV.3. Synthesis of Vanadium Oxide Thin films .....	50
IV.3.1. Effect of vanadium precursors .....	50
IV.3.1.1. Vanadyl (IV) acetylacetonate precursor .....	50
IV.3.1.2. Vanadium dioxide (VO <sub>2</sub> ) precursor .....	53
IV.3.1.3. Ammonium decavanadate (NH <sub>4</sub> ) <sub>6</sub> [V <sub>10</sub> O <sub>28</sub> ] precursor .....	55
IV.3.2. Effect of acidic catalysts and chemical additives .....	57
IV.3.2.1. FTIR spectroscopy .....	60
IV.3.2.2. X-ray powder diffraction (XRD) .....	60
IV.3.2.3. Energy Dispersive X-ray Analysis (EDX) .....	61
IV.3.2.4. Optical behaviours .....	63
IV.3.3. Effect of tenside .....	65
IV.3.4. Characterisation of vanadium oxide layers.....	65
IV.3.4.1. <sup>51</sup> V MAS NMR measurements .....	67
<b>V. Conclusion.....</b>	<b>69</b>
<b>VI. References .....</b>	<b>71</b>
<b>Appendix .....</b>	<b>85</b>

## List of abbreviations

Al<sub>2</sub>O<sub>3</sub>: Aluminum Oxide

FCC: Face-Centered Cubic

VO<sub>2</sub>: Vanadium Dioxide

V<sub>2</sub>O<sub>5</sub>: Vanadium Pentoxide

IGEPAL: Octylphenoxypolyethoxyethanol

AliPr: Aluminum isopropoxide

MIT: Metal Insulator Transition

MOR: Metal alkoxides

pH:  $-\log[\text{H}^+]$

DC: Dip-coating

ALD: Atomic layer deposition

CVD: Chemical vapor deposition

SP: Spray pyrolysis

XRD: X-ray powder diffraction

SEM: Scanning electron microscopy

EDAX: Energy-dispersive X-ray spectroscopy

GIXRD: Grazing incidence X-ray diffraction

FTIR: Fourier-transform infrared spectroscopy

AFM: Atomic force microscopy

ATR: Attenuated total reflection

Fig: Figure

## List of figures

Figure 1. Thin film deposition on the substrate .....	11
Figure 2. Lattice of $\gamma$ - $\text{Al}_2\text{O}_3$ composed of 4 layers of tetrahedral and octahedral planes .....	14
Figure 3. Lattice of vanadium oxide red atoms represent the vanadium atoms and the blue patterns represent the oxygen atoms .....	18
Figure 4. The crystalline structure of $\text{V}_2\text{O}_5$ within one unit cell. The orthorhombic unit cell of $\text{V}_2\text{O}_5$ is marked as blue dashed lines. The 3D view and the projected views of (100), (010), and (001) facets are depicted.....	18
Figure 5. Sol–gel thin films deposition process .....	20
Figure 6. Sequential stages of the dip-coating process: (a) dipping, (b) withdrawal and (c) evaporation of the solvent .....	23
Figure 7. Transmittance of layers prepared from boehmite and aluminum oxide suspensions and commercial $\text{Al}_2\text{O}_3$ layer products .....	33
Figure 8. The probable connections between the octa- and tetraordinated Al ions on the surface of boehmite .....	34
Figure 9. Transmittance of layers prepared from boehmite sol in the function of acetic acid.	34
Figure 10. Transmittance of layers prepared from boehmite sol in the function of HAc molar ratio.....	35
Figure 11. Transmittance of layers in the function of concentration of boehmite sol prepared with 0.5 molar ratio of HAc/Al .....	35
Figure 12. XRD diffractions of böhmite vs. temperature .....	36
Figure 13. SEM images of $\text{Al}_2\text{O}_3$ layer obtained from boehmite suspension with 0.5 molar ratio of HAc/Al. Magnification: 25 000x; 100 000x, 65 000x (110-120 nm).....	37
Figure 14. SEM images of $\text{Al}_2\text{O}_3$ layer obtained from $\text{Al}_2\text{O}_3$ suspension. ....	37
Figure 15. EDAX measurement of $\text{Al}_2\text{O}_3$ layer obtained from boehmite suspension with 0.5 molar ratio of HAc/Al .....	38
Figure 16. Transmittance of sol-gel derived layers prepared from Al acetate in the function of HCl .....	39
Figure 17. Transmittance of sol–gel derived layers prepared from Al acetate in the function of acetic acid (HAc).....	40
Figure 18. Transmittance of sol-gel derived layers prepared from Al acetate (AlAc) with various additives.....	41

Figure 19. XRD spectrum of sol-gel derived Al <sub>2</sub> O <sub>3</sub> layers prepared from Al acetate with HCl (upper), HAc (middle), and boehmit (lower) .....	42
Figure 20. SEM of sol-gel derived layers prepared from Al acetate (AlAc) with HCl .....	43
Figure 21. SEM of sol-gel derived layers prepared from Al acetate (AlAc) with HAc.....	43
Figure 22. SEM of sol-gel derived layers prepared from Al acetate (AlAc) with boehmite. Magnification: 25 000x; 100 000x, 120 000x. Layer thickness is 50-60 nm.....	44
Figure 23. Transmittance of sol-gel derived layers prepared from Al nitrate.....	44
Figure 24. SEM of sol-gel derived layers prepared from Al nitrate. ....	45
Figure 25. GIXRD spectrum of sol-gel derived Al <sub>2</sub> O <sub>3</sub> layers prepared from Al nitrate.....	45
Figure 26. Transmittance of sol-gel derived layers prepared by Yoldas and our methods from Al isopropoxide .....	46
Figure 27. SEM images. Upper layers were prepared by Yoldas method from Al isopropoxide. Lower layers were produced by our sol-gel technique from Al isopropoxide ..	47
Figure 28. Comparison of the transmittance of $\gamma$ -Al <sub>2</sub> O <sub>3</sub> layers prepared by various techniques with commercial products (Heraus, Chyoda, and Lighttech).....	49
Figure 29. SEM images of samples prepared from VO(acac) <sub>2</sub> and heated in air and N <sub>2</sub> atmosphere .....	51
Figure 30. XRD patterns of vanadium oxide thin films prepared from VO(acac) <sub>2</sub> and heated in air and N <sub>2</sub> atmosphere .....	52
Figure 31. <sup>51</sup> V NMR spectra of VO <sub>2</sub> vs. temperature. V <sub>2</sub> O <sub>5</sub> provides for comparison.....	54
Figure 32. SEM images of vanadate layers prepared from VO <sub>2</sub> sol solution .....	55
Figure 33. <sup>51</sup> V NMR spectra of (NH <sub>4</sub> ) <sub>6</sub> [V <sub>10</sub> O <sub>28</sub> ] .....	56
Figure 34. SEM images of vanadate layers prepared from NH <sub>4</sub> VO <sub>3</sub> with various additives: nitric acid, citric acid, oxalic acid, ascorbic acid, ethyl acetate, and after ion exchange .....	58
Figure 35. FTIR spectra of vanadium pentoxide thin films on glass substrates prepared with different chemical additives: (a) ethyl acetate; (b) nitric acid; (c) oxalic acid.....	60
Figure 36. XRD patterns of vanadium oxide thin films on glass substrates prepared with three types of most promising chemical additives: (a) nitric acid; (b) ethyl acetate; (c) oxalic acid	61
Figure 37. Energy Dispersive X-ray Analysis (EDX) of vanadium pentoxide thin films on glass substrates prepared with different solvents at 400 °C: (a) nitric acid; (b) ethyl acetate; (c) oxalic acid .....	62
Figure 38. Transmittance spectra of vanadium pentoxide thin films on glass substrates prepared with different additives: (a) nitric acid; (b) ethyl acetate; (c) oxalic acid .....	63

Figure 39. The optical band gap ( $E_g$ ) of vanadium oxide thin films: (a) ethyl acetate; (b) nitric acid; (c) oxalic acid .....	64
Figure 40. Reflection optical microscopy images of vanadate layers prepared from $\text{NH}_4\text{VO}_3$ and nitric acid, a without, b with surfactant (Triton X 100).....	65
Figure 41. SEM images of vanadium pentoxide thin films on glass substrates prepared with nitric acid.....	66
Figure 42. TG curve of dried V-containing layer.....	67
Figure 43. $^{51}\text{V}$ NMR spectra of layer synthesized from $\text{NH}_4\text{VO}_3$ and catalysed with $\text{HNO}_3$ vs temperature.....	68

## Introduction and objectives

Functional inorganic oxide layers have attracted significant attention in recent years due to their unique properties and potential applications in various fields, including environmental protection. Among the different types of inorganic oxides, aluminum oxide ( $\text{Al}_2\text{O}_3$ ) and vanadium oxides ( $\text{V}_2\text{O}_5$ ) stand out as particularly promising materials. Aluminum oxide ( $\text{Al}_2\text{O}_3$ ) and vanadium oxide ( $\text{V}_2\text{O}_5$ ) thin films are functional inorganic materials that have been extensively studied due to their high chemical stability [1,2], thermal resistance [3,4], good absorption ability [5,6], and excellent catalytic effect [7,8].

Previous research has explored various methods for the synthesis of aluminum oxide ( $\text{Al}_2\text{O}_3$ ) and vanadium oxide ( $\text{V}_2\text{O}_5$ ) thin films, including sol-gel [9,10], deposition methods such as dip coating [11], and pulsed laser deposition [12]. These studies have focused on optimizing the synthesis conditions to achieve high-quality thin films with desirable properties for specific applications, such as photocatalysis [13–15], energy storage [16,17], and water treatment [18].

This research aims to contribute to the current understanding of the synthesis and characterization of aluminum oxide and vanadium oxide thin films and their potential applications.

The focus of the research is to understand how these thin films can be utilized for environmental protection and to determine their suitability for various applications.

The aim also is to provide a comprehensive analysis of the synthesis and characterization of  $\text{Al}_2\text{O}_3$  and  $\text{V}_2\text{O}_5$  thin films, and to identify the optimal conditions and to develop the synthesis techniques and methodologies to produce these thin films, as well as to characterize their physical and chemical properties.

The synthesis of  $\text{Al}_2\text{O}_3$  and  $\text{V}_2\text{O}_5$  thin films was realized by using various methods such as sol-gel, co-precipitation by dip coating deposition techniques.

The characterization of the synthesized thin films was performed by various techniques such as grazing incidence X-ray diffraction (GI-XRD), scanning electron microscopy (SEM), thermal analysis, nuclear magnetic resonance spectroscopy (NMR), and energy-dispersive X-ray spectroscopy (EDX) being used to study the structure, composition, and morphology.

## Motivation

There are several reasons why one might choose to study the synthesis and characterization of aluminum oxide ( $\text{Al}_2\text{O}_3$ ) and vanadium oxide ( $\text{V}_2\text{O}_5$ ) thin films. Firstly, both aluminum oxide ( $\text{Al}_2\text{O}_3$ ) and vanadium oxide ( $\text{V}_2\text{O}_5$ ) are important functional materials with a wide range of applications, particularly in the fields of environmental protection, energy conversion, and electronics. Thin films of these materials have unique properties that make them particularly suitable for use in the applications, such as their ability to efficiently adsorption, catalysis, and convert and store energy.

Additionally, the synthesis and characterization of  $\text{Al}_2\text{O}_3$  and  $\text{V}_2\text{O}_5$  thin films is a complex and challenging field that requires a deep understanding of the underlying chemical and physical processes involved. Studying these materials provides an opportunity to gain a deeper understanding of these processes and to develop new and improved methods for synthesizing and characterizing these materials.

Finally, the increasing demand for environmentally friendly and sustainable technologies has driven significant interest and investment in the development of new and improved materials for use in these technologies, making the synthesis and characterization of  $\text{Al}_2\text{O}_3$  and  $\text{V}_2\text{O}_5$  thin films a particularly important and relevant field of study.

# I. Literature review

## I.1. Thin films

Thin films are continuous layers of material with thicknesses ranging from a few nanometers to several micrometers (Fig. 1). Thin films are typically deposited onto a substrate using various techniques such as sol-gel method, physical vapor deposition, chemical vapor deposition, and dip-coating. Due to their thickness and surface area, thin films also exhibit unique physical and chemical properties that are different from bulk materials, such as increased surface area, higher reactivity, tunable optical and electrical properties.

Thin films are used in a variety of applications, including electronic devices, solar cells, and various coatings [19, 20]. Thin films of materials such as aluminum oxide thin films and vanadium oxide thin films can exhibit different properties than their bulk counterparts due to their nanoscale dimensions, making them of particular interest for research and development. Therefore, the investigation of thin films of materials like aluminum oxide ( $\text{Al}_2\text{O}_3$ ) and vanadium oxide ( $\text{V}_2\text{O}_5$ ) is crucial for the advancement of nanotechnology and the development of new technologies.

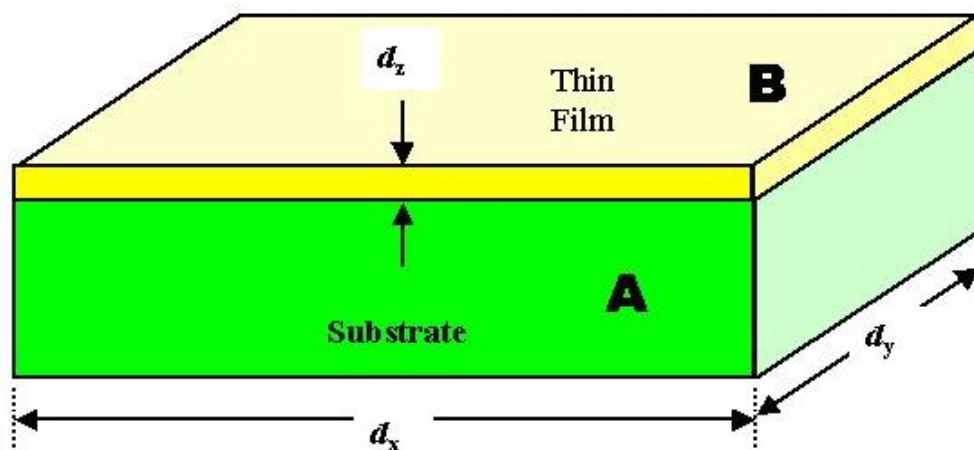


**Figure 1.** Thin film deposition on the substrate. [21]

## I.2. Overview of aluminum oxide

$\text{Al}_2\text{O}_3$  is commonly referred to as alumina or aluminum oxide, which is a white or almost colorless crystalline material. The main natural source of alumina is bauxite, and it contains varying proportions of hydrous (water-containing) aluminum oxides. The crystalline polymorphic phases of  $\text{Al}_2\text{O}_3$  can be found in nature in the mineral corundum, ruby, and sapphire.

The various crystalline phases of alumina can be divided into two groups based on whether they include a face-centered cubic (FCC) lattice or a hexagonal compact-packed (HCP) of oxygen ions. This last group is the most numerous [22], it contains the  $\kappa$  (orthorhombic) and  $\chi$  (hexagonal), monoclinic  $\theta'$ ,  $\theta''$  and  $\lambda$  phases in addition to the most stable  $\alpha$ - $\text{Al}_2\text{O}_3$  phase [23].

The four metastable polymorphs that make up the FCC oxygen network alumina group are the  $\theta$  (monoclinic) [24],  $\delta$  (tetragonal or orthorhombic), and  $\eta$  (cubic spinel-type) phases. The  $\theta$ - $\text{Al}_2\text{O}_3$  structure is the only known exactly among these metastable phases. The  $\gamma$  and  $\eta$  phases are quite similar, many authors refer to any cubic alumina phase as  $\gamma$ - $\text{Al}_2\text{O}_3$  due to its significant prominence [25]. Both spinel structures have one aluminum vacancy in the site of every 9 Al atoms. The distinction between the two phases is made according to whether the vacancies are all in site A, tetrahedral ( $\gamma$ - $\text{Al}_2\text{O}_3$ ) [26], or all in site B, octahedral ( $\eta$ - $\text{Al}_2\text{O}_3$ ). It's interesting to note that despite the similarity of their crystal structures,  $\gamma$  and  $\eta$ - $\text{Al}_2\text{O}_3$  have very different properties.

Aluminum oxide ( $\text{Al}_2\text{O}_3$ ) thin films have attracted a lot of attention due to their excellent transparency [27], broadband gap [28], chemical and thermal stability and aluminum oxide ( $\text{Al}_2\text{O}_3$ ) possesses several great properties (Table 1). Its transparency extends throughout a broad spectrum, from ultra-violet to mid-infrared. Aluminum oxide thin films have several uses in optoelectronics, microelectronics, wear-resistant technology, catalysis [29,30,31], anticorrosive coatings [32], adsorption techniques [33] and surface passivation for solar cells [34].

**Table 1.** Properties of Aluminum oxide [35]

Crystal structure	Trigonal
Molar Mass	101.96 g. mol <sup>-1</sup>
Density	3.95-4.1 g /cm <sup>3</sup>
Melting point	2072 °C
Boiling point	2977 °C
Thermal conductivity	30W.m <sup>-1</sup> . K <sup>-1</sup>
Electrical resistivity	1x10 <sup>14</sup> to 1x10 <sup>15</sup> Ω.cm
Tensile strength	69 to 665 MPa
Compressive strength	690 to 5500 MPa
Mohs hardness	9
Bulk modulus	137-324 GPa
Shear modulus	88-165 GPa
Young's modulus	215-413 GPa

- Gamma aluminum oxide ( $\gamma$ -Al<sub>2</sub>O<sub>3</sub>)

Gamma aluminum oxide ( $\gamma$ -Al<sub>2</sub>O<sub>3</sub>) is commonly employed as a support due to its excellent mechanical strength, ability to be synthesized with a large surface area, and cost-effectiveness. The surface characteristics of a substance are considered an extension of its bulk and thin films. Although  $\gamma$ -Al<sub>2</sub>O<sub>3</sub> has been utilized for many years, there is still ongoing debate about its structure. This is primarily because the production of macrocrystalline  $\gamma$ -Al<sub>2</sub>O<sub>3</sub> has not been achieved, with only nanocrystalline  $\gamma$ -Al<sub>2</sub>O<sub>3</sub> being successfully prepared (Fig. 2).

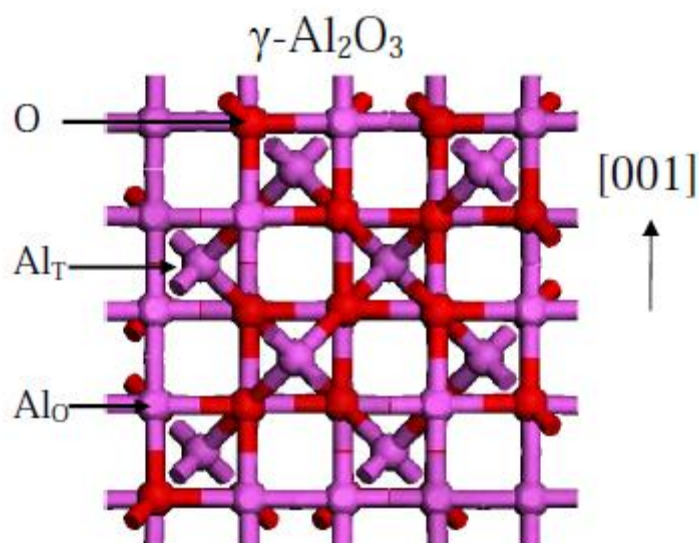


**Figure 2.** The lattice of  $\gamma\text{-Al}_2\text{O}_3$  is composed of 4 layers of tetrahedral and octahedral planes.

- Surface of  $\gamma\text{-Al}_2\text{O}_3$

Understanding the surface properties of  $\gamma\text{-Al}_2\text{O}_3$  is crucial. Gamma aluminum oxide serves as an acidic catalyst and acts as a primary support for catalytic metal, metal oxide, and metal sulfide particles. The morphology of  $\gamma\text{-Al}_2\text{O}_3$  particles is inherited from boehmite particles, as boehmite undergoes a topotactic transformation to become  $\gamma\text{-Al}_2\text{O}_3$ . Typically, boehmite nanoparticles exhibit a rhombohedral shape, characterized by a prominent (010) basal surface and (100), (001), and (101) edge surfaces. These four boehmite surfaces correspondingly transform into the (110), (110), (100), and (111) surfaces of  $\gamma\text{-Al}_2\text{O}_3$  [36]. The arrangement and coordination states (5-, 4-, or 3-coordinated) of  $\text{Al}^{3+}$  cations on the surface play a significant role, as surface  $\text{Al}^{3+}$  cations with incomplete coordination are responsible for the Lewis acidity observed on the  $\gamma\text{-Al}_2\text{O}_3$  surface, which holds significant importance.

### **I.2.1. Preparation of aluminum oxide**

Aluminum oxide thin films can be developed using a number of chemical and physical processes, including atomic layer deposition (ALD) [37], chemical vapor deposition (CVD) [38], pulsed laser deposition (PLD) [39], reactive magnetron sputtering [40], spray pyrolysis deposition (SPD) [41], and dip coating (DP) [42], and sol-gel route [43,44]–[48]. Due to its simplicity, affordability, and ability to regulate the structure and textural qualities, the sol-gel technique is one of the best methods for producing aluminum oxide thin films [48].

The aluminum alkoxides, such as aluminum isopropoxide and sec-butoxide are often chosen to make aluminum oxide thin film by sol-gel process [49, 50]. A few organic stabilizers are used to enhance the quality and transparency of thin films as well as speed up or limit the rate of hydrolysis of metal alkoxides [7,46]. Yoldas used the sol-gel approach to create the first alumina thin films by applying an Al alkoxide precursor over a lengthy period of time [52].

From the inorganic Al salts, nitrate and chloride are also used in the sol gel process [53]. Several authors have studied the effect of acids e.g., hydrochloric, or acetic acids to create sols. Sols may be controlled by various factors, including molar ratio, time, and pH [54].

### **I.3. Overview of vanadium oxides**

Vanadium oxides belong to the class of semiconducting metal oxides. Due to the different material characteristics depending on the oxidation state, they have attracted increasing study over the past few decades. Vanadium oxide can exist in various oxidation states from  $V^{2+}$  to  $V^{5+}$  [55].

The most well-known substances are vanadium dioxide ( $VO_2$ ) and vanadium pentoxide ( $V_2O_5$ ). These numerous substances have demonstrated their ability to be used in various real-world contexts. At roughly 68 °C [56], vanadium dioxide undergoes an intriguing metal-insulator-transition (MIT) phenomenon [57], changing its phase structure from a low-temperature insulating state to a high-temperature metallic state [58]. One application of these unique properties is for electrical and optical switching [54, 55]. On the other hand, vanadium pentoxide  $V_2O_5$  is a widely used substance in catalytic applications [61].

Vanadium oxide phases, which consist of mixed oxidation states are exist in two phases: the Magnéli phases with  $V_nO_{2n-1}$  or the Wadsley phases with  $V_{2n}O_{5n-2}$  [8], [62]. Due to the large number of vanadium-oxygen combinations that may be formed, they have a direct relationship with their oxidation states. The frequently observed mixed valence oxides, which include both  $V^{4+}$  and  $V^{5+}$  ions, can significantly affect the material's properties, giving rise to the opportunity to modify the vanadium oxide composition to suit different application domains.

- Sol-gel vanadium oxide thin films

The synthesis of vanadium oxide thin films using this approach is the most versatile method. This technique offers a cost advantage compared to costly vacuum methods. Additionally, it boasts other benefits such as zero material loss and the ability to coat both sides of the substrate.

The first step of the procedure is the formation of a colloidal sol solution serving as the precursor for the second step, in which a continuous gel network is developed. Commonly employed starting materials include metal alkoxides and metal chlorides, which undergo different hydrolysis and polycondensation reactions.

Vanadium oxide ( $V_2O_5$ ) can be readily produced from both inorganic and metalorganic precursors. Vanadium oxide gel exhibits long-term stability when stored in a sealed container, lasting for months or even years. The emergence of the sol-gel process has generated fresh enthusiasm for  $V_2O_5$  gels, leading to rapid advancements in this area.

Numerous studies have documented various methods for synthesizing  $V_2O_5$  sols and gels in the literature [63–65]. The sol-gel process relies on the hydrolysis and condensation reactions of molecular precursors.

Aiping et al. [65] utilized a combination of the sol-gel technique and a hydrothermal method to deposit Mo-doped  $V_2O_5$  electrochromic films. The introduction of doping enhanced the electrochemical and electrochromic properties of films. El Mandouh et al. [63] employed an inorganic sol-gel method to deposit  $V_2O_5$  films on glass substrates. The substrates were immersed in the sol and gradually withdrawn, allowing for the film formation process. The gel formed on the substrate was allowed to air dry for 24 hours at room temperature. The prepared films underwent a heat treatment process (ranging from 127 to 327 °C) to enhance their adhesion and microstructure.

The researchers found that the direct band gaps of  $V_2O_5$  films prepared via the sol-gel method on glass substrates were 2.49 eV in their initial state and 2.42 eV after annealing at 200 °C. The annealed films exhibited reduced band gaps due to the decrease in localized states within the band gap caused by the annealing process.  $V_2O_5 \cdot nH_2O$  gels are composite materials that consist of solvent molecules ( $H_2O$ ) trapped within an oxide network ( $V_2O_5$ ). These gels possess electronic properties originating from electron hopping within the mixed-valence oxide network, as well as ionic properties arising from proton diffusion in the aqueous phase [66].

### I.3.1. Structural and electrical properties of V<sub>2</sub>O<sub>5</sub>

Vanadium oxide has interesting structural and electrical properties that make it useful in various applications. The saturated (highest oxidation state) oxide is V<sub>2</sub>O<sub>5</sub>, and consequently, that is the most stable in the V–O system.

Vanadium pentoxide has an orthorhombic crystal structure [67]. The Pm-nm space group has unit cell structure with lattice parameters  $a=11.510 \text{ \AA}$ ,  $b=3.563 \text{ \AA}$ , and  $c=4.369 \text{ \AA}$ . It is made up of deformed trigonal bipyramidal coordination polyhedra of O ions around V ions and has a layer-like structure (Fig. 3 and 4).

Vanadium pentoxide has an orthorhombic crystal structure with Pm-mn symmetry made up of VO<sub>6</sub> octahedra structures that are connected from the unit cell's corners and edges by bridging oxygen atoms as shown in (Fig. 3). The structure possesses a relatively open framework, and introducing oxygen vacancies into a crystal could potentially enhance its structural properties.

Most applications for vanadium oxide have been in the field of catalysis. The potential application of V<sub>2</sub>O<sub>5</sub> as an electrode material in lithium-ion batteries has garnered significant attention [68]. Its use as an additional layer in solar cells has also been widely studied and is of considerable interest [69]. According to most sources, the V<sub>2</sub>O<sub>5</sub> phase is an n-type semiconductor [61,62].

The existence of oxygen vacancies in the structure of the films, mostly because of lower valence V<sup>4+</sup> ions, and the hopping conduction mechanism that results have been widely acknowledged as the basis for the electric conductivity of the V<sub>2</sub>O<sub>5</sub> phase [72]. The unpaired electron is positioned on two vanadium sites connected to an oxygen vacancy in this way. By hopping electrons from lower valence states to higher levels, the electrical conductivity is created [73]. The preliminary orthorhombic V<sub>2</sub>O<sub>5</sub> crystal structure can be distorted, leading to a new symmetry when the concentration of V<sup>4+</sup> ions and associated oxygen vacancies exceeds a particular threshold. Additionally, it has been demonstrated that vanadium oxide thin films and semiconducting with a mixed valence state composed of V<sup>5+</sup> and V<sup>4+</sup> ions are p-type semiconductors [74].

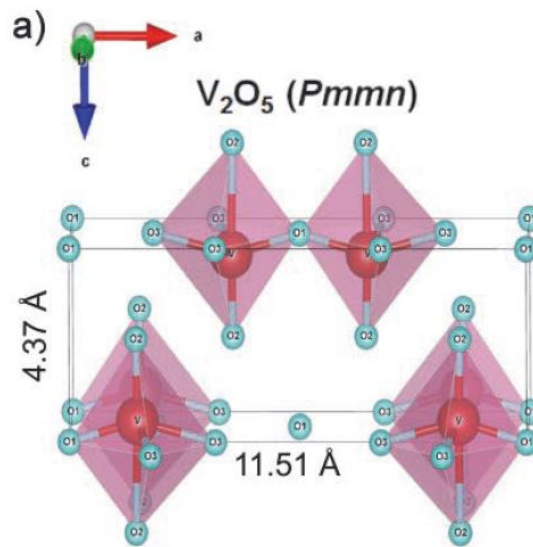


**Figure 3.** Lattice of vanadium oxide red atoms represent the vanadium atoms and the blue patterns represent the oxygen atoms [75].

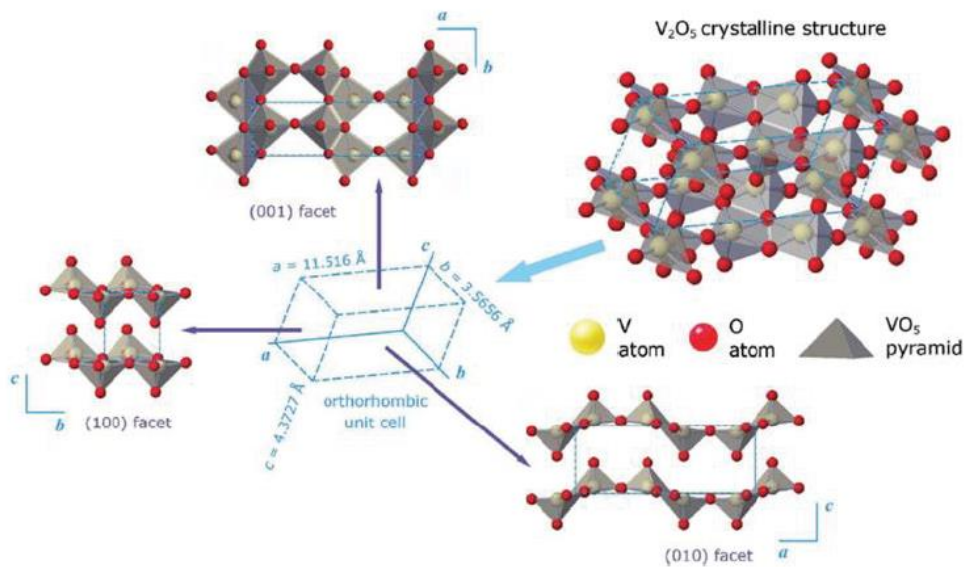


**Figure 4.** The crystalline structure of  $V_2O_5$  within one unit cell. The orthorhombic unit cell of  $V_2O_5$  is marked as blue dashed lines. The 3D view and the projected views of (100), (010), and (001) facets are depicted as well [76].

Vanadium pentoxide thin films ( $V_2O_5$ ) were made using a variety of techniques, including pulsed laser deposition [77], spray pyrolysis [69,70], chemical vapor deposition [80], sol-gel [81], [82], spin coating [74,75], atomic layer deposition [85], sputtering [86] and dip coating [87]. These applications mostly focus on the film-growing techniques and the material properties connected to the shape and crystallinity of the film surface [88]. Dip coating is an affordable and straightforward experimental method for maintaining uniformity, quality, and repeatability. Various parameters, such as immersion time and dipping rate, can influence the properties of the resulting films [65].

Margoni et al. studied the effect of substrate temperature on the structural, optical, morphological, and electrical properties of  $V_2O_5$  by adding nitric acid [89], Chu et al. prepared nanostructure  $V_2O_5$  film using oxalic acid by hydrothermal treatment [90], George et al., reported the preparation of vanadium pentoxide by dip coating using polyethylene glycol and nitric acid [91].

## II. Methods of synthesis and characterization

### II.1. Synthesis methods

#### II.1.1. Sol-gel technique

This method produces highly homogeneous, cost-effective materials with defined, proposed structure. The sol-gel method is an excellent cost- and energy efficient technique. The sol-gel process is a versatile technique, it produces coatings and thin films, monoliths, composites, porous membranes, powders and fibers [92]. The texture and surface qualities of the materials may be well controlled due to the solvent medium of technique. Controlling and tailoring the material structures is possible even in the nanoscale or molecular range.

In general, the sol-gel process can be divided into five stages, which are outlined below (Fig. 5). The fundamental reactions such as hydrolysis and condensation of molecular precursors produce a transparent colloidal system: sols or gels (1,2 stages). The 3. stage is the aging, 4. is drying, and 5. the heat treatment [93] (Fig. 5).

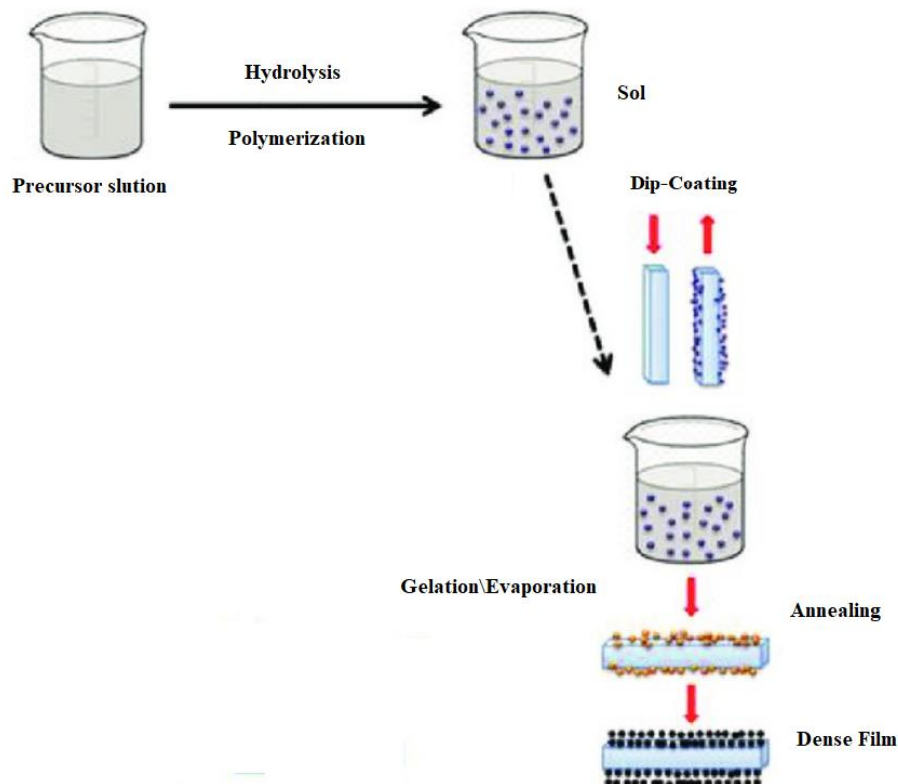


**Figure 5.** Sol-gel thin films deposition process [94].

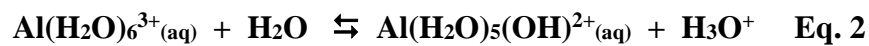
### *II.1.1.1. Hydrolysis*

Hydrolysis means a reaction of precursor molecules with water. The typical precursor molecules are metal alkoxides (M-OR). The following is the general chemical reaction for the hydrolysis process:



where M=metal atoms, R=alkyl groups ( $\text{C}_n\text{H}_{2n+1}$ ). The amount of water strongly influences the gel formation, a higher water content facilitates the development of loose structures.

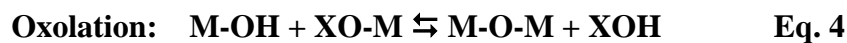
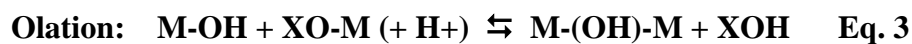
But inorganic metal salts are also applied as precursor molecules. Its hydrolysis reaction:



### *II.1.1.2. Condensation*

When water or alcohol molecules are removed from the hydrolyzed compounds, bonds develop between the compounds. Condensation may be realized through two processes: olation, which involves the formation of a shared hydroxyl ( $-\text{OH}-$ ) group between two metal centers; and oxolation, which means the development of an oxo ( $-\text{O}-$ ) bridge between two metal centers.

The following is the general chemical reaction for condensation:



X may be H or R groups.

### ***II.1.1.3. Aging***

Structural changes persistently occur following the formation of a 3D gel network. The processes of aging are categorized as polymerization, coarsening, and phase transformation. Polymerization results in an increase in the connectivity of the network. The gel network becomes denser. Coarsening or ripening is a process of dissolution and reprecipitation driven by differences in solubility and it leads to an increase in the size of particles and a decrease in the size of pores.

### ***II.1.1.4. Drying***

Different drying techniques can be employed to extract the liquid from the gel, resulting in different gel structures: atmospheric/thermal drying leads to the formation of xerogel, supercritical drying yields aerogel, and freeze-drying produces cryogel. Each technique has a unique effect on the structure of the gel network.

### ***II.1.1.5. Thermal treatment***

This final calcination step is used to remove any remaining residues, by-products, and solvent molecules from the powder. The important aim is to create the final bonding structures. Calcination temperature is a critical parameter in controlling the material's pore size and density.

### ***II.1.1.6. Structural influential parameters***

The following factors significantly influence sol-gel chemistry [95]:

- **pH:** Under acid-catalyzed conditions ( $\text{pH} < 5$ ), the hydrolysis is favored, the condensation reactions are limiting. Under basic conditions ( $\text{pH} > 8$ ) the condensation will be favored.
- **Catalysis:** Acidic or basic catalysts are often employed to influence the density of the 3D gel structure.
- **Solvent quality:** Alkoxides are not miscible in water, the precursors, water, and potentially the catalyst must all be mixed in a single solvent. To avoid probable interactions between the different components and the alteration of the kinetics reactions, the alcohol-related to the ligand -OR of the alkoxide must be used.
- **Solvent content:** considerably determines the density of the 3D gel structure.
- **Additives:** drive and control the structure.

## II.2. Deposition methods

### II.2.1. Dip-coating (DP)

Dip-coating is a rapid and versatile film-formation technique that effectively complements sol-gel methods [96]. Dip-coating is a method of depositing thin films on a substrate by dipping it into a viscous or colloidal solution of precursors and then withdrawing it at a controlled rate.

This process is repeated multiple times to build up the desired film thickness. The dipping and withdrawal process is typically carried out at regular intervals to ensure a uniform coating on the substrate. The characteristics of precursor solutions have a significant impact on the quality of the deposited layer. It is important to choose a suitable solvent, which must be simple to remove during subsequent annealing [97]. The surface of the substrate should not be permeable and must permit the crystallization of a film on it [98]. The substrate must be able to endure the chemical properties of the layer while keeping structural integrity throughout subsequent heating processes.

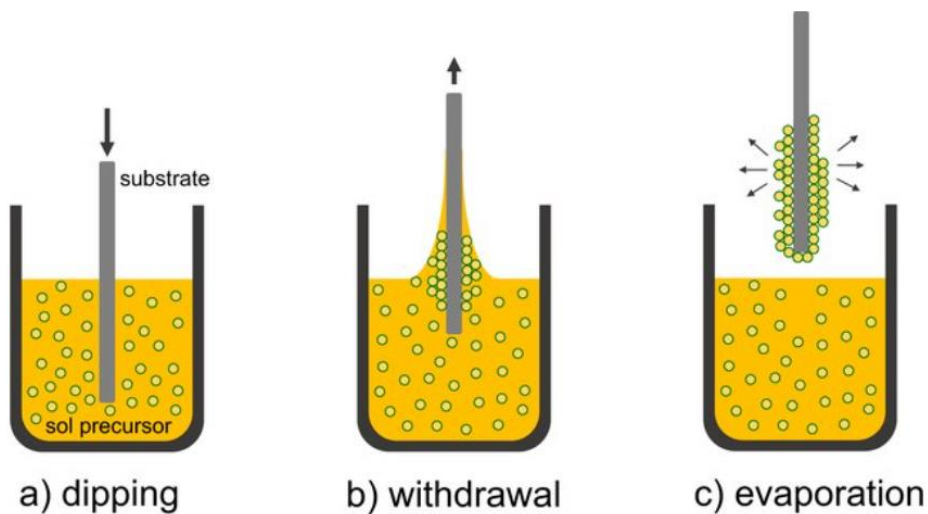


**Figure 6.** Sequential stages of the dip-coating process: (a) dipping, (b) withdrawal and (c) evaporation of the solvent [99].

To achieve an equilibrium between the substrate surface and the solution, the substrate should be given a short period of rest after being submerged in the liquid (Fig. 6).

Apart from other factors like liquid viscosity, surface tension, and evaporation rate. The deposition rate is a critical parameter in dip-coating. The withdrawal rate of the substrate from the precursor solution significantly affects the outcome of the deposition process [92,93]. A slower withdrawal rate results in a thinner layer on the substrate.

### **II.2.2. Atomic layer deposition (ALD)**

During ALD, a sample substrate is subjected to alternating dosages of various vapor- or gas-phase species, and thin films are built up layer by layer in cycles. A sub-monolayer of material is deposited in each [102]. A typical ALD cycle consists of four steps.

The sample is exposed to a precursor in the first stage. Cleaning is carried out in the second stage to cleanse the reactor of any remaining precursor. The sample is then exposed to a co-reactant in the next phase. Both half-cycles are saturated, resulting in a specific amount of growth per cycle, or GPC. The two half-cycles are repeated in an ABAB pattern to achieve the desired film thickness. ALD produces highly conformal and homogeneous films with exact thickness control, which is required for a variety of micro- and nano-scale applications due to its self-limiting surface reactions. Metal oxides, nitrides, carbides, chalcogenides, metals, and other materials are currently among the materials that ALD may create [102].

### **II.2.3. Chemical vapor deposition (CVD)**

Chemical vapor deposition (CVD) is a widely used method for depositing high-quality and high-performance thin films on a substrate through a chemical reaction between a vapor-phase precursor and a surface. The reaction occurs at high temperatures and/or pressures, which activate the precursor and promote the desired chemical reaction. The process can be optimized by understanding the chemistry involved, and theoretical chemical modeling can provide detailed information about the surface and gas phase chemistry [103]. Chemical vapor deposition is commonly used in the semiconductor industry for depositing thin films of various materials and in other industries for producing hard coatings and wear-resistant surfaces. There are different types of chemical vapor deposition techniques, each with its own advantages and limitations, which are chosen based on the specific application and desired properties of the thin film.

#### **II.2.4. Spray pyrolysis (SP)**

Spray pyrolysis is a technique primarily utilized in industrial settings rather than in laboratories for synthesizing submicron materials. Spray pyrolysis is an efficient, cost-effective, and adaptable approach, often considered a bridge between liquid and gas-phase techniques [104]. The different precursor solutions might be colloidal or a real solution that contains metal ions. The subsequent steps outline the process of fabrication [105]:

- Dissolve the inorganic precursors in a suitable solvent to acquire the liquid source.
- Utilize a two-fluid atomization or an ultrasonic atomizer to produce droplets from this liquid source.
- A carrier gas is used to transport the droplets into a heated chamber.
- The droplets are vaporized within the chamber and subsequently captured using a filter, enabling the disintegration of the droplets to generate the corresponding materials, often oxides.
- The use of two-fluid atomization provides the benefit of high throughput, but the drawback is the wide particle size distribution.

Spray pyrolysis, like any other technology, has some limitations, including difficulty scaling up (lower yield) and challenges determining the growth temperature.

### **III. Experimental details**

#### **III.1. Synthesis of aluminum oxide thin films**

##### **III.1.1. Layer from Al<sub>2</sub>O<sub>3</sub> suspension**

An aqueous colloidal sol was prepared from Al<sub>2</sub>O<sub>3</sub> powders. The sol was stirred for 2 hours at 70 °C. Various sol concentrations (1 M, 0.75 M, 0.5 M, and 0.25 M) were used for the layer procedure [106]. To enhance the adhesion of the layer on a quartz substrate, an IGEPAL solution was introduced to each precursor system under ultrasonic conditions [107]. Each layer was applied using the dip-coating method, and the solvent was eliminated by heating the samples at temperatures between 80-90 °C.

In all instances, the Al<sub>2</sub>O<sub>3</sub> layer was subjected to a heat treatment at 600 °C. The layers as commercial materials obtained by this widely used industrial technique make for comparison purposes.

##### **III.1.2. Layer from boehmite suspension**

A colloidal boehmite sol has been obtained by partial dissolution of boehmite powders (BASF) in an acid medium. The most suitable acid medium is the aqueous solution of acetic acid (HAc). Boehmite powders were reacted with acetic acid in various molar ratios to Al: 0; 0.05; 0.1; 0.5; 1.0; and 2.0 [108]. The reaction was carried out under stirring at 70 °C for 2 hours. The final sol concentration was also varied. The subsequent preparation steps align with those described in paragraph 3.1.1.

##### **III.1.3. Layer by sol-gel method starting from basic Al acetate**

The starting solution has been prepared by dissolving the aluminum acetate (Al (OCH<sub>2</sub>CH<sub>3</sub>)<sub>2</sub>OH, AlAc) in NaOH solution in 0.11 molar ratio of OH/Al and heated at 55 °C for 1 hour under reflux. Various acids (HCl, acetic acid, and citric acid) were added to the basic solution to achieve pH=7 [108].

In another sol-gel preparation route, the layer synthesis started using two types of Al precursors. Basic aluminum acetate and boehmite sol were reacted in a common solution. The aluminum acetate was separately dissolved in NaOH solution in molar ratio 0.11 and stirred at room temperature for 1 hour. The boehmite colloid solution was also separately prepared from boehmite powders with acetic acid in molar ratio of 0.5. The boehmite sol and the basic solution

of AlAc were mixed in various ratios and heated at 55 °C for 1 hour under reflux. The subsequent preparation steps align with those described in paragraph 3.1.1.

#### **III.1.4. Layer by sol-gel method starting from Al nitrate**

Aluminum nitrate ( $\text{Al}(\text{NO}_3)_3 \cdot 9 \text{H}_2\text{O}$ , Aln) was dissolved in 1-propanol in a molar ratio of 0.12. This solution was kept under stirring at 80 °C for 15 hours. During the treatment, hydrolysis reactions occur, along with condensation reactions at a lower rate. A concentrated solution is obtained through partial evaporation of the solvent, which promotes further condensation reactions. The viscous solution is then dried at 80 °C. The macroporous foam product obtained can be immersed in distilled water, using 10 or 20 mass ratios of water/solid material [108].

#### **III.1.5. Layer by sol-gel method starting from Al isopropoxide**

The experiments using Al isopropoxide serve two purposes: first, as a comparative sol-gel preparation based on the Yoldas method; and second, as the development of a new sol-gel procedure originating from a typical sol-gel precursor, such as Al isopropoxide.

In accordance with Yoldas's approach [47], AliPr was dissolved in distilled water with a molar ratio of 156 and stirred at 80 °C for 1 hour, resulting in the formation of a slurry. Acetic acid was then introduced to the slurry in a molar ratio of 4.9  $\text{Al}^{3+}/\text{HAc}$ . This system was stirred at 80 °C for 8 hours, leading to the conversion of the slurry into a transparent sol solution.

In our sol-gel application, we dissolved aluminum isopropoxide ( $\text{Al}(\text{OCH}(\text{CH}_3)_2)_3$ , AliPr, 98%) in 1-propanol with an Al to propanol molar ratio of 0.04 and stirred the mixture at 60 °C for 2 hours. To the solution, we added ethyl acetate (EtAc) or acetic acid (as a peptizing agent) and water in an  $\text{Al}^{3+}/\text{Ac}$  molar ratio of 12.25 and a distilled water to  $\text{Al}^{3+}$  ratio of 10. The solution was then treated at 60 °C for 3 hours. The resulting sol required an additional 24-hour treatment to achieve a gel-like structure.

In every sol-gel approach, an IGEPAL solution was employed as a non-ionic surfactant to improve the bonding between the layer and the quartz substrate [109].

Maintaining clean surfaces is crucial for a wide range of applications, particularly in the fields of semiconductor devices and microelectronics [110].

The dip-coating technique was utilized to apply all solutions onto a quartz substrate. When devising strategies for substrate cleaning, it is imperative to ensure that the selected methods efficiently eliminate contaminants while preserving the surface's integrity. Prior to coating, the substrate underwent through a cleaning procedure that included the use of acetone, ethanol, and deionized water. Then the layers were dried at 70 °C for 1 hour and subsequently heated at 600 °C for 3 hours.

### **III.2. Synthesis of vanadium oxide thin films**

In these experiments, the primary method of preparation was sol-gel synthesis, complemented by thermal decomposition. Additionally, melting was employed as a comparative process. Ammonium metavanadate ( $\text{NH}_4\text{VO}_3$ , Merck,  $\geq 99\%$  purity), volatile vanadate salts, our custom-created ammonium decavanadate ( $(\text{NH}_4)_6[\text{V}_{10}\text{O}_{28}]$ ) as a precursor containing  $\text{V}^{5+}$ , and vanadyl acetylacetonate ( $\text{VO}(\text{acac})_2$ , Merck,  $\geq 99\%$ ), as well as  $\text{VO}_2$  (Merck, 98%) as  $\text{V}^{4+}$  containing precursors were used in our syntheses.

The effect of various chemical additives, including acids, reducing agents, and surfactants, was examined to assess their influence on the quality of the deposited layers. Vanadium oxide thin films were deposited on glass substrates using the dip-coating technique, with the process conducted at a temperature of 400°C.

#### **III.2.1. Sol-gel synthesis starting from $\text{NH}_4\text{VO}_3$**

Ammonium metavanadate ( $\text{NH}_4\text{VO}_3$ ) was mixed with distilled water to dissolve resulting 0.21  $\text{mol}\cdot\text{dm}^{-3}$  concentration and stirred at 50 °C. Without an acidic medium is not possible to get a clear solution yellow sol.

To obtain a transparent homogeneous system, it is necessary to maintain a pH of 2, leading to the formation of vanadic acid ( $\text{H}_3\text{VO}_4$ ) in the orange-coloured solution. In the synthesis experiments, various acid reagents, such as nitric acid ( $\text{HNO}_3$ ), acetic acid ( $\text{HAc}$ ), and citric acid were added to the solution. In addition to acids, a cation exchange process was employed to obtain vanadic acid ( $\text{H}_3\text{VO}_4$ ).

Several experiments were conducted using different chemical additives, including oxalic acid at a concentration of 40 % by weight of metavanadate, ascorbic acid at a concentration of 120 % by weight of metavanadate, and ethyl acetate at a concentration range of 30-50% by weight of metavanadate. Various surfactants, such as Pluronic L61 (a polyoxyethylene block

copolymer), non-ionic Triton X 100 (glycol tert-octyl phenyl ether), and cationic CTAB (cetyltrimethylammonium bromide) at concentrations of 5-10 % by weight, were also used. These systems were found to be suitable for dip-coating. The optimal concentration for the dipping process was determined to be 35% by weight of metavanadate. Dip-coating was found to be more effective, resulting in high-quality layers, particularly when surfactants were employed. Heat treatment was carried out at both 70 °C and 400 °C [111].

### **III.2.2. Synthesis starting from VO<sub>2</sub>**

Ethanol was used to disperse VO<sub>2</sub> in 20 g · dm<sup>-3</sup> concentration, followed by the addition of oxalic acid (10 g · dm<sup>-3</sup>). The resulting solution is stirred at 50 °C for 2 hours to create a sol solution. The substrate could then be dipped into the sol to obtain thin films, which are subsequently treated at temperatures of 80 and 400 °C [111].

### **III.2.3. Synthesis starting from vanadyl acetylacetonate, VO(ac)<sub>2</sub>**

To prepare the solution, vanadyl acetylacetonate VO(acac)<sub>2</sub> is dissolved in propanol with a concentration of 0.125 mol · dm<sup>-3</sup>. The solution was then stirred at ambient temperature for a duration of 24 hours. Dipping of the layer can be performed using this highly viscous system [111].

The addition of ethylene glycol can elevate the viscosity of alcoholic solutions. The layer was subjected to drying at a temperature of 80 °C for a duration of 1 hour. To prevent the oxidation of V<sup>4+</sup> to V<sup>5+</sup>, the heat treatment should be conducted within the range of 400 - 600 °C under a N<sub>2</sub> atmosphere.

### **III.2.4. Synthesis starting from ammonium decavanadate**

The most stable form of V<sub>10</sub> can be achieved in acidic conditions (pH 3 to 6). A decavanadate salt, [V<sub>0.50</sub>(H<sub>2</sub>O)<sub>5</sub>]<sub>2</sub>[H<sub>2</sub>(V<sub>10</sub>O<sub>28</sub>)] · 4(H<sub>2</sub>O), was obtained by the reaction of NaVO<sub>3</sub> with quinhydrone (C<sub>12</sub>H<sub>10</sub>O<sub>4</sub>) (in 1:3 molar ratio) in a medium of pH 5-6 adjusted with glacial acetic acid. The mixture of reactants is dissolved in the ethanol-water mixture (40: 60 v/v ratio) and refluxed at 60 °C with stirring. As a result, the solution of ammonium decavanadate can be directly used for layer formation. The resulting layers are then treated at 80 and 400 °C.

During the dip-coating process for thin film preparation, the glass substrates underwent ultrasonic cleaning using acetone, ethanol, and deionized water. Afterwards, the substrates were

immersed in the colloidal solution for a duration of 2 minutes, with a withdrawal speed of 30 mm/min using an automated dip-coater (PTL-MM<sub>01</sub> Dip Coater). The films were left to air-dry at room temperature and subsequently heat-treated at 400 °C. This procedure was repeated to achieve the desired film thickness.

### **III.3. Investigation Methods**

#### **III.3.1. Scanning electron microscopy (SEM)**

The surface coverage and layer thickness were examined using an FEI Quanta 3D FEG scanning electron microscope. SEM images were obtained using the Everhart-Thornley secondary electron detector (ETD), which provides an ultimate resolution of 1-2 nm. Due to the high conductance of the particles studied, electric charges on the surface were readily removed, allowing for SEM imaging in a high vacuum without any coverage on the specimen surface. For optimal SEM visibility, the particles were deposited onto a HOPG (graphite) substrate surface. Additionally, SEM combined with energy dispersive X-ray spectroscopy (EDX) was used for spatially resolved chemical analysis of monolith samples.

#### **III.3.2. Reflection optical microscopy (ROM)**

The surface of layers has also been investigated by reflection optical microscopy, which is part of the atomic force microscopy (AFM) instrument (Park System, XE-100, South Korea) Measurements were performed in air at 25 °C in non-contact mode.

#### **III.3.3. Grazing incidence X-ray diffraction (GIXRD)**

GIXRD measurements were performed by a Rigaku Smartlab X-ray diffractometer equipped with a 1.2 kW copper source (radiation wavelength: CuK $\alpha$ ;  $\lambda = 0.15418$  nm). To reduce the effect of the substrate, a grazing incidence parallel-beam geometry was used with an incidence angle of  $\omega = 1^\circ$ . Scans were performed in the range  $2\Theta$  between  $10^\circ$ – $110^\circ$  with a 1D silicon strip detector (D/Tex ultra-250) at a speed  $0.2^\circ/\text{min}$ .

#### **III.3.4. UV–Visible spectroscopy**

The transmittance of thin films was measured using a Dynamica spectrophotometer equipped with a UV-detection program at room temperature, covering the wavelength range of 200-1000 nm through UV-Visible spectroscopy.

### **III.3.5. FTIR spectroscopy**

The IR spectra were recorded on a Bruker Alpha Fourier transform spectrometer equipped with a single reflection diamond Attenuated total reflection (ATR) unit with a resolution of  $2\text{ cm}^{-1}$ .

### **III.3.6. $^{51}\text{V}$ nuclear magnetic resonance spectroscopy (NMR)**

$^{51}\text{V}$  ( $I=7/2$ , 99,75% abundance) NMR measurements were performed on Bruker Avance-III NMR spectrometer with a 4 mm MAS probe at 11.744 Tesla. All samples were measured at 131.48 MHz resonance frequency with a single pulse sequence using a 15-degree flip angle, and a 1 s relaxation delay. 2 K data points were accumulated at 9, 10, or 11 kHz MAS rotation speed. Typically, 1024 FID signals were accumulated to increase the signal-to-noise ratio. 4 K real spectrum points were calculated applying zero filling and 100-500 Hz line broadening on the FID data points.  $\text{VOCl}_3$  was used for the external standard of the ppm scale. Vanadium (V) spectra were observed in a 4750-ppm spectrum window. Vanadium (IV) nuclei were measured in a 9500-ppm wide window because of their bigger CSA, quadrupole, and paramagnetic anisotropy. The very wide spectrum range resulted in strong baseline distortions of the spectra which were eliminated by a modified SOLA computer simulation program of BRUKER TopSpin software. The advantageous possibility of  $^{51}\text{V}$  NMR measurements is vanadium isotope frequency of 99.75%, well measurable in oxidation state of 5+, the evaluation of  $^{51}\text{V}$  NMR spectra is reliable and unambiguous however, this method also presents some challenges.

### **III.3.7. pH meter**

The pH has been measured by education line EL20 (Mettler-Toledo) calibrated with different buffer solutions of pH 4.01, 7.00, and 9.21.

### **III.3.8. Dip Coater Machine**

Desktop dip coater with variable speed (1-200 mm/min) - PTL-MM01

## IV. Results and discussion

The gamma-aluminum oxide ( $\gamma\text{-Al}_2\text{O}_3$ ) thin films can serve as effective protective coatings in energy-efficient compact fluorescent lamps which contain the mercury gas, enhancing their durability and performance [112]. The alumina layer protects the glass against the formation of sodium amalgam black pattern or HgO layer, since the blackening of the glass reduces the UV emission. The high energy of UV radiation furthers the diffusion of sodium ions from the glass body to the inner surface of quartz tube, and neutral sodium atoms may be created by the electrons of the discharge region. On the inner wall of the quartz tube, sodium amalgam black pattern forms by reaction of the mercury atoms with sodium atoms.

The  $\gamma\text{-Al}_2\text{O}_3$  layer serves to prevent the discharge of mercury ions and blackening of the glass surface in compact fluorescent lamps, thereby contributing to their environmental performance. To ensure that the  $\gamma\text{-Al}_2\text{O}_3$  layer meets this requirement, it must maintain transparency. The transparency of the coated quartz tube is monitored using UV-Visible spectroscopy, with a particular focus on transmittance measurements within the UV range.

### IV.1. Synthesis of gamma-aluminum oxide thin films

The main aim of the syntheses process is to create high-quality transparent  $\gamma\text{-Al}_2\text{O}_3$  nanofilms that form a continuous, uniform coverage over the surface of the quartz substrate. The other aim was to investigate which precursor system is preferred for layer formation. The sol (suspension or slurry) or the gel-like system. In the sol or slurry systems content separated particles of nano or  $\mu\text{m}$  ranges, respectively. The gel-like systems consist of a three-dimensional (3D) network structure. During the synthesis the starting materials, additives, catalysts, and the synthesis techniques were varied.

#### IV.1.1. Layer from boehmite suspension

In the first experiments, thin films were prepared from aqueous sol solutions of boehmite [ $\text{AlO}(\text{OH})$ ] or  $\text{Al}_2\text{O}_3$  using a dip-coating technique. Based on the transmittance results obtained from UV-Visible spectroscopy, the layers produced from boehmite sols exhibit significantly better transparency compared to those derived from  $\text{Al}_2\text{O}_3$  sols (Fig. 7). Different commercially available  $\text{Al}_2\text{O}_3$  layer products (German Heraus and Japanese Chyoda tubes) were served the comparison. The notable disparity in their characteristics can be attributed to the incorporation of acids during the synthesis procedure.

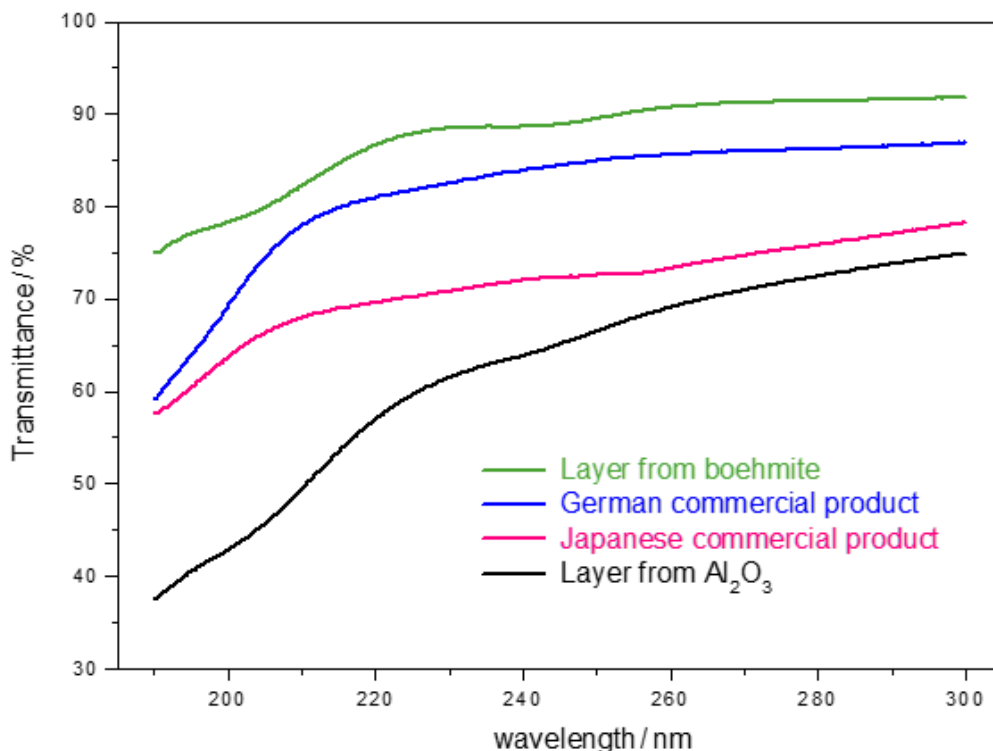


**Figure 7.** Transmittance of layers prepared from boehmite and aluminum oxide suspensions and commercial Al<sub>2</sub>O<sub>3</sub> layer products.

Among the investigated acids (HCl, HNO<sub>3</sub>, HAc), acetic acid (HAc) demonstrated the highest efficiency in terms of enhancing the overall quality of the prepared layers. The acetic acid can attack and partly dissolve the surface of boehmite particles. Moreover, the acetate anions can connect two Al ions from surfaces as a bidentate ligand (Fig. 8). The shared OH groups and the bidentate acetate ligands support and stabilize the formation of a continuous layer.

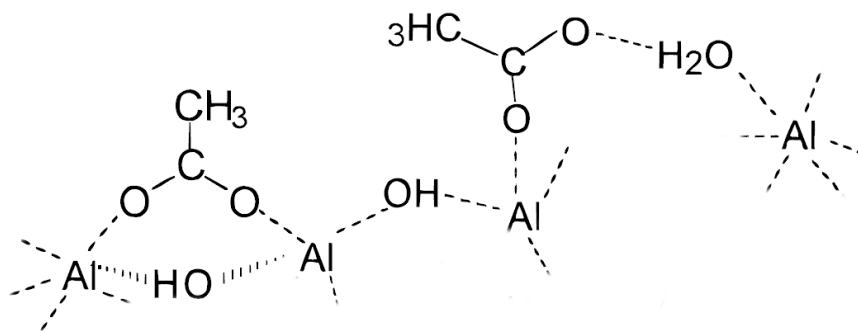


**Figure 8.** The probable connections between the octa- and tetra-coordinated Al ions on the surface of boehmite.

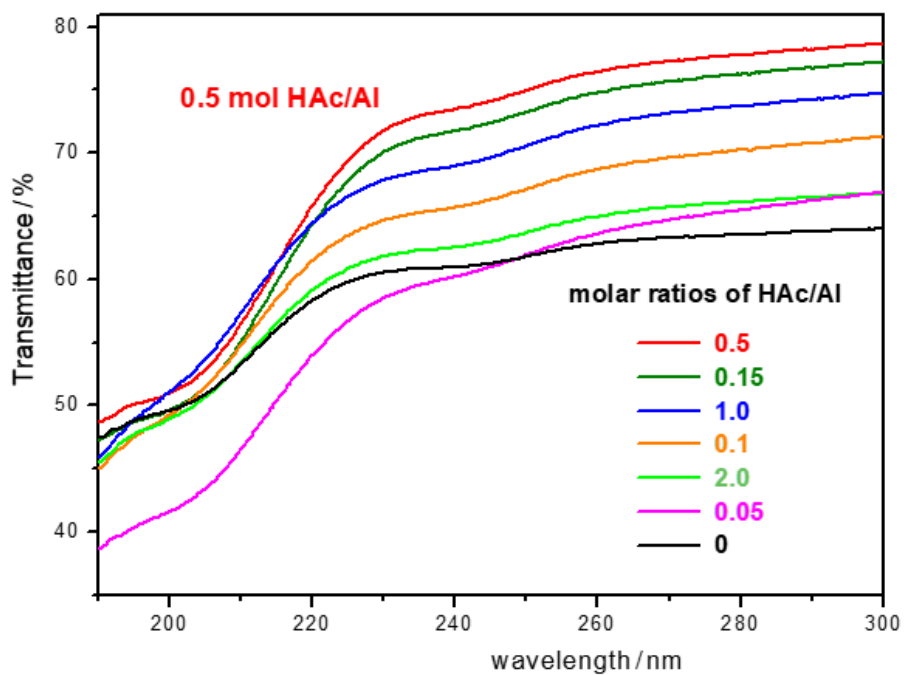


**Figure 9.** Transmittance of layers prepared from boehmite sol in the function of acetic acid.

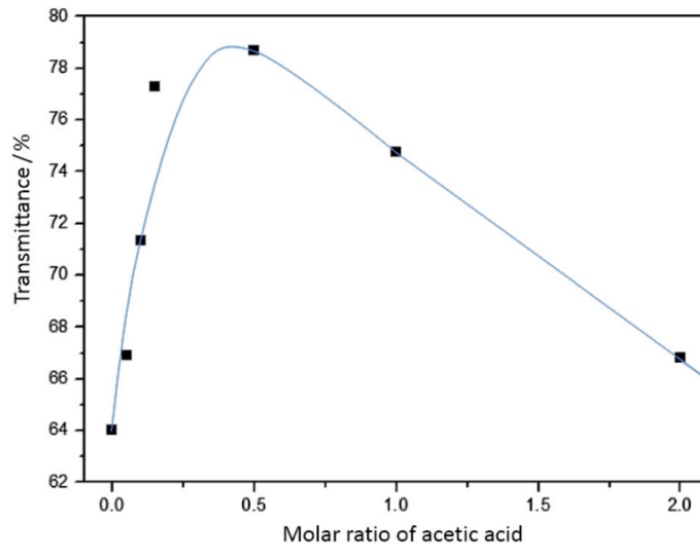


**Figure 10.** Transmittance of layers prepared from boehmite sol in the function of HAc molar ratio.

The optimal molar ratio of HAc has been identified in the precursor sol solution. The ideal HAc/Al molar ratio was found to be 0.50 for optimal layer quality (Fig. 9,10). The larger HAc volume results in too strong acidity, which hinders the OH and acetate substitution and the condensation reactions. The concentration of the initial sol solutions was also investigated. As illustrated in (Fig. 11), a lower concentration of boehmite results in thinner layers and higher transmittance values.

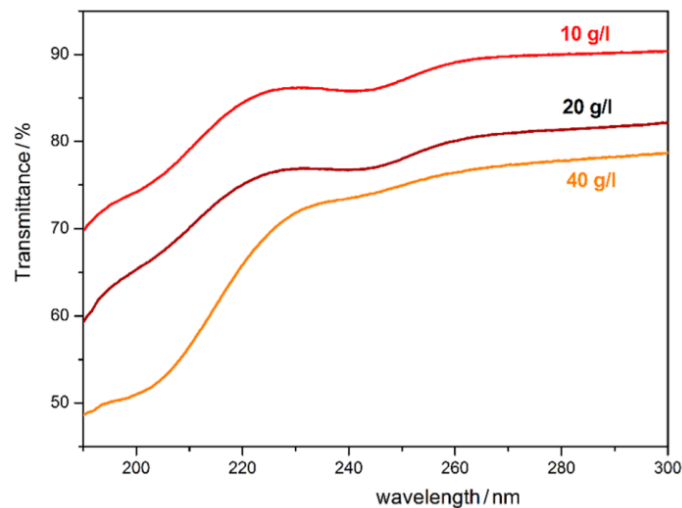


**Figure 11.** Transmittance of layers in the function of concentration of boehmite sol prepared with 0.5 molar ratio of HAc/Al.

To identify the temperature at which boehmite transforms into gamma-aluminum oxide ( $\gamma$ - $\text{Al}_2\text{O}_3$ ), the boehmite sol particles were subjected to various heat treatments and analyzed using a grazing incidence X-ray diffractometer (Fig. 12). The findings indicate that the optimal heat treatment temperature range for the formation of  $\gamma$ - $\text{Al}_2\text{O}_3$  lies between 600-800 °C.

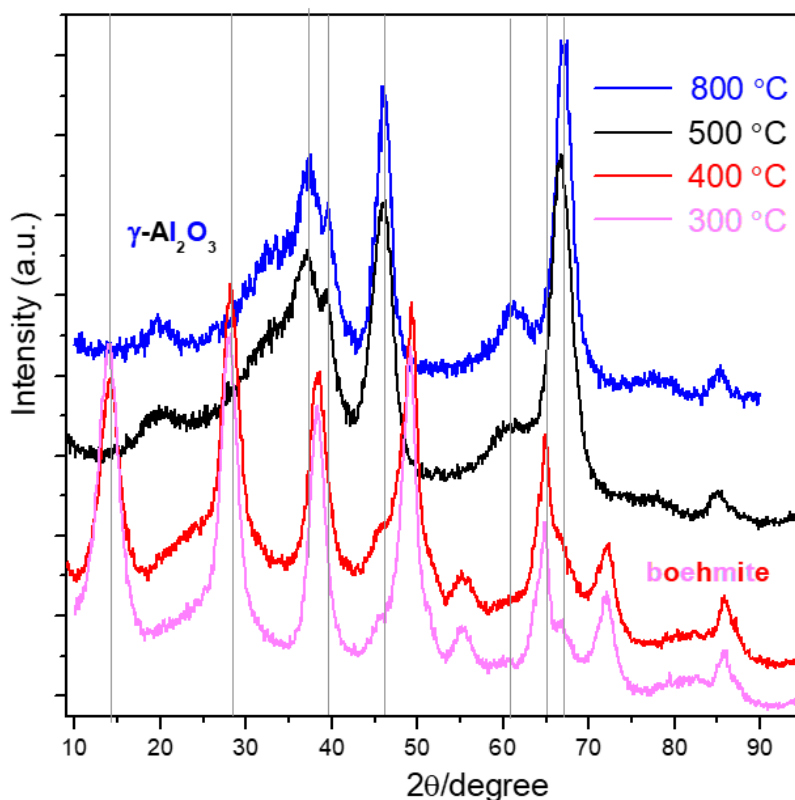


**Figure 12.** Grazing incidence X-ray diffraction (GI-XRD) of boehmite vs. temperature

The goal of the scanning electron microscopy investigation, as depicted in (Fig. 13), was to assess the surface coverage of the quartz substrate and the thickness of the layers. The layer derived from boehmite sol exhibited complete and uniform coverage of the substrate, with a thickness of 110-120 nm. The optimal preparation conditions were identified as a 0.5 molar ratio of HAc/Al and a sol concentration of 10 g/l.

Scanning electron microscopy investigation represents the layer formed from  $\text{Al}_2\text{O}_3$  suspension was less homogeneous and contained some particles of  $\leq 1 \mu\text{m}$  (Fig. 14). The thickness of this layer (135-145 nm) was greater than that of the boehmite-derived layer, resulting in reduced

transmittance. The lower quality of this layer can be attributed to the reduced reactivity of  $\text{Al}_2\text{O}_3$ .

The EDAX analysis presented in (Fig. 15) confirms the existence of aluminum (Al) and oxygen (O) atoms within the layer derived from boehmite sol.

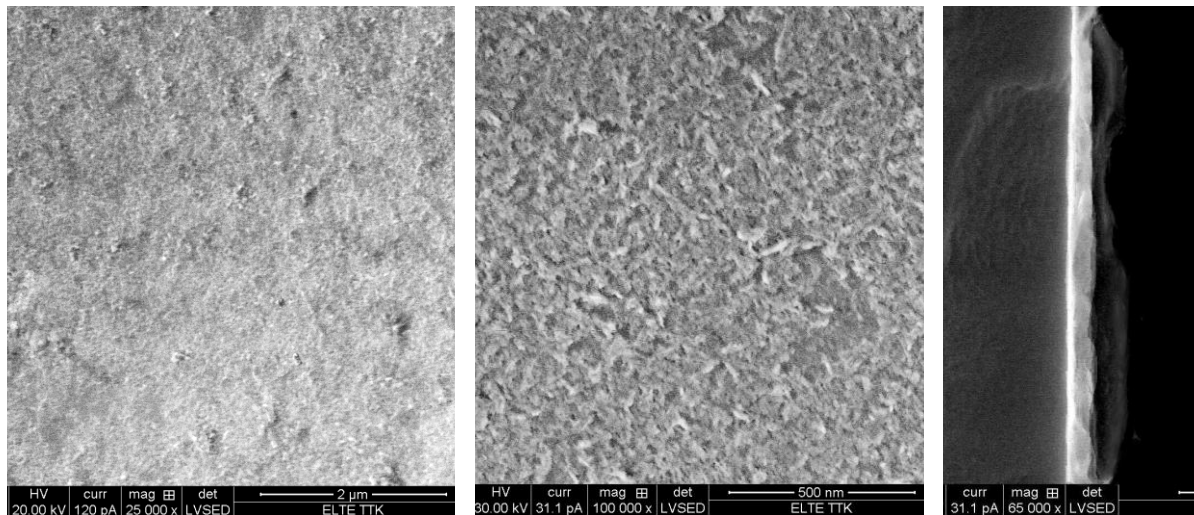


**Figure 13.** SEM images of  $\text{Al}_2\text{O}_3$  layer obtained from boehmite suspension with 0.5 molar ratio of HAc/Al. The layer thickness is 110-120 nm. Magnification: 25 000x; 100 000x, 65 000x.

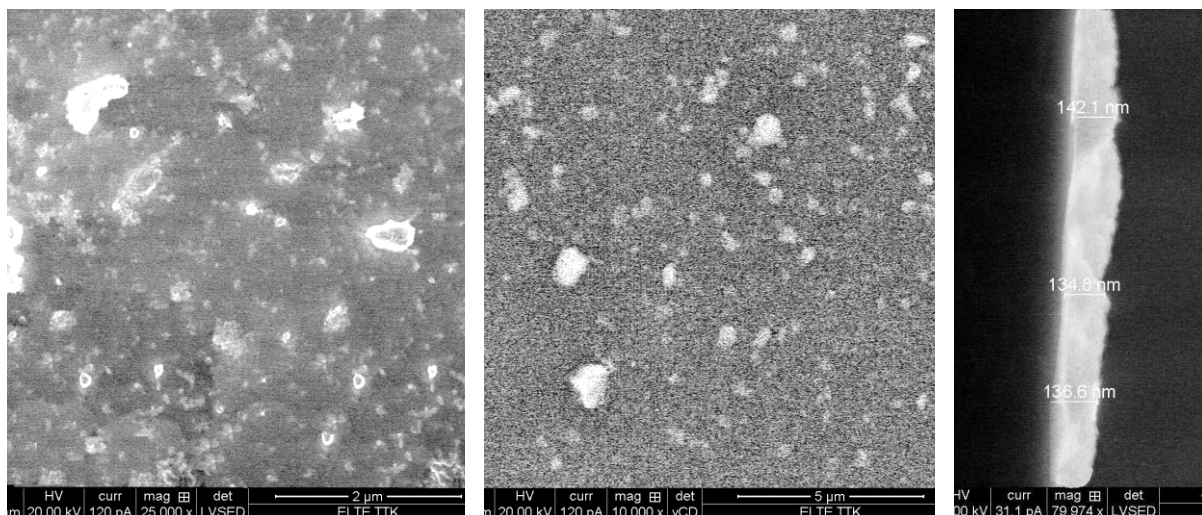


**Figure 14.** SEM images of  $\text{Al}_2\text{O}_3$  layer obtained from  $\text{Al}_2\text{O}_3$  suspension. The layer thickness is 135-145 nm. Magnification: 25 000x; 10 000x, 80 000x.

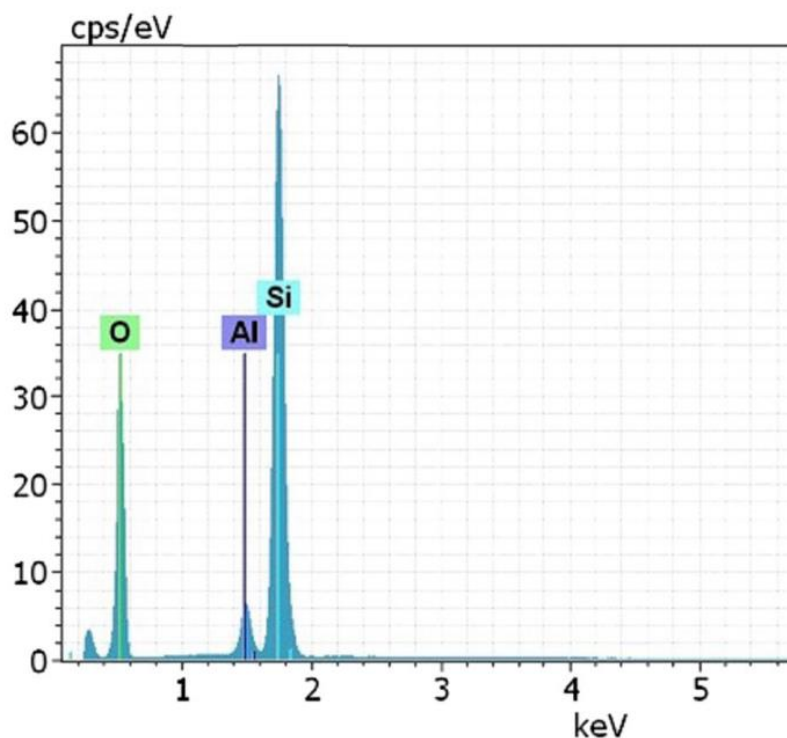


**Figure 15.** EDAX measurement of  $\text{Al}_2\text{O}_3$  layer obtained from boehmite suspension with 0.5 molar ratio of HAc/Al on quartz substrate.

#### IV.1.2. Layer by sol-gel method starting from basic Al acetate (AlAc) salt

Various parameters were varied in the sol-gel syntheses, including the initial materials such as aluminum acetate, nitrate, and isopropoxide, as well as the concentration of acid catalysts such as hydrochloric acid (HCl), acetic acid (HAc), citric acid, and nitric acid ( $\text{HNO}_3$ ). Additionally, additives like boehmite powder were introduced. The application of aluminum acetate and nitrate yielded significant innovations, while the use of aluminum isopropoxide served as a basis for comparison.

The application of acetate anions can be attributed, in part, to their environmental benefits. These anions can decompose into harmless molecules ( $\text{CO}_2$  and  $\text{H}_2\text{O}$ ) during the heat treatment process. Another aspect of acetate's application is its role as bidentate ligands, facilitating the bonding between aluminum ions.

The transmittance values vigorously depend on the acid concentrations. The best transmittance value can be achieved at 2 molar ratios in the case of strong acid such as hydrochloric acid (HCl) (Fig. 16). In the treatment with weak acid (HAc), the molar ratio of 10 proved to be

optimum value. The larger ratios than 10 mol HAc/Al did not appear to improve the transmittance (Fig. 17).

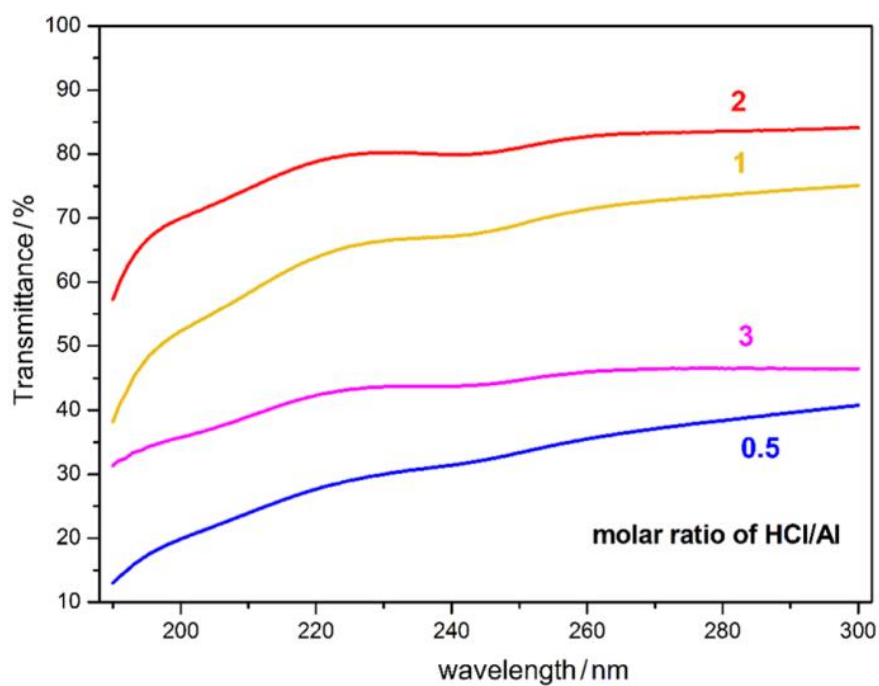


**Figure 16.** Transmittance of sol-gel derived layers prepared from Al acetate in the function of HCl.

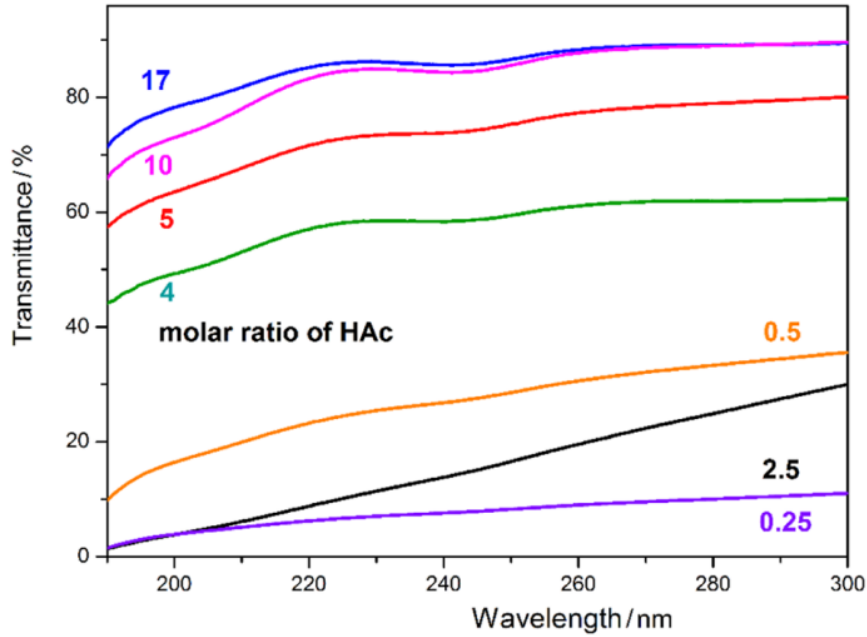


**Figure 17.** Transmittance of sol-gel derived layers prepared from Al acetate in the function of acetic acid (HAc).

The gel-like system obtained from aluminum acetate were subjected to treatment with different additives, such as citric acid and boehmite powders. Citric acid played a role in coordinating with aluminum ions, aiding in the formation of a continuous layer. The presence of boehmite powders initiates first the formation boehmite then gamma  $\text{Al}_2\text{O}_3$  phases. In this system, citric acid could be applied up to a maximum molar ratio of 1.0. Ratios exceeding 1.0 resulted in the formation of inhomogeneous layers. (Fig. 18) illustrates the impact of different acids, along with their optimal ratios, and additives on the transmittance. The layer created using aluminum acetate in the presence of boehmite demonstrated the highest transmittance value. The mass ratio between aluminum acetate and boehmite was 1:1.

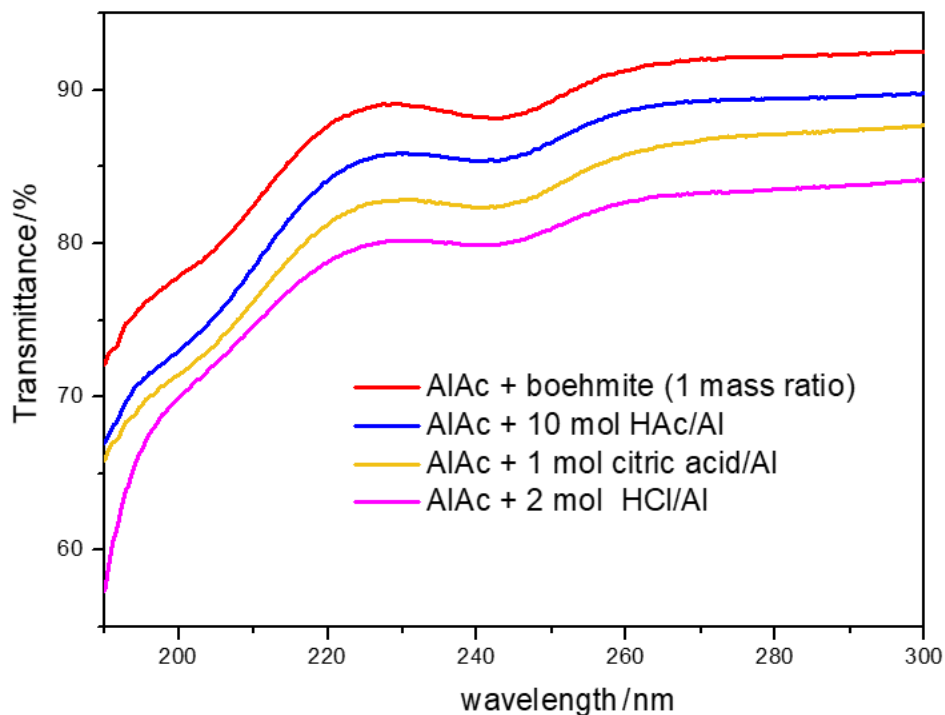


**Figure 18.** Transmittance of sol-gel derived layers prepared from Al acetate (AlAc) with various additives.

The utilization of both acids and boehmite results in the formation of gamma  $\text{Al}_2\text{O}_3$  layers upon heat treatment at 600 °C, as depicted in (Fig. 19). The analysis of GIXRD spectra was conducted using reference cards from JCPDS, namely JCPDS 29-0063 for gamma  $\text{Al}_2\text{O}_3$ , JCPDS 46-1215 for delta  $\text{Al}_2\text{O}_3$ , and JCPDS 21-1307 for pseudo-boehmite.

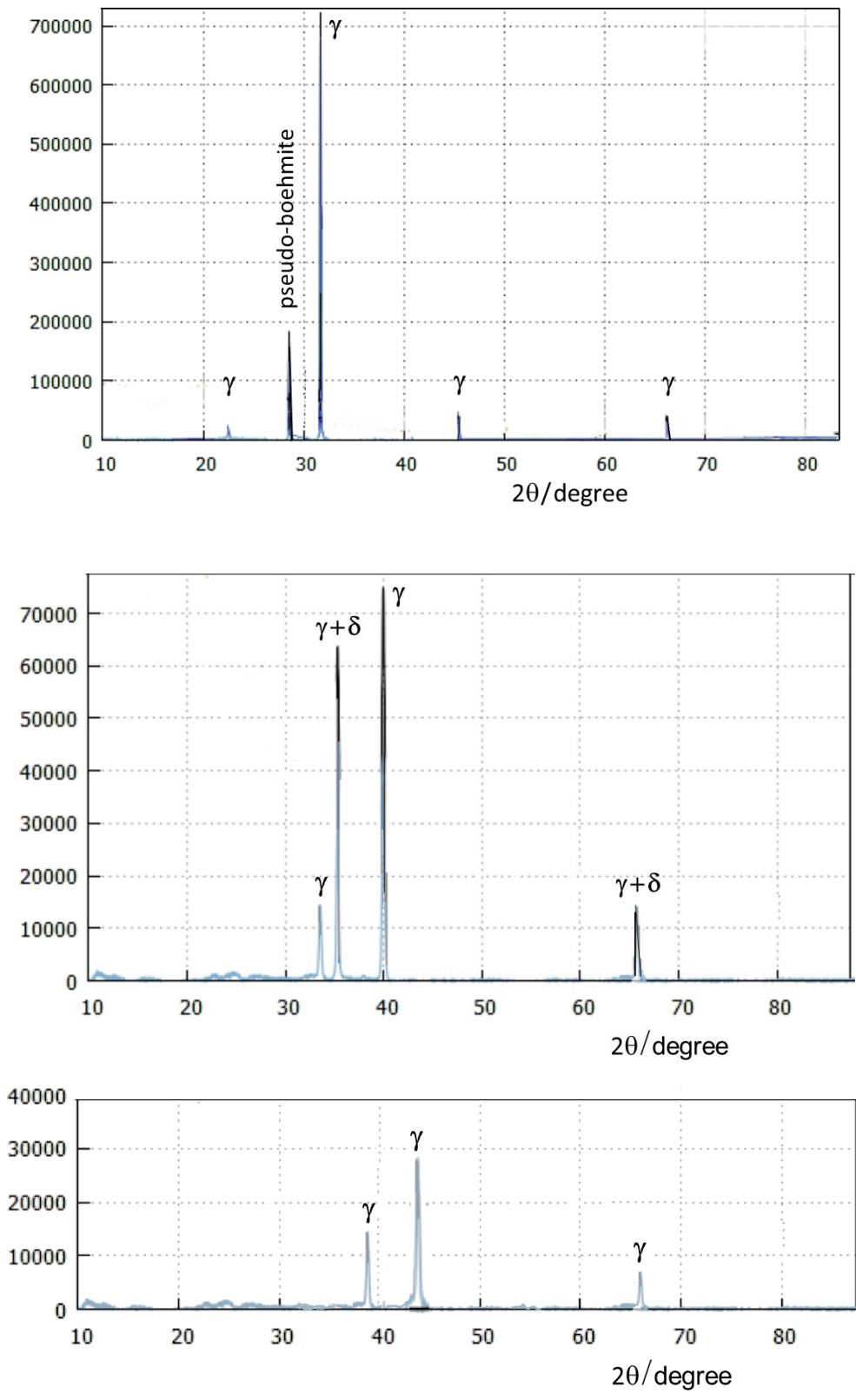


**Figure 19.** XRD spectrum of sol-gel derived  $\text{Al}_2\text{O}_3$  layers prepared from Al acetate with HCl (upper), HAc (middle), and boehmite (lower)

Regarding the SEM images of the layers generated from aluminum acetate in the presence of HCl, HAc, and boehmite, each layer exhibits a continuous and crack-free coverage of the quartz surface (Fig. 20-22). The thinnest layer, measuring 50-60 nm in thickness, is achieved by combining aluminum acetate and boehmite (Fig. 22). The surface of this layer closely resembles that of the layer derived from the sole precursor, boehmite.

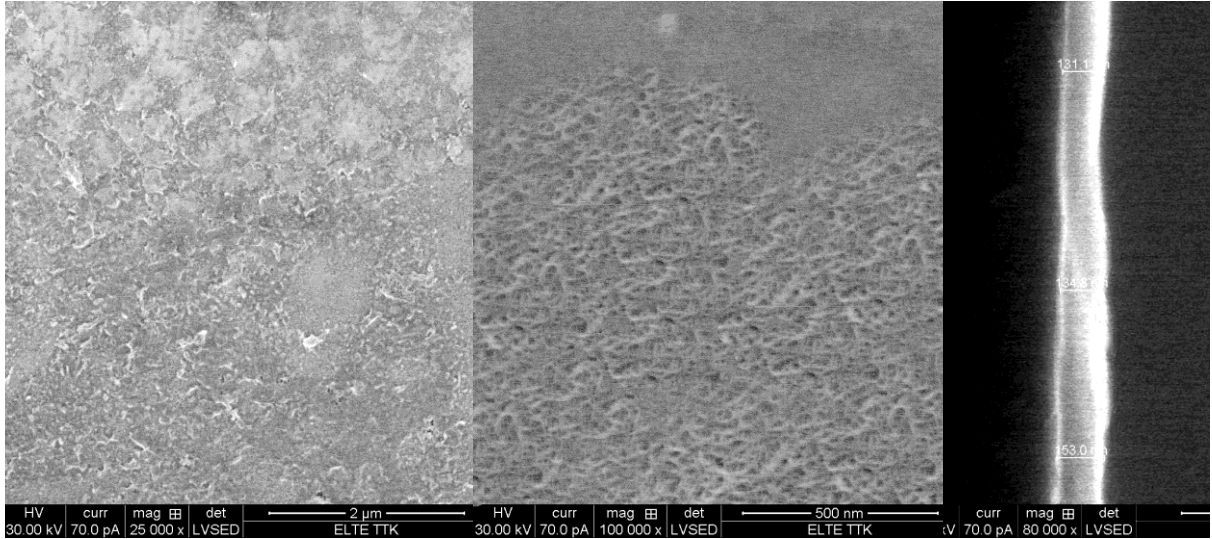


**Figure 20.** SEM of sol-gel derived layers prepared from Al acetate (AlAc) with HCl.

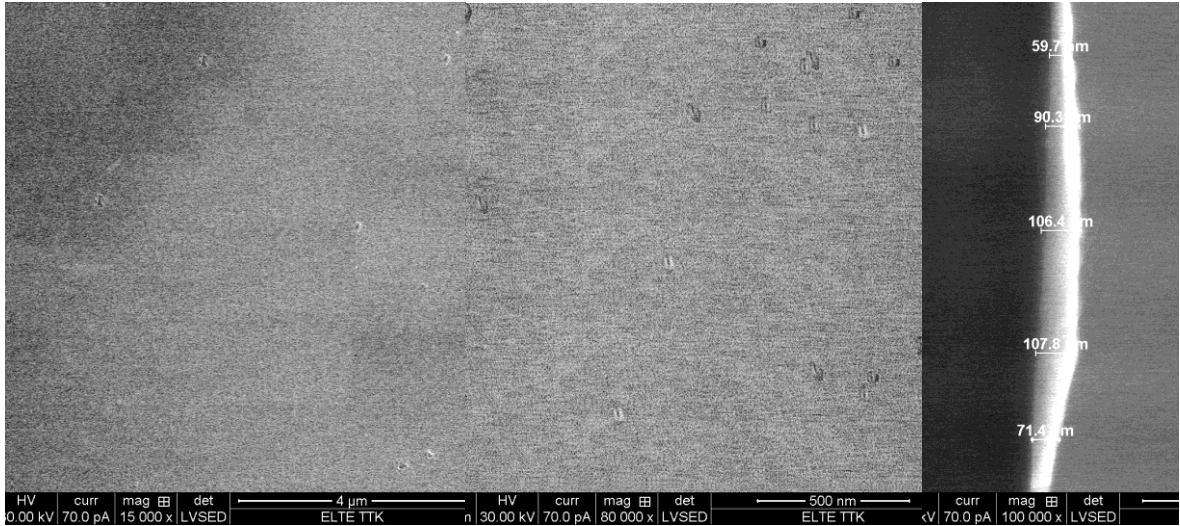


**Figure 21.** SEM of sol-gel derived layers prepared from Al acetate (AlAc) with HAc.

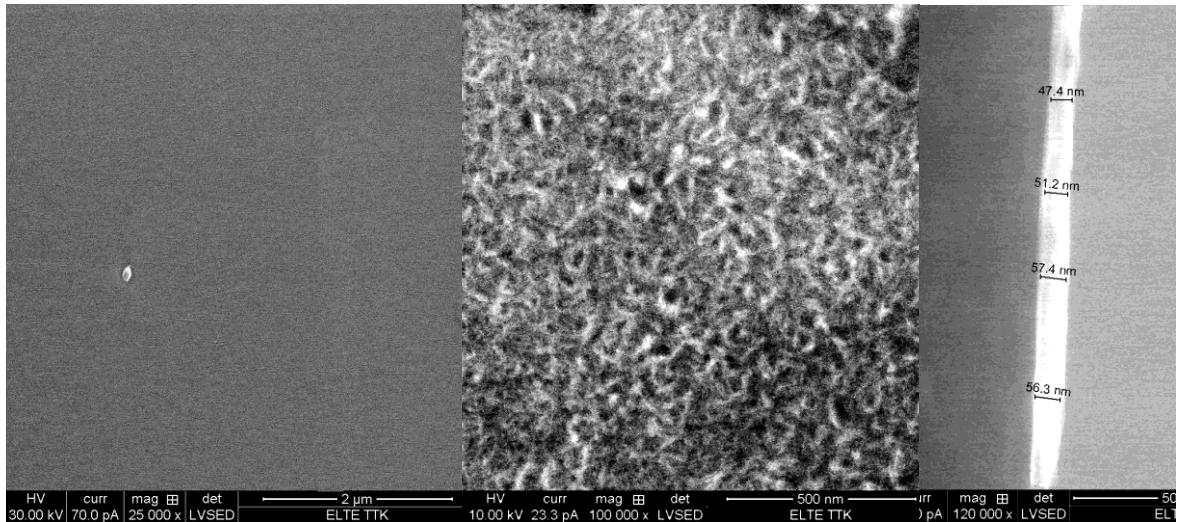


**Figure 22.** SEM of sol-gel derived layers prepared from Al acetate (AlAc) with boehmite. Magnification: 25 000x; 100 000x, 120 000x. Layer thickness is 50-60 nm.

#### IV.1.3. Layer by sol-gel method starting from Al nitrate

By employing Al nitrate as the precursor, the highest-quality layer can be obtained when using a water-to-dried gel mass ratio of 20. Diluting the mixture further does not result in the production of continuous coatings. The Al nitrate layer exhibits exceptional transmittance, as illustrated in (Fig. 23).

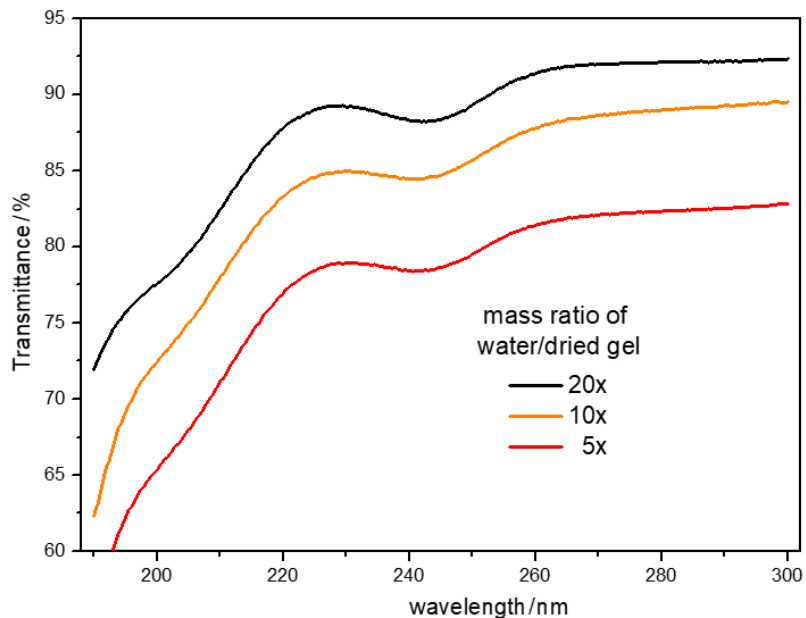


**Figure 23.** Transmittance of sol-gel derived layers prepared from Al nitrate.

The layer exhibits a smooth surface and crack-free surface, as depicted in (Fig. 24). With a thickness ranging from 55 to 65 nm, it qualifies as a nanofilm. Following the heat treatment at 600 °C, a slightly disordered  $\gamma$ -Al<sub>2</sub>O<sub>3</sub> phase emerges. However, the GIXRD diagram shown in (Fig. 25) reveals the absence of the 100 peaks of  $\gamma$ -Al<sub>2</sub>O<sub>3</sub> at 67°. The use of Al nitrate precursor presents a single drawback, namely the release of nitrous gases during both the gelation process and heat treatment.

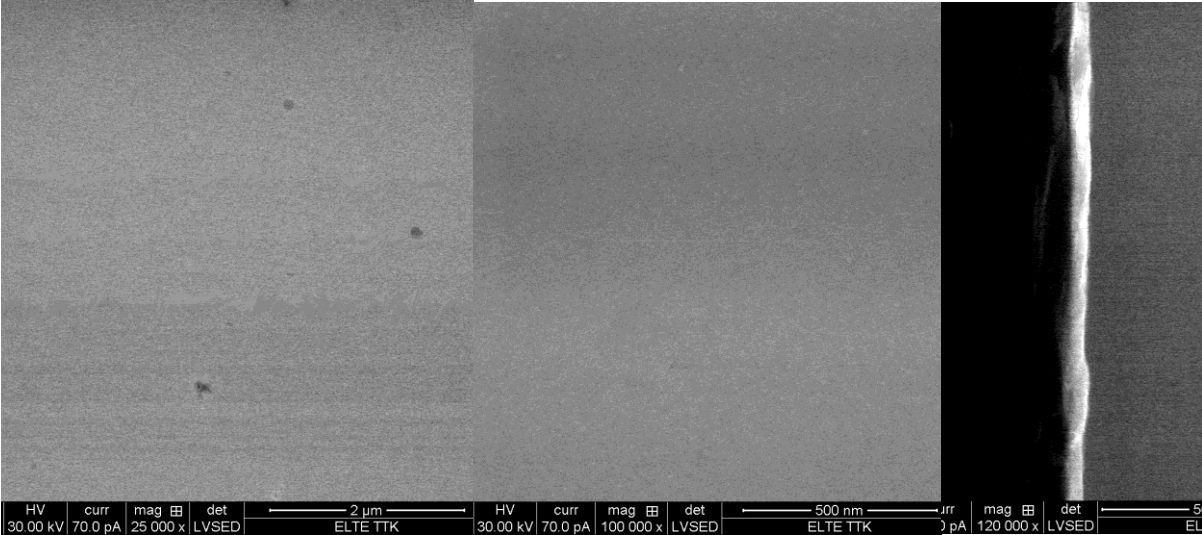


**Figure 24.** SEM of sol-gel derived layers prepared from Al nitrate.

Magnification: 25 000x; 100 000x, 120 000x. The layer thickness is 55-65 nm.

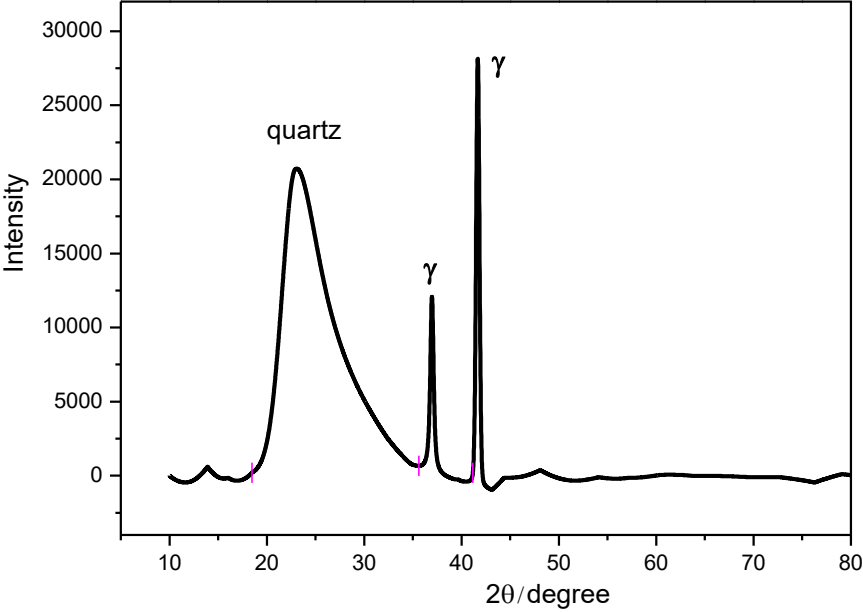


**Figure 25.** GIXRD spectrum of sol-gel derived Al<sub>2</sub>O<sub>3</sub> layers prepared from Al nitrate.

#### IV.1.4. Layer by sol-gel method starting from Al isopropoxide

The application of Al isopropoxide (AliPr) in experiments does not yield layers of optimal quality. However, employing the Yoldas synthesis method produces layers with respectable quality, featuring a thickness of 75-85 nm and sufficient transmittance. Based on these results, attempts were made to develop a new approach starting with Al isopropoxide. However, the layer quality achieved through our method was deemed insufficient when compared to layers obtained through other methods (Fig. 26, 27). Considering the quality of the layers and the cost of AliPr, the application of AliPr was dismissed.

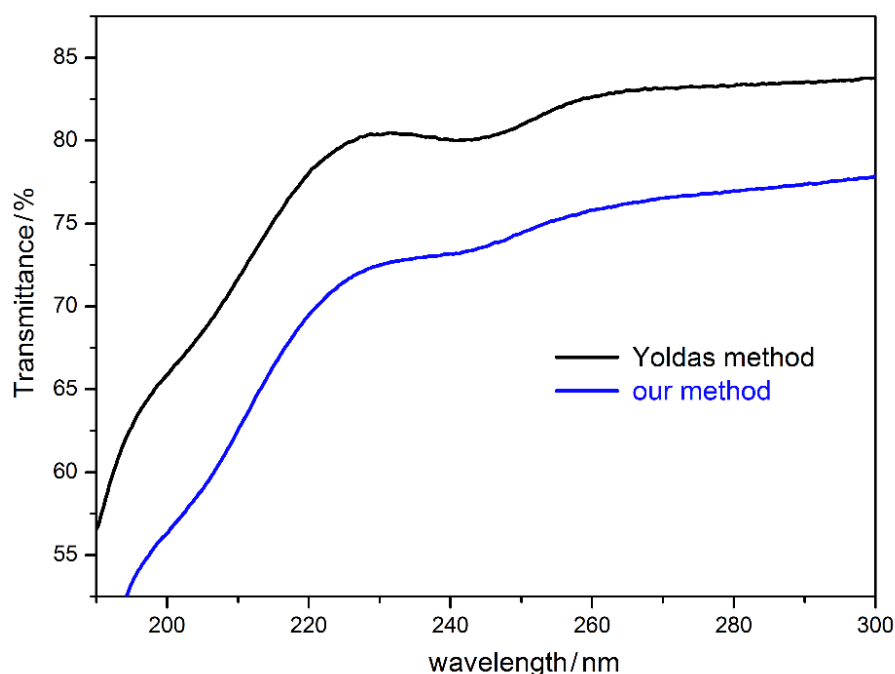


**Figure 26.** Transmittance of sol-gel derived layers prepared by Yoldas and our methods from Al isopropoxide.

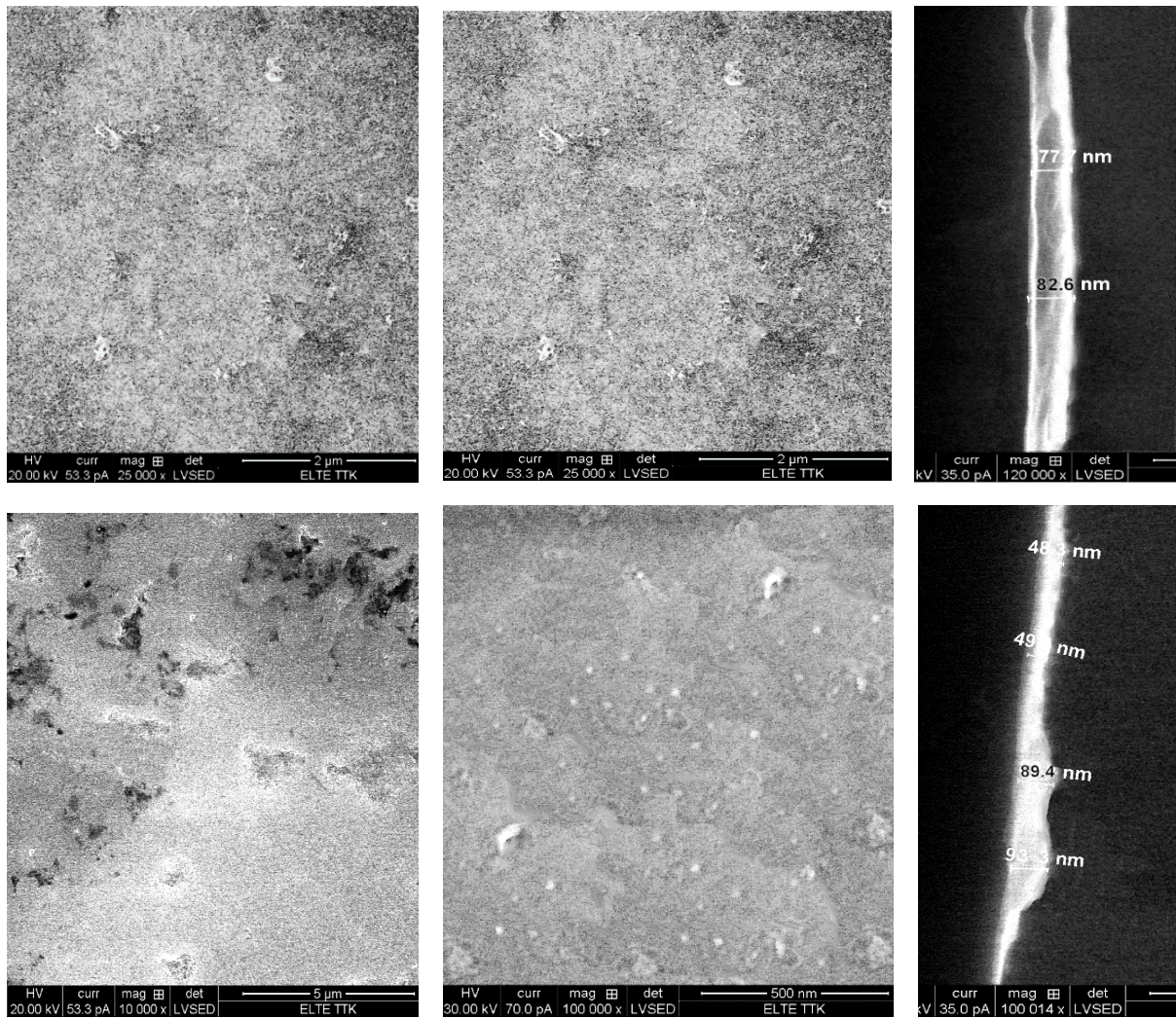


**Figure 27.** SEM images. The upper layers were prepared by the Yoldas method from Al isopropoxide. Lower layers were produced by our sol-gel technique from Al isopropoxide. Magnification upper: 25 000x; 100 000x, 120 000x; lower: 10 000x, 100 000x, 100 000x.

## IV.2. Comparison of Al<sub>2</sub>O<sub>3</sub> layers prepared by various synthesis routes

The following table and figure are provided to facilitate the comparison of aluminum oxide layers based on specific layer parameters (Table 2 and Fig. 28). Among the sol-gel syntheses conducted, two methods yield the highest quality layers: one starting from Al acetate with the addition of boehmite and HAc, and the other starting from Al nitrate (Table 2 and Fig. 28). These layers exhibit a long-lasting protective nature, as they were monitored over a 500-hour period of application.

**Table 2.** Comparison of Al<sub>2</sub>O<sub>3</sub> layers prepared by various synthesis routes.

Synthesis ( (precursor + additive)	Transmittance at 254 nm (%)	Layer thickness (nm)	Quality of layer
Boehmite (0.5 mr HAc)	90.1	110-120	good
Al <sub>2</sub> O <sub>3</sub>	67.7	135-145	moderate
AlAc (NaOH + 10 mr HAc)	86.6	60-105	good
AlAc (NaOH + 2 mr HCl)	81.8	130-150	moderate
AlAc (NaOH + boehmite + HAc)	90.3	50-60	excellent
Al nitrate (20x water)	90.3	55-65	excellent
AliPr (our synthesis)	75.1	45-100	moderate
AliPr (Yoldas synthesis) [27]	81.8	75-85	excellent
German commercial product	85.3	130-170	excellent
Japanese commercial product	72.9	–	good

AlAc: basic Al acetate, HAc: acetic acid, mr: molar ratio to Al, x: mass ratio of water to dried gel, AliPr: Al isopropoxide.

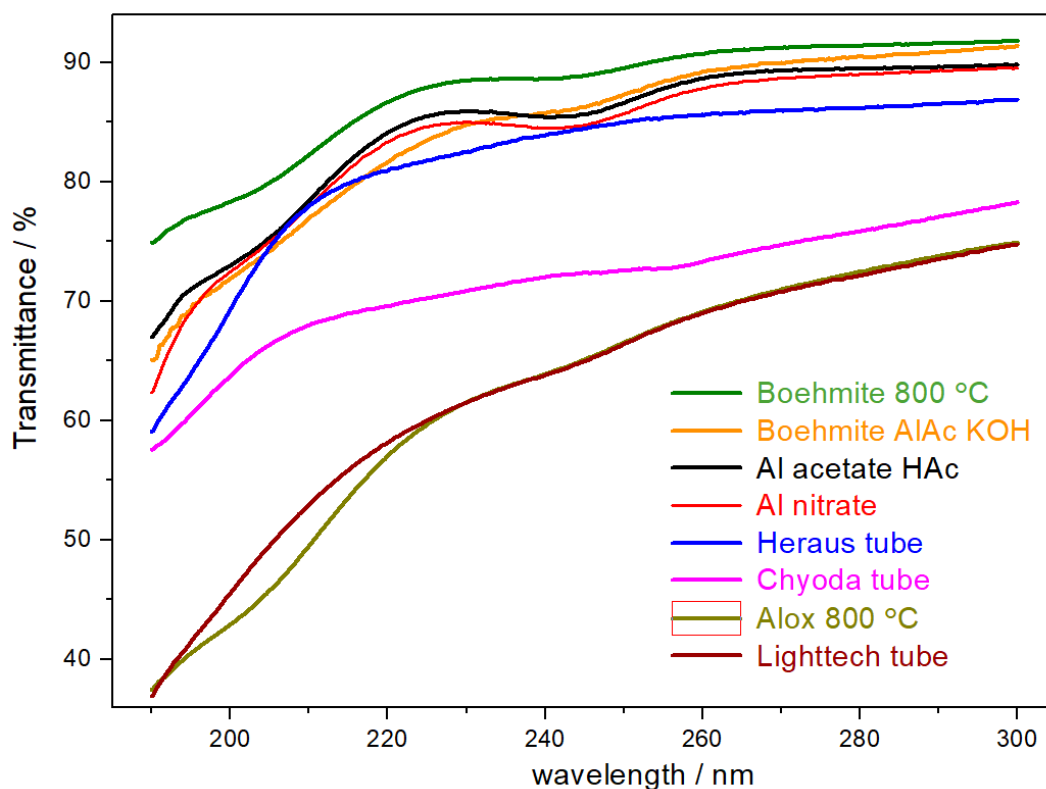


**Figure 28.** Comparison of the transmittance of  $\gamma$ -Al<sub>2</sub>O<sub>3</sub> layers prepared by various techniques with commercial products (Heraus, Chyoda, and Lighttech).

Al acetate is the best initial material due to its environmentally friendly decomposition and the acetate ions support and stabilize the formation of continuous layers by connecting two Al ions as a bidentate ligand. Acetic acid and boehmite powders as additives proved to be most efficient for the improvement of layer quality. Acetic acid is capable partly dissolve boehmite powders and boehmite initializes the development of gamma-aluminum oxide ( $\gamma$ -Al<sub>2</sub>O<sub>3</sub>) phase.

In the comparison between colloidal suspensions (sol or slurry) and gel-like systems for layer formation, the gel-like systems have demonstrated greater suitability. The three-dimensional network developed by gel systems derived from gel-like precursors ensures the creation of continuous films and enables precise regulation of layer thickness. Conversely, suspensions, particularly slurries, are commonly used as precursor systems for coating applications. However, they often yield thicker layers that may not provide optimal surface coverage due to the presence of larger particles.

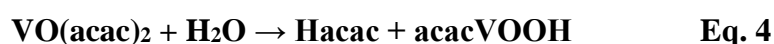
### IV.3. Synthesis of Vanadium Oxide Thin films

#### IV.3.1. Effect of vanadium precursors

The choice of vanadium-containing materials has a significant impact on the structure of the resulting layers. When using  $\text{NH}_4\text{VO}_3$  as the starting material, it is crucial to achieve a pH of approximately 2 in the initial solution to form  $\text{H}_3\text{VO}_4$  molecules. Only  $\text{H}_3\text{VO}_4$  molecules can realize condensation reactions and form a three-dimensional network. The presence of the  $\text{VO}^{3-}$  anion hinders condensation and leads to the formation of polyvanadate. In these experiments, only vanadium(V)-containing materials were prepared. The optimal concentration for the dipping process is a 35% weight-to-weight ratio of metavanadate solution. The quality of the layers is strongly influenced by the degree of acidification.

##### IV.3.1.1. Vanadyl (IV) acetylacetonate precursor

The aim of the application of vanadyl (IV) acetylacetonate ( $\text{VO}(\text{acac})_2$ ) was to prepare a  $\text{V}^{\text{IV}}$ -containing layer.  $\text{V}^{\text{IV}}$ -content is needed for more intensive electrical properties [113].  $\text{VO}_2$  was proved to have better electrochemical performance compared with  $\text{V}_2\text{O}_5$  [114].  $\text{VO}(\text{acac})_2$  has several advantages compared to vanadium alkoxides as typical sol-gel precursors.  $\text{VO}(\text{acac})_2$  can be characterized by its low price, low toxicity, highly stable against precipitation, and rapid hydrolysis. From  $\text{VO}(\text{acac})_2$  an ester forms by elimination of a  $\text{C}_3\text{H}_4$  group, which transforms into anhydride in the first step, then into  $\text{VO}_2$  by further heat treatment [115].



The synthesis and heat treatment must be performed in a  $\text{N}_2$  atmosphere to produce  $\text{VO}_2$  film. The precursor films can turn into crystalline  $\text{VO}_2$  by heat treatment. The final heat treatment needs 500-600 °C for efficient (monoclinic or orthorhombic) crystallization of  $\text{VO}_2$ . The layer dipped from the viscous solution of  $\text{VO}(\text{acac})_2$  and dried in the air is not homogeneous, 1-2  $\mu\text{m}$  NaCl phase separation can be observed by SEM and EDX techniques (Fig. 29).

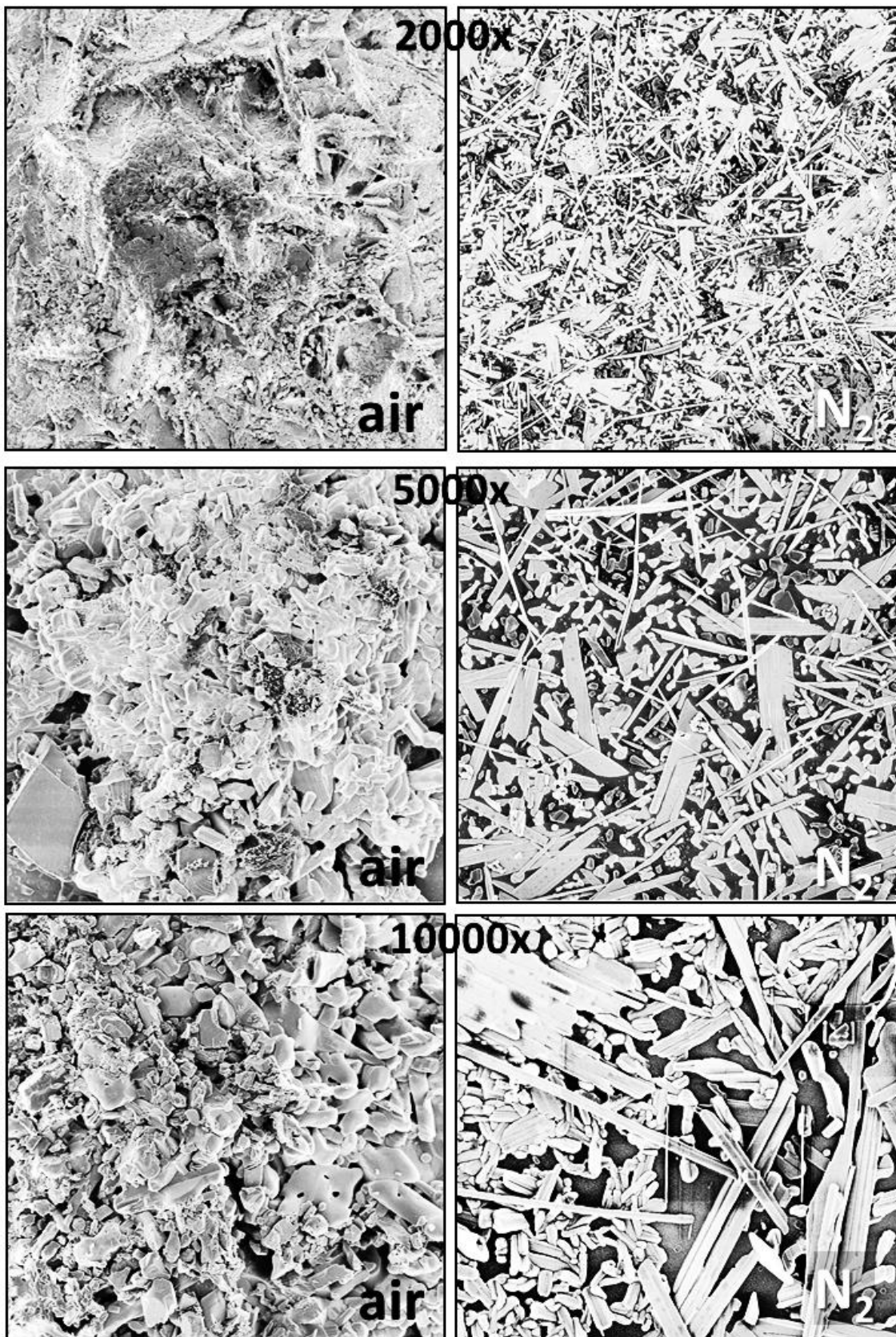


**Figure 29.** SEM images of samples prepared from VO (acac)<sub>2</sub> and heated in air and N<sub>2</sub> atmosphere.

The diagram in (Fig. 30) shows the different crystalline structures of the layers created using VO (acac)<sub>2</sub>, which were subjected to heating either in a nitrogen atmosphere or in the air at a temperature of 500 °C.

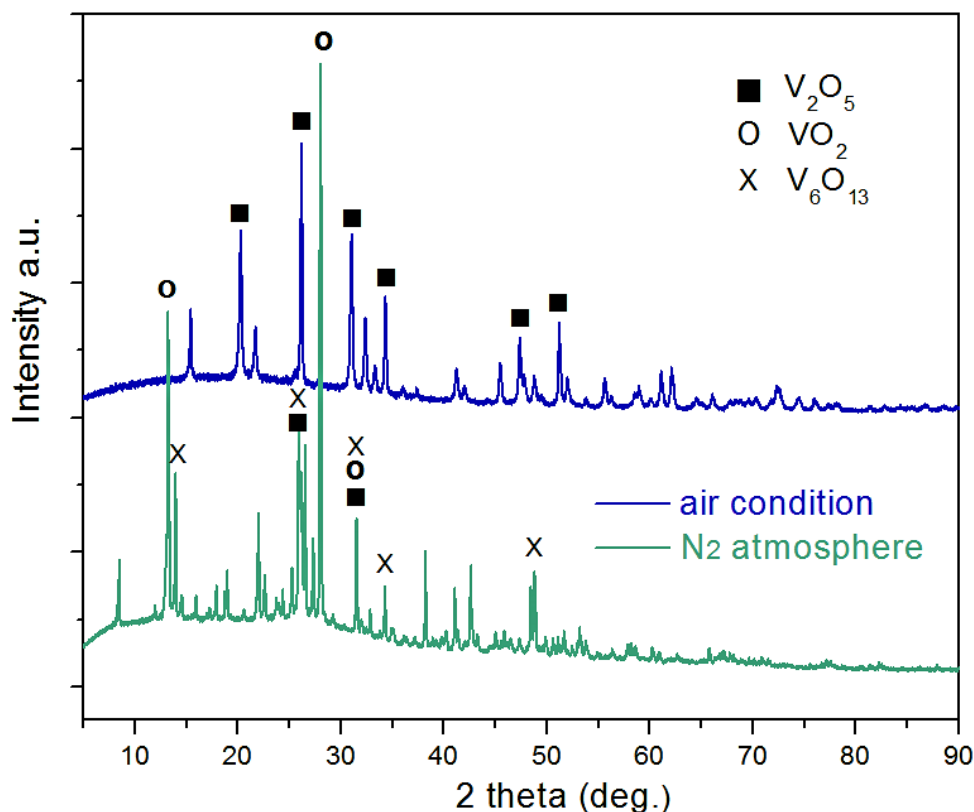


**Figure 30.** XRD patterns of vanadium oxide thin films prepared from VO (acac)<sub>2</sub> and heated in air and N<sub>2</sub> atmosphere.

The XRD analysis confirms that the vanadate sample, which was heated at 500 °C in the air, consists solely of the V<sub>2</sub>O<sub>5</sub> crystalline phase with specific characteristics such as a peak at 26° and 110 planes. This identification was made using card #98-002-2114. On the other hand, the sample heated at 500 °C in a nitrogen atmosphere exhibits multiple crystalline structures, as depicted in (Fig. 30).

The main crystalline phase is VO<sub>2</sub>, with characteristic peaks at 28° and 13.3°, as identified by JCPDS card #65-7960. This dominance of VO<sub>2</sub> is attributed to the use of an N<sub>2</sub> atmosphere during the heating process. VO<sub>2</sub> coexists with the V<sub>6</sub>O<sub>13</sub> monoclinic crystalline phase, which appears at 13.97°, 26°, 26.5°, 34°, and 48.7°, as identified by JCPDS card #71-2235. V<sub>6</sub>O<sub>13</sub> consists of a combination of V<sup>4+</sup> and V<sup>5+</sup> vanadium states. The tunnel-like V<sub>6</sub>O<sub>13</sub> comprises alternative single and double vanadium oxide layers with shared corners.

It is possible that a small amount of a single  $V_2O_5$  phase (peaks at  $26^\circ$  and  $31.4^\circ$ ) is also present, although its presence cannot be definitively confirmed. Both  $VO_2$  and  $V_6O_{13}$  can be effectively utilized as cathode materials.

The  $^{51}V$  NMR measurements were not feasible for the systems synthesized from  $VO(acac)_2$  due to significant challenges arising from chemical shift anisotropy, paramagnetic electrons of  $V^{IV}$ , and quadrupole interaction with asymmetric electron environments. The presence of paramagnetic electrons leads to the wide overlapping of rotation sidebands, making it impossible to accurately evaluate the NMR spectra. The spectra do not confirm any presence of  $V^V$  neither in precursor materials nor in the final layer materials heated in  $N_2$ .

#### *IV.3.1.2. Vanadium dioxide ( $VO_2$ ) precursor*

The objective of the experiments with  $VO_2$  dispersed in ethanol and oxalic acid was to examine the chemical and structural modifications of  $VO_2$  based on varying heating temperatures. Even in an air environment, oxalic acid potentially exhibits a reducing effect [116]. The changes in the chemical structure were examined using  $^{51}V$  NMR. Determining the oxidation state of vanadium in solid materials is a complex task, even with the use of NMR spectroscopy.

The NMR signals corresponding to vanadium ions with different oxidation states can appear widely separated from each other in the spectrum. In solutions, it is possible to effectively detect the vanadium ion with a nuclear spin of  $7/2$ , a natural abundance of 99.75%, and an oxidation state of +5 using NMR techniques. However, in solid phases, identifying the vanadium species becomes more difficult. The spectrum exhibits a broad range of approximately 4000 ppm, a quadrupole coupling of a few MHz, an anisotropic shading of 1000 ppm, a line broadening of 5000 Hz due to the quadrupole relaxation, strong baseline deformation, and many spinning sidebands make the evaluation of spectra more complicated.

At room temperature, the stable monoclinic  $\beta$ - $VO_2$  transforms into rutile  $\alpha$ - $VO_2$  at  $68^\circ C$ , which reverts to  $\beta$ - $VO_2$  when returning to room temperature. As a result, this phase transition cannot be detected by NMR at room temperature. The oxidation of  $VO_2$  begins in the air even at  $200^\circ C$ , as shown in (Fig. 31). The presence of the  $V_2O_5$  phase can be unambiguously observed in the sample treated at  $200^\circ C$ . The oxidation becomes more significant at  $350^\circ C$  and is completed by  $500^\circ C$ , at which point the  $VO_2$  phase disappears (Fig. 31). Based on these NMR findings, it is evident that a mixed oxidation state involving  $V^{IV}$  and  $V^V$  can only be achieved in the air between  $100$  and  $200^\circ C$ . The electrical properties of vanadate systems can be

effectively regulated by the vanadium's charge in the structural units, and the ratio of  $V^{IV}$  and  $V^V$  plays a crucial role in determining their electric properties [113].

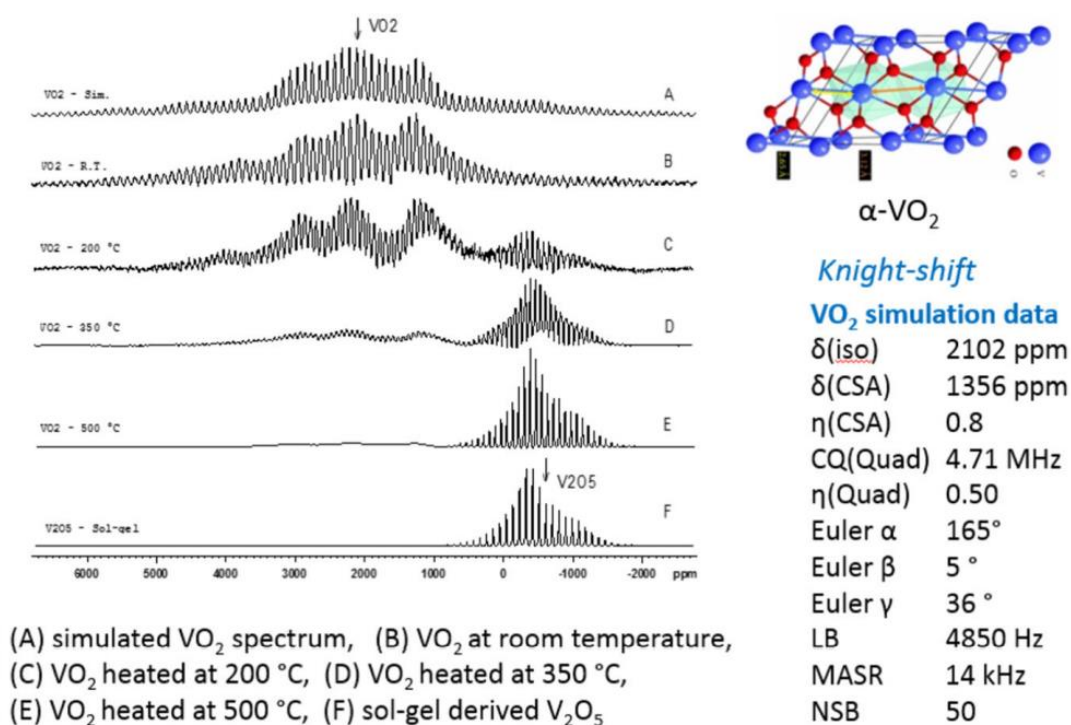


**Figure 31.**  $^{51}\text{V}$  NMR spectra of VO<sub>2</sub> in the function of temperature.

The layer surface obtained from the VO<sub>2</sub> sol solution, as depicted in (Fig. 32), displays a non-uniform texture, and lacks a smooth surface. It contains a mixture of small and larger particles, attributed to the characteristics of the sol system. Analysis using energy-dispersive X-ray spectroscopy (EDX) confirms that each particle is composed of vanadium and oxygen elements.

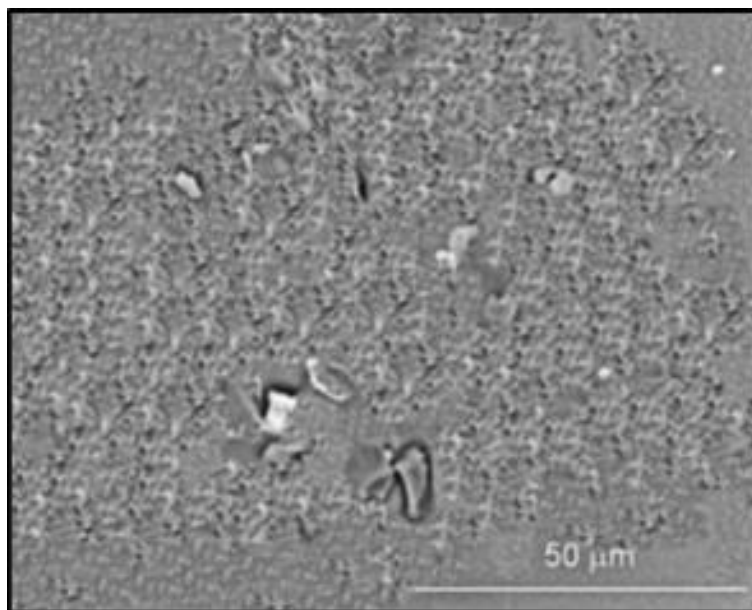


**Figure 32.** SEM images of vanadate layers prepared from VO<sub>2</sub> sol solution.

#### *IV.3.1.3. Ammonium decavanadate (NH<sub>4</sub>)<sub>6</sub>[V<sub>10</sub>O<sub>28</sub>] precursor*

The orange colour ammonium decavanadate (NH<sub>4</sub>)<sub>6</sub>[V<sub>10</sub>O<sub>28</sub>] that contains 10 vanadium atoms is a stable species for several days at neutral pH, but at higher pH immediately converts to the structurally and functionally distinct lower oxo-vanadate such as the monomer, dimer, or tetramer. The most stable form of V<sub>10</sub> is in the acidic pH range (pH 3 to 6). Decavanadate anions consist of three chemically different vanadium sites; the metal sites at the central junction correspond to two central VO<sub>6</sub> octahedra containing only bridging oxygen atoms, and two types of peripheral vanadium units including a V=O bond are assembled around the central units [117].

Although the precursor solution of ammonium decavanadate covers excellently the surface of the glass substrate, the layer will be fragmented after a drying process. Various rates, temperatures, and atmospheres of drying were checked out but without success. The material of the substrate was changed from glass to carbon, which results in layers with low quality already in the wet state.

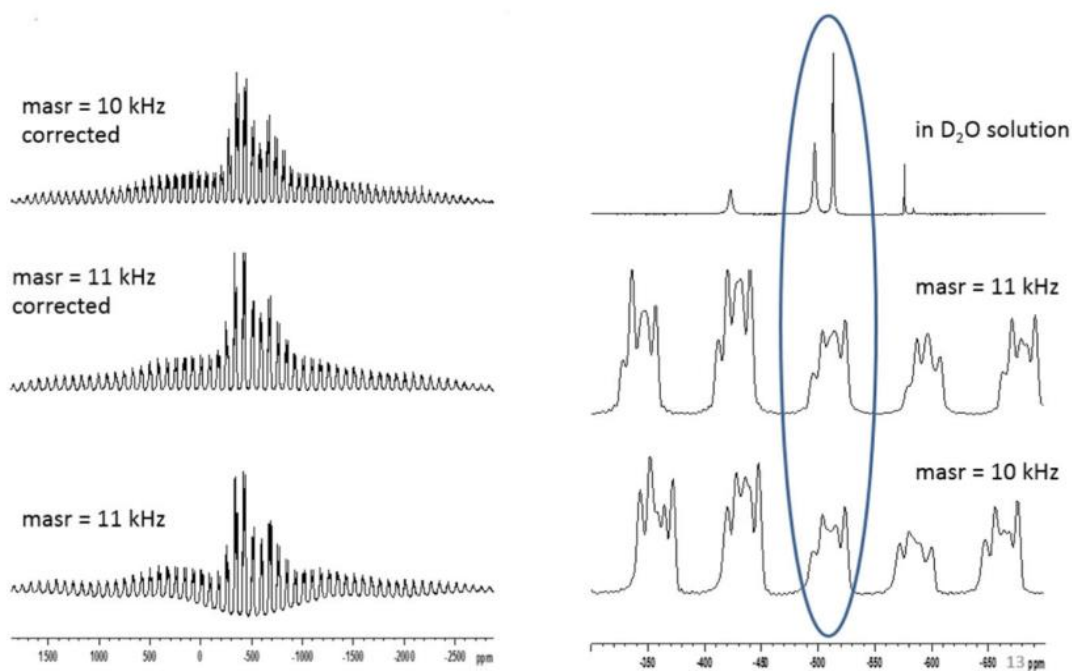


**Figure 33.**  $^{51}\text{V}$  NMR spectra of  $(\text{NH}_4)_6[\text{V}_{10}\text{O}_{28}]$ .

The  $^{51}\text{V}$  NMR spectrum demonstrates dozens of sidebands in the wide frequency range of 1800 ppm to -2800 ppm (Fig. 33). The strong chemical shift anisotropy (CSA) and quadrupole couplings were determined for these sites by computer simulation. Three kind of decavanadate sites were identified at -418 ppm ( $\delta\text{CSA}=-1192$  ppm,  $\eta\text{CSA}=0.92$ ,  $C_Q=-2.06$  MHz,  $\eta_Q=0.99$ ), -504 ppm ( $\delta\text{CSA}=-2151$  ppm,  $\eta\text{CSA}=0.94$ ,  $C_Q=-3.99$  MHz,  $\eta_Q=0.6$ ) and -514 ppm ( $\delta\text{CSA}=-373$  ppm,  $\eta\text{CSA}=0.44$ ,  $C_Q=-0.01$  MHz,  $\eta_Q=0.19$ ) according to the cluster structure of the anion [118].

### IV.3.2. Effect of acidic catalysts and chemical additives

Starting from  $\text{NH}_4\text{VO}_3$ , the compulsory step of synthesis is to create  $\text{pH} = 2$  in the initial solution. The  $\text{pH}$  value can be regulated by acids or cation exchanged.

From the various acids used for setting  $\text{pH} = 2$ , the application of nitric acid ( $\text{HNO}_3$ ) results in complete and transparent layers (Fig. 34). A 3D colloid network is formed by employing nitric acid catalyst, consisting of compact particles sized between  $0.6\text{-}0.8\ \mu\text{m}$  that are connected in a random manner. This network forms a continuous, porous, and see-through coating as depicted in (Fig. 34).

$\text{HCl}$  and citric acid do not produce uniform layers (as shown in Fig. 34). The layer created with citric acid is incomplete and consists of fibers and filaments. In addition to the filaments, there are also some tiny fragments at the nanoscale. The fibers typically have a length of  $4\text{-}5\ \mu\text{m}$  (as seen in Fig. 34).

Ascorbic acid also fails to produce continuous and homogeneous layers or reduce  $\text{V}^{\text{V}}$  units. EDAX measurements indicate that both types of particles have a significant amount of vanadium ( $\text{V}$ ) content without any carbon content. Therefore, it is possible that the larger spherical particles ( $5\ \mu\text{m}$ ) are amorphous, while the smaller units ( $1\text{-}10\ \text{nm}$ ) are crystalline in nature (refer to Fig. 34).

Oxalic and ascorbic acids are not strong enough to achieve a  $\text{pH}$  of 2, but they may still have a mild reducing effect [110–112]. This reduction process could potentially result in the formation of  $\text{V}^{\text{IV}}$  ions. However, in this study, no measurable reduction was observed using NMR; only  $\text{V}^{\text{V}}$  ions were detectable. Acidification through proton exchange increases the coordination of  $\text{V}^{\text{V}}$  from 5 to 6, as exemplified by the hexacoordinated species  $[\text{VO}(\text{OH})_3(\text{OH}_2)_2]$ . When oxalic acid is used, it does not produce a uniform coating. The particles, sized between  $2\text{-}3\ \mu\text{m}$ , form a dense layer on a limited surface area. The remaining part of the substrate surface is covered by individual particles measuring  $100\text{-}200\ \text{nm}$  in size (refer to Fig. 34).

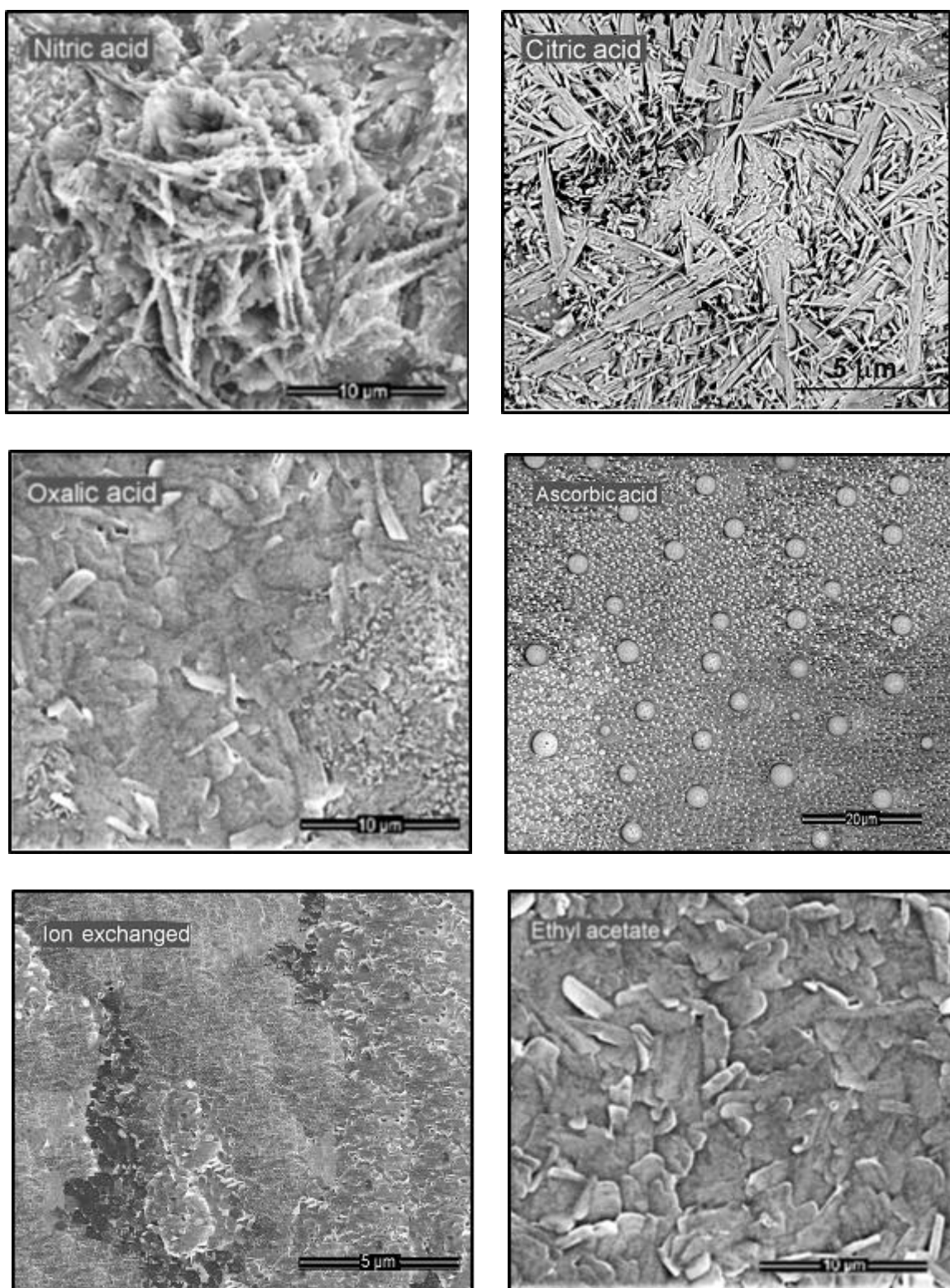


**Figure 34.** SEM images of vanadate layers prepared from  $\text{NH}_4\text{VO}_3$  with various additives: nitric acid, citric acid, oxalic acid, ascorbic acid, ethyl acetate, and after ion exchange.

The use of ethyl acetate also aids in the creation of a solid, unbroken coating. Most of the particles possess cylindrical shape with a diameter of approximately 500 nm and a length of around 3  $\mu\text{m}$ . Additionally, there are some plate-like particles with a diameter of 2-3  $\mu\text{m}$  that can be observed. These particles exhibit a narrow size distribution, as shown in (Fig. 34).

The coating obtained from an ion-exchanged solution is not seamless. It consists of individual units measuring 100-300 nm in size, as well as aggregates of these units' forming structures of 4-6  $\mu\text{m}$ . This layer arrangement is illustrated in (Fig. 34).

#### IV.3.2.1. FTIR spectroscopy

FTIR spectroscopy helps to analyse the phase composition of thin films of vanadium oxide (as shown in Fig. 35). The oxides exhibit distinctive characteristics at frequencies below  $1200\text{ cm}^{-1}$ , specifically around  $1008$ ,  $806$ , and  $595\text{ cm}^{-1}$ . These frequencies correspond to three main vibration modes of vanadium oxide, namely the symmetric stretching vibration of  $\text{V}=\text{O}$ , the asymmetric stretch of  $\text{V}-\text{O}-\text{V}$ , and the symmetric stretch of  $\text{V}-\text{O}-\text{V}$ , respectively. The intensity and frequency of the  $\text{V}-\text{O}$  vibrational bands show slight variations within the range of  $400\text{-}1012\text{ cm}^{-1}$  due to the influence of different additives.

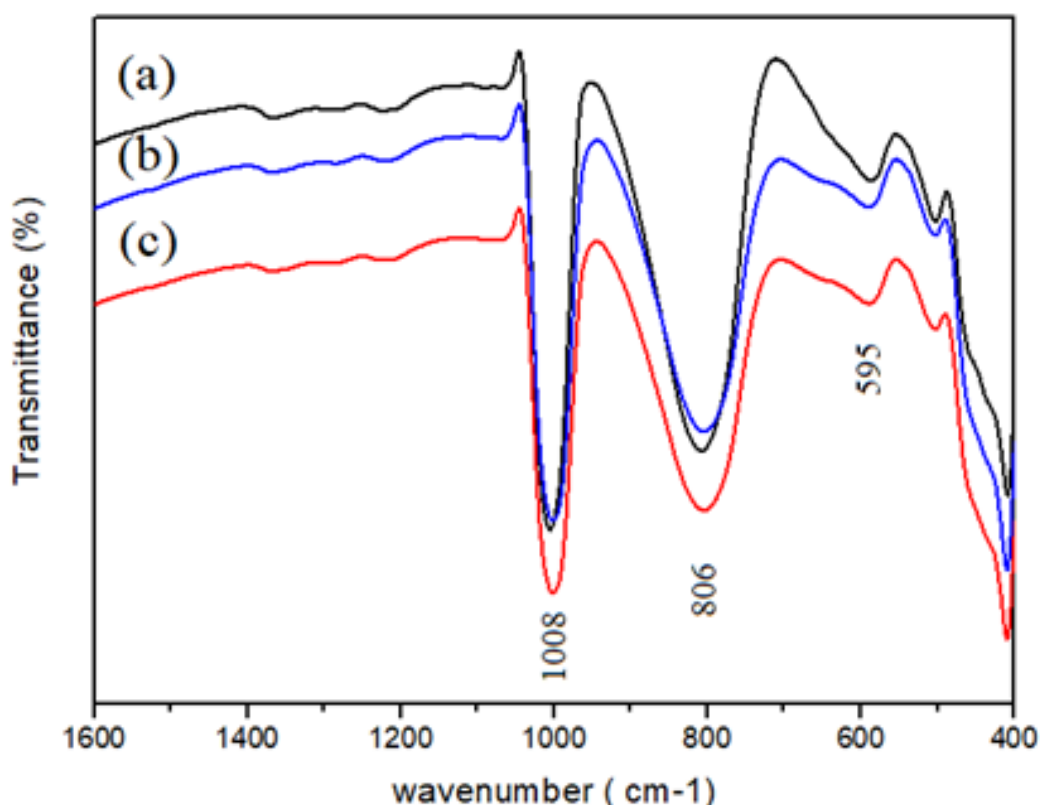


**Figure 35.** FTIR spectra of vanadium pentoxide thin films on glass substrates prepared with different chemical additives: (a) ethyl acetate; (b) nitric acid; (c) oxalic acid

#### IV.3.2.2. X-ray powder diffraction (XRD)

The XRD measurements were used to assess the level of crystallinity in the deposited vanadium pentoxide, which was prepared using three highly promising chemical additives (Fig. 36). Crystallization of the films occurred after subjecting them to annealing at  $400\text{ }^{\circ}\text{C}$  for 30 minutes in a muffle furnace. Despite using different chemical additives (nitric acid, ethyl acetate, oxalic acid), no noticeable changes in crystallinity were observed. The intensity of the (101) peak

decreased when the preparation involved (a) nitric acid, (b) ethyl acetate, or (c) oxalic acid, indicating an enhancement in film crystallinity. The entire thin films exhibited peaks at  $20.30^\circ$  and  $41.24^\circ$  ( $2\theta$ ) corresponding to the (001) and (002) orientations, respectively, confirming the presence of the  $V_2O_5$  phase in the orthorhombic system as identified in the JCPDS file (JCPDS card #41-1426). The XRD measurements did not detect any  $V^{IV}$  content in the sample synthesized with oxalic acid.

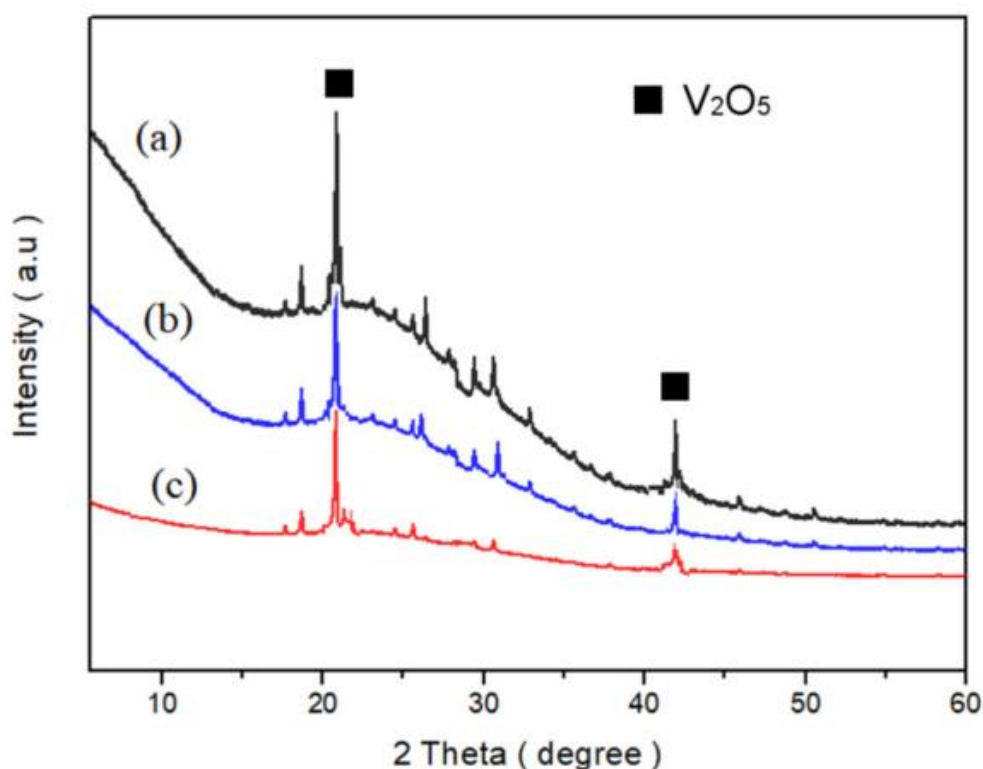


**Figure 36.** XRD patterns of vanadium oxide thin films on glass substrates prepared with three types of most promising chemical additives: (a) nitric acid; (b) ethyl acetate; (c) oxalic acid.

#### ***IV.3.2.3. Energy Dispersive X-ray Analysis (EDX)***

EDX technique provides information about the chemical composition of the thin layers (Fig. 37). The EDX spectra reveal the presence of vanadium (V) and oxygen (O) on the thin films. However, the presence of substrate peak is also prominent as the thickness of the film is so thin [122]. EDX analysis also verified that the film prepared with nitric acid (Fig. 37/a) exhibited complete coverage. This layer had the highest concentration of vanadium. If the primary reason for this was the greater thickness of the layer, then the oxygen content should also be higher.

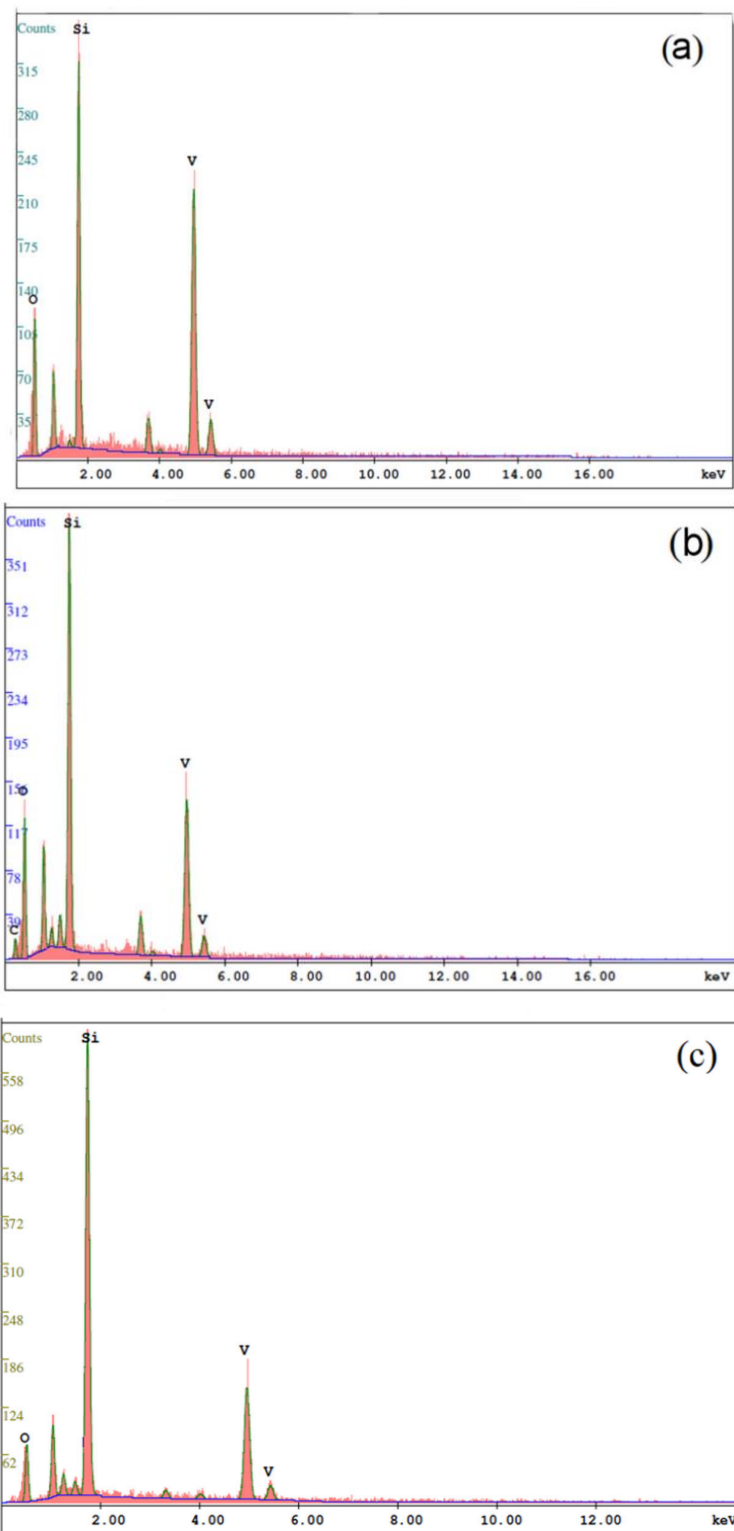


**Figure 37.** Energy Dispersive X-ray Analysis (EDX) of vanadium pentoxide thin films on glass substrates prepared with different solvents at 400 °C: (a) nitric acid; (b) ethyl acetate; (c) oxalic acid.

#### IV.3.2.4. Optical behaviours

(Fig. 38) illustrates the transmittance spectrum of vanadium pentoxide thin films prepared using different additives within the wavelength range of 250 to 1000 nm. In the range of 550 to 1000 nm, the transmittance of the films exceeded 70%, indicating their good uniformity. However, the transmittance decreased with the use of nitric acid (a), ethyl acetate (b), and oxalic acid (c). The maximum transmittance values for the films were as follows: nitric acid, 81.2%; ethyl acetate, 78.9%; and oxalic acid, 74.4%.

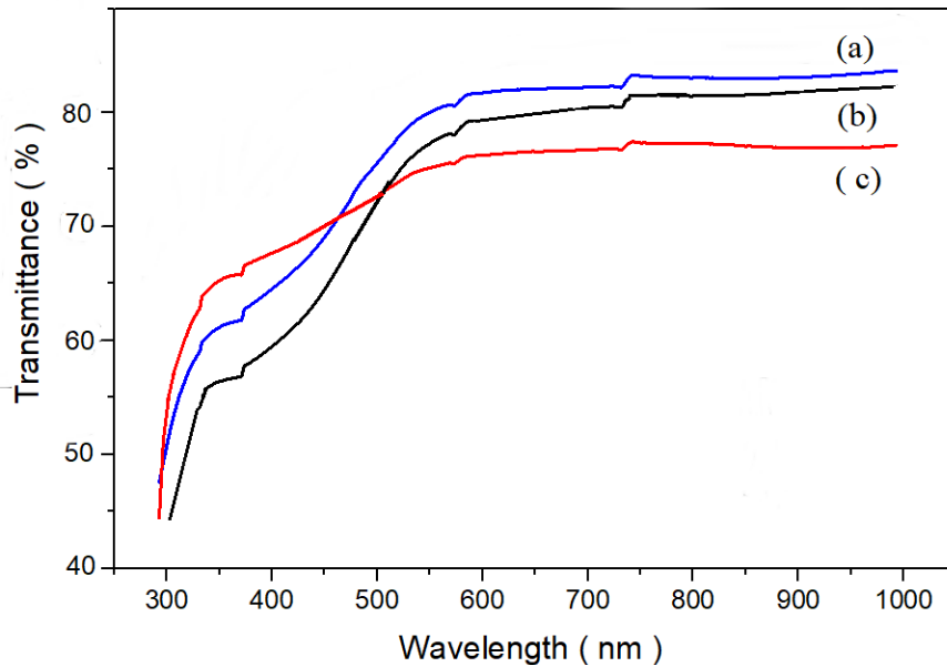


**Figure 38.** Transmittance spectra of vanadium pentoxide thin films on glass substrates prepared with different additives: (a) nitric acid; (b) ethyl acetate; (c) oxalic acid.

The Tauc plot was utilized to calculate the optical band gap ( $E_g$ ) of vanadium oxide thin films that were prepared using various additives:

$$(\alpha h\nu)^2 = A (h\nu - E_g) \quad \text{Eq. 6}$$

In the equation, where  $\alpha$  represents the absorption coefficient,  $A$  is a constant,  $h$  is the Planck constant, and  $E_g$  stands for the optical band gap (Fig. 39), the band gap ( $E_g$ ) can be estimated

by extrapolating the linear portion of the curves until they intersect the photon energy axis. The calculated band gap values for the thin films prepared with oxalic acid, nitric acid, and ethyl acetate are 1.98 eV, 2.11 eV, and 2.17 eV, respectively. It is worth noting that the variation in band gap energy is attributed to the non-stoichiometry level and the thickness of the thin films [91], [122]–[124].

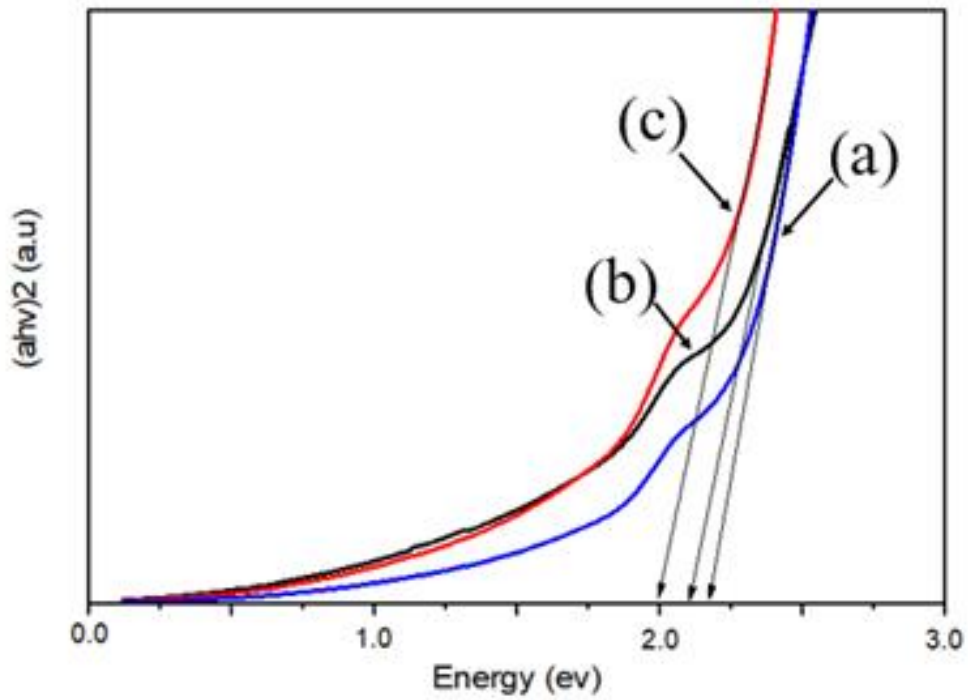


**Figure 39.** The optical band gap ( $E_g$ ) of vanadium oxide thin films: (a) ethyl acetate; (b) nitric acid; (c) oxalic acid

### IV.3.3. Effect of tenside

The presence of surfactants enhances the effectiveness of dip-coating, leading to higher-quality layers (Fig. 40). Among the different surfactants tested (Pluronic L61, non-ionic Triton X-100, cationic CTAB), Triton X-100 demonstrated the highest level of effectiveness.

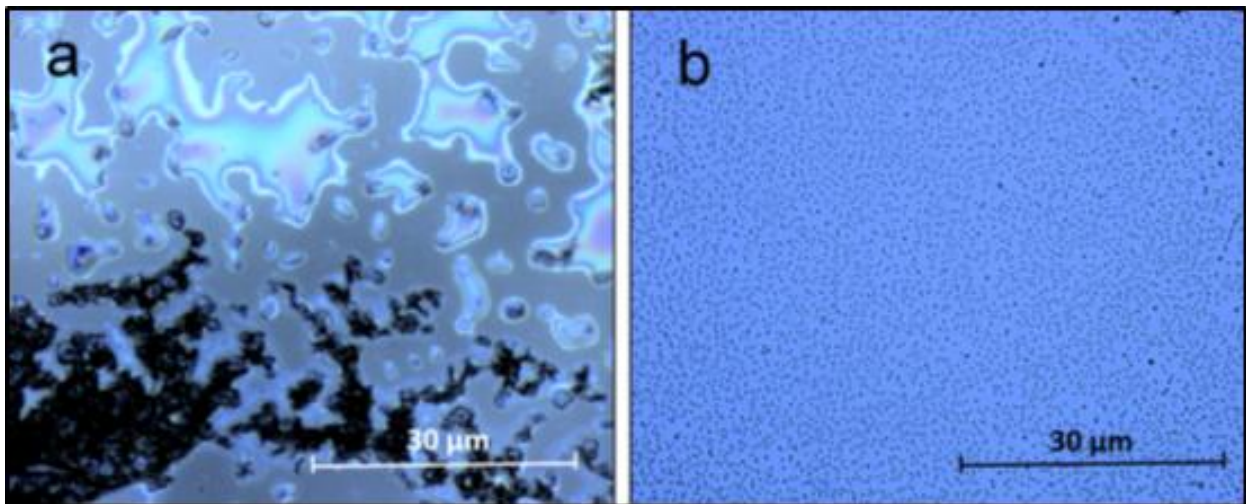


**Figure 40.** Reflection optical microscopy images of vanadate layers prepared from  $\text{NH}_4\text{VO}_3$  and nitric acid, a without, b with surfactant (Triton X 100)

### IV.3.4. Characterisation of vanadium oxide layers

Based on previous experiments, the most promising synthesis for the  $\text{V}_2\text{O}_5$  layer started from Ammonium metavanadate ( $\text{NH}_4\text{VO}_3$ ) precursor with nitric acid as a catalyst and Triton X 100 as a surfactant. Additionally, the application of ethyl acetate contributes to the successful production of high-quality layers. The synthesis process should be conducted at a temperature of  $70\text{ }^\circ\text{C}$  for a duration of 5 hours. By single dipping in the aqueous viscous solution, a uniform thin layer with a thickness ranging from 26 to 32 nm can be obtained (Fig. 41).

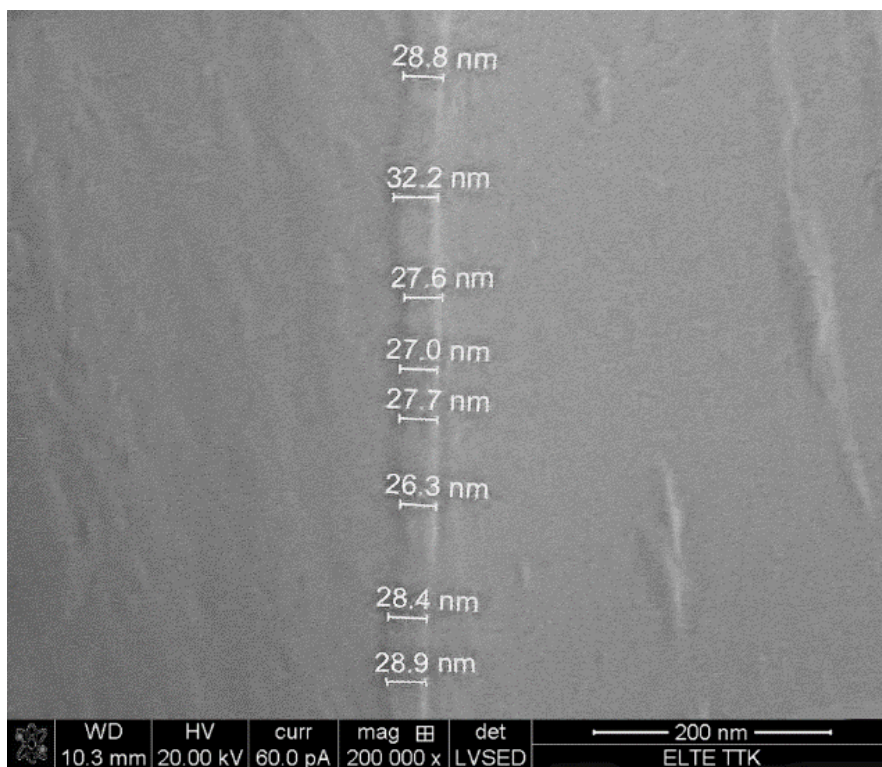


**Figure 41.** SEM images of vanadium pentoxide thin films on glass substrates prepared with nitric acid.

Based on thermal analysis (TG), the mass of the layer changes strongly above 360 °C (Fig. 42). Therefore, the formation of  $V_2O_5$  necessitates a temperature range of 360-400 °C in this process. The differential thermal analysis (DTA) reveals the release of ammonia at 200 °C.

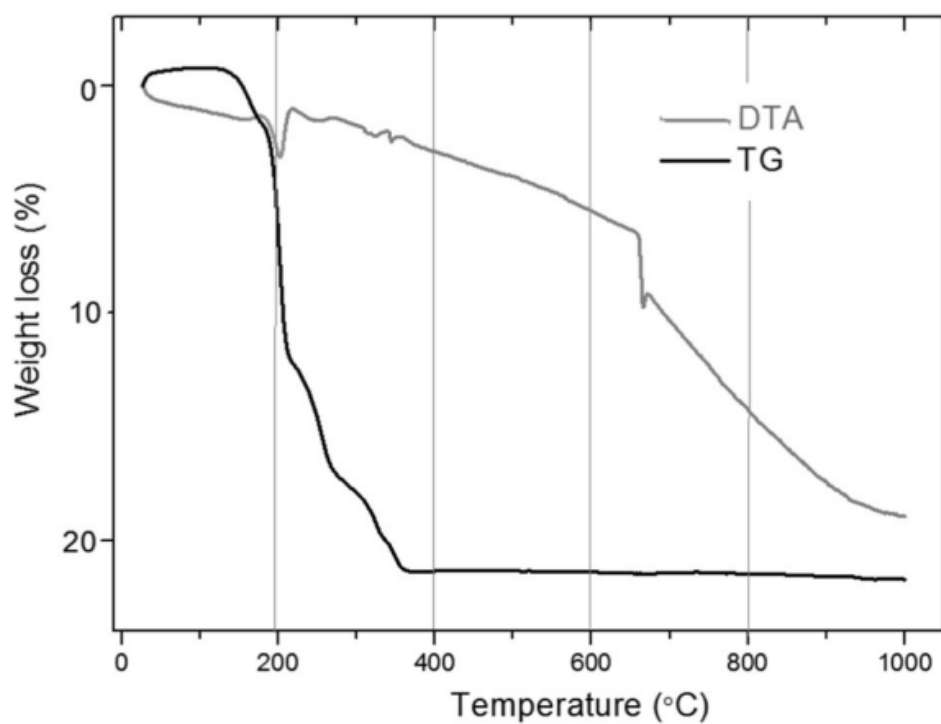


**Figure 42.** TG curve of dried V-containing layer

#### *IV.3.4.1. <sup>51</sup>V MAS NMR measurements*

The <sup>51</sup>V NMR spectroscopy confirms that the vanadate ions undergo a transformation into first VO<sup>2+</sup> and V<sub>3</sub>O<sub>10</sub><sup>5+</sup> at 100 °C, followed by the formation of V<sub>2</sub>O<sub>5</sub> ( $\alpha$ -V<sub>2</sub>O<sub>5</sub>) at 300 °C (Fig. 43, Table 3). The V<sub>2</sub>O<sub>5</sub> samples demonstrate thermal stability up to the measured temperature of 600 °C, encompassing both  $\alpha$ -V<sub>2</sub>O<sub>5</sub> and  $\beta$ -V<sub>2</sub>O<sub>5</sub> phases (Fig. 43, Table 3).

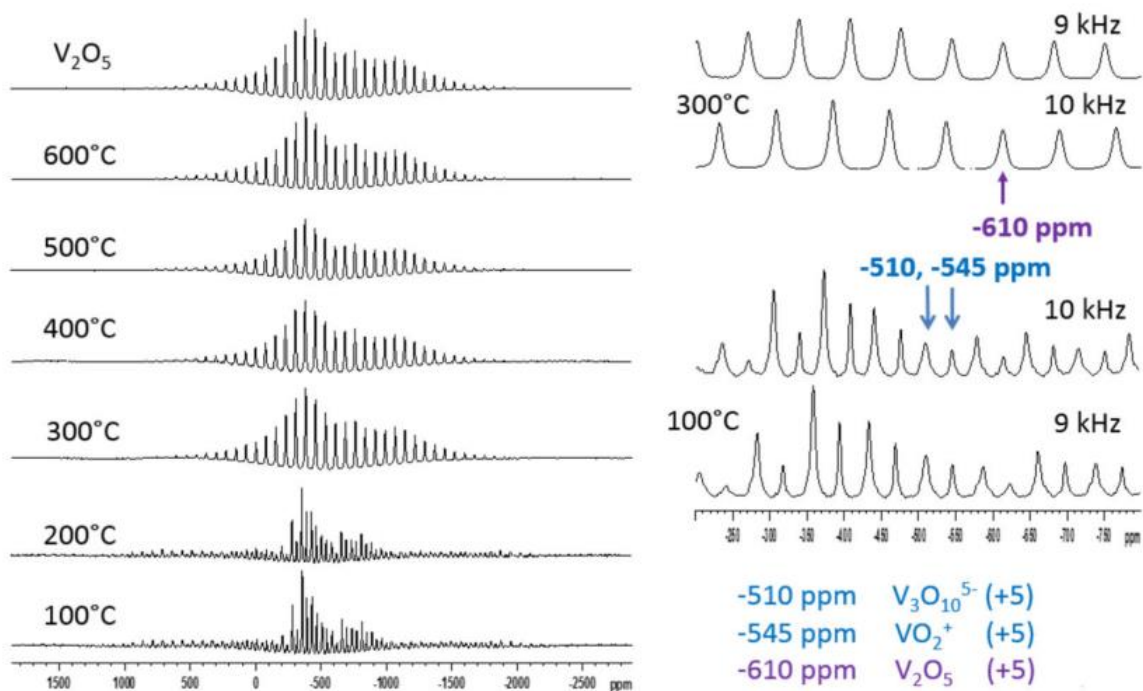


**Figure 43.**  $^{51}\text{V}$  NMR spectra of layer synthesized from  $\text{NH}_4\text{VO}_3$  and catalyzed with  $\text{HNO}_3$  vs temperature.

**Table 3.**  $^{51}\text{V}$  NMR results

Sample	-508 – -509 ppm	-545 – -546 ppm	-610 ppm
$\text{NH}_4\text{VO}_3$ , $\text{HNO}_3$ , 100 °C	$\text{V}_3\text{O}_{10}^{5-}$ (+5)	$\text{VO}_2^+$ (+5)	
$\text{NH}_4\text{VO}_3$ , $\text{HNO}_3$ , 200 °C	$\text{V}_3\text{O}_{10}^{5-}$ (+5)	$\text{VO}_2^+$ (+5)	
$\text{NH}_4\text{VO}_3$ , $\text{HNO}_3$ , 300 °C			$\text{V}_2\text{O}_5$
$\text{NH}_4\text{VO}_3$ , $\text{HNO}_3$ , 400 °C			$\text{V}_2\text{O}_5$
$\text{NH}_4\text{VO}_3$ , $\text{HNO}_3$ , 500 °C			$\text{V}_2\text{O}_5$
$\text{NH}_4\text{VO}_3$ , $\text{HNO}_3$ , 600 °C			$\text{V}_2\text{O}_5$
$\text{V}_2\text{O}_5$ (RT)			$\text{V}_2\text{O}_5$
$\text{V}_2\text{O}_5$ heated at 500 °C			$\text{V}_2\text{O}_5$

## V. Conclusion

In my Ph.D. research, the primary objective was to synthesize and characterize transparent gamma -aluminum oxide ( $\gamma\text{-Al}_2\text{O}_3$ ) and vanadium oxide ( $\text{V}_2\text{O}_5$ ) thin films, as well as optimize the synthesis parameters. The investigation encompassed various synthesis routes, surface morphology analysis, thin film thickness determination, phase purity assessment, element distribution examination, and estimation of bandgap energy. Through a combination of experimental techniques including scanning electron microscopy (SEM), energy-dispersive X-ray spectroscopy (EDXS), infrared spectroscopy, X-ray diffraction (XRD), and UV-Visible absorption spectroscopy, valuable information could be gained about the properties of the thin films.

In the first part of the thesis, the focus was on the synthesis and characterization of aluminum oxide thin films. Several solution-based techniques were employed, including colloidal methods and sol-gel chemistry, using different starting materials such as Al acetate, nitrate isopropoxide, boehmite, and  $\text{Al}_2\text{O}_3$  powders, along with various additives including acetic acid, HCl,  $\text{HNO}_3$ , and citric acid. The films were deposited via a dip-coating process and subjected to heat treatment at 600 °C.

Among the synthesis routes, the sol-gel technique demonstrated remarkable results in terms of achieving high-quality transparent gamma-aluminum oxide thin films. Starting from Al nitrate or a mixture of Al acetate and boehmite powders in the presence of acetic acid, nanolayers with excellent characteristics were obtained. These layers exhibited exceptional transparency with approximately 90% transmittance, a thickness ranging from 50 to 60 nm, and perfect covering. Furthermore, the use of Al nitrate as a precursor resulted in nanolayers with an extremely smooth surface. The sol-gel technique offered precise control over the film's thickness, ensuring a continuous and homogeneous coating.

The developed  $\gamma$ -aluminum oxide thin films hold significant potential for environmental protection applications. The  $\gamma\text{-Al}_2\text{O}_3$  thin layer acts as a protective or absorbent layer, contributing to the preservation of the environment. The remarkable transmittance properties of the films, even in the ultraviolet range, make them suitable for various industrial utilizations. LightTech company, for instance, has already adopted this newly developed technique. LightTech company applies the  $\gamma\text{-Al}_2\text{O}_3$  layer as a protective layer in spot amalgam lamps on quartz bulbs.

In the second part of the PhD study, the research concentrated on vanadium oxide thin films. The effect of chemical substances was studied on the structure, surface morphology, and material properties of vanadium oxide thin films. The investigation of the chemical substances covers the examination of initial materials (e.g.,  $\text{NH}_4\text{VO}_3$ ,  $\text{NaVO}_3$ ,  $\text{VO}_2$ , vanadyl acetylacetonate, ammonium decavanadate,  $(\text{NH}_4)_6[\text{V}_{10}\text{O}_{28}]$ ) and various additives (e.g., acids, chelate ligand, reduction reagent, and tensides). The syntheses are based on sol-gel chemistry. The main task of the sol-gel experiments was to optimize the chemical conditions such as catalyst and solvent for the preparation of perfect  $\text{V}^{5+}$ -containing layers. The other aim of study on vanadium-containing systems was to check the controllability of the  $\text{V}^{4+}/\text{V}^{5+}$  ratios. The control was carried out in the air in the presence of reducing agents or in a nitrogen atmosphere. The application of  $\text{NH}_4\text{VO}_3$  and  $\text{HNO}_3$  catalyst results in the best, complete and transparent  $\text{V}_2\text{O}_5$  layers. GI XRD data confirmed the orthorhombic structure of the thin films, exhibiting a preferred orientation along the (101) direction. The different chemical substances and the quality of solvent had a notable impact on the surface morphology of the films. UV-Visible spectroscopy analysis revealed that the average visible transmittance was influenced by the variation of chemical conditions due to the modification of the morphology of the films. The bandgap values measured for the thin films produced from different solvents were 1.98 eV by oxalic acid, 2.11 eV by nitric acid, and 2.17 eV by ethyl acetate.

The other aim was to adjust the  $\text{V}^{\text{IV}}/\text{V}^{\text{V}}$  ratios. The ratio of  $\text{V}^{\text{IV}}$  and  $\text{V}^{\text{V}}$  possesses an important role in the electric properties. The complete and homogeneous layers can be prepared from  $\text{VO}_2$  and vanadyl (IV) acetylacetonate in the presence or absence of reducing agents. Mixed oxidation states ( $\text{V}^{\text{IV}}$  and  $\text{V}^{\text{V}}$ ) can be achieved in the air only between 100 and 200 °C without or with mild reducing agent. The state of  $\text{V}^{\text{IV}}$  can be held only in nitrogen atmosphere above 200 °C or with strong reducing agent. The oxalic and ascorbic acids as reducing agents cannot prevent the oxidation of  $\text{V}^{\text{IV}}$ . The control of oxidation state was verified by  $^{51}\text{V}$  NMR. The ability to control the  $\text{V}^{\text{IV}}/\text{V}^{\text{V}}$  ratio, as well as the choice of solvents, provides a means to modulate the electrical properties of the thin films.

## VI. References

- [1] D. Wu *et al.*, “Durable lubricant-infused anodic aluminum oxide surfaces with high-aspect-ratio nanochannels,” *Chem. Eng. J.*, vol. 368, no. November 2018, pp. 138–147, 2019, doi: 10.1016/j.cej.2019.02.163.
- [2] M. Zhu, H. Wang, C. Li, H. Qi, D. Zhang, and W. Lv, “Thickness-modulated thermochromism of vanadium dioxide thin films grown by magnetron sputtering,” *Surf. Coatings Technol.*, vol. 359, no. August 2018, pp. 396–402, 2019, doi: 10.1016/j.surfcoat.2018.12.077.
- [3] A. M. Abyzov, “Aluminum Oxide and Alumina Ceramics (review). Part 1. Properties of Al<sub>2</sub>O<sub>3</sub> and Commercial Production of Dispersed Al<sub>2</sub>O<sub>3</sub>,” *Refract. Ind. Ceram.*, vol. 60, no. 1, pp. 24–32, 2019, doi: 10.1007/s11148-019-00304-2.
- [4] A. P. Y. S. Chauhan, and A. Verma, “Vanadium dioxide thin films synthesized using low thermal budget atmospheric oxidation,” *Thin Solid Films*, vol. 706, no. November 2019, p. 138003, 2020, doi: 10.1016/j.tsf.2020.138003.
- [5] W. Xu, H. Wang, F. Xie, J. Chen, H. Cao, and J. Bin Xu, “Facile and Environmentally Friendly Solution-Processed Aluminum Oxide Dielectric for Low-Temperature, High-Performance Oxide Thin-Film Transistors,” *ACS Appl. Mater. Interfaces*, vol. 7, no. 10, pp. 5803–5810, 2015, doi: 10.1021/am508775c.
- [6] E. K. Koussi, F. Bourquard, T. Tite, D. Jamon, F. Garrelie, and Y. Jourlin, “Synthesis of vanadium oxides by pulsed laser deposition and rapid thermal annealing,” *Appl. Surf. Sci.*, vol. 521, no. October 2019, p. 146267, 2020, doi: 10.1016/j.apsusc.2020.146267.
- [7] M. Sarno *et al.*, “Electrical conductivity of carbon nanotubes grown inside a mesoporous anodic aluminium oxide membrane,” *Carbon N. Y.*, vol. 55, pp. 10–22, 2013, doi: 10.1016/j.carbon.2012.10.063.
- [8] S. Surnev, M. G. Ramsey, and F. P. Netzer, “Vanadium oxide surface studies,” *Prog. Surf. Sci.*, vol. 73, no. 4–8, pp. 117–165, 2003, doi: 10.1016/j.progsurf.2003.09.001.

- [9] A. R. Phani and S. Santucci, "Evaluation of structural and mechanical properties of aluminum oxide thin films deposited by a sol-gel process: Comparison of microwave to conventional anneal," *J. Non. Cryst. Solids*, vol. 352, no. 38–39, pp. 4093–4100, 2006, doi: 10.1016/j.jnoncrsol.2006.06.013.
- [10] O. Berezina, D. Kirienko, A. Pergament, G. Stefanovich, A. Velichko, and V. Zlomanov, "Vanadium oxide thin films and fibers obtained by acetylacetonate sol-gel method," *Thin Solid Films*, vol. 574, pp. 15–19, 2015, doi: 10.1016/j.tsf.2014.11.058.
- [11] C. Glynn, D. Creedon, H. Geaney, J. O'Connell, J. D. Holmes, and C. O'Dwyer, "Optimizing vanadium pentoxide thin films and multilayers from dip-coated nanofluid precursors," *ACS Appl. Mater. Interfaces*, vol. 6, no. 3, pp. 2031–2038, 2014, doi: 10.1021/am4051102.
- [12] C. Cibert *et al.*, "Properties of aluminum oxide thin films deposited by pulsed laser deposition and plasma enhanced chemical vapor deposition," *Thin Solid Films*, vol. 516, no. 6, pp. 1290–1296, 2008, doi: 10.1016/j.tsf.2007.05.064.
- [13] K. B. Kusuma *et al.*, "Photocatalytic and electrochemical sensor for direct detection of paracetamol comprising  $\gamma$ -aluminium oxide nanoparticles synthesized via sonochemical route," *Sensors Int.*, vol. 1, no. July, p. 100039, 2020, doi: 10.1016/j.sintl.2020.100039.
- [14] K. Patty, S. M. Sadeghi, A. Nejat, and C. B. Mao, "Enhancement of emission efficiency of colloidal CdSe quantum dots on silicon substrate via an ultra-thin layer of aluminum oxide," *Nanotechnology*, vol. 25, no. 15, 2014, doi: 10.1088/0957-4484/25/15/155701.
- [15] T. F. R. Shen, M. H. Lai, T. C. K. Yang, I. P. Fu, N. Y. Liang, and W. T. Chen, "Photocatalytic production of hydrogen by vanadium oxides under visible light irradiation," *J. Taiwan Inst. Chem. Eng.*, vol. 43, no. 1, pp. 95–101, 2012, doi: 10.1016/j.jtice.2011.06.004.
- [16] M. A. Azam, K. Isomura, S. Ismail, N. Mohamad, and T. Shimoda, "Electrically conductive aluminum oxide thin film used as cobalt catalyst-support layer in vertically aligned carbon nanotube growth," *Adv. Nat. Sci. Nanosci. Nanotechnol.*, vol. 6, no. 4, p. 45008, 2015, doi: 10.1088/2043-6262/6/4/045008.

- [17] F. Azadian and A. C. Rastogi, “Energy storage performance of thin film nanocrystalline vanadium oxide with fluorinated tin oxide current carrier electrode for solid-state transparent supercapacitors based on ionic liquid gel electrolyte,” *Electrochim. Acta*, vol. 330, no. xxxx, p. 135339, 2020, doi: 10.1016/j.electacta.2019.135339.
- [18] M. Kaur, S. Ishii, S. L. Shinde, and T. Nagao, “All-ceramic solar-driven water purifier based on anodized aluminum oxide and plasmonic titanium nitride,” *Opt. InfoBase Conf. Pap.*, vol. Part F125-, pp. 1–8, 2018, doi: 10.1364/jsap.2018.19a\_211b\_3.
- [19] G. Gregory, C. Feit, Z. Gao, P. Banerjee, T. Jurca, and K. O. Davis, “Improving the Passivation of Molybdenum Oxide Hole-Selective Contacts with 1 nm Hydrogenated Aluminum Oxide Films for Silicon Solar Cells,” *Phys. Status Solidi Appl. Mater. Sci.*, vol. 217, no. 15, 2020, doi: 10.1002/pssa.202000093.
- [20] J. Sastre *et al.*, “Aluminum-Assisted Densification of Cosputtered Lithium Garnet Electrolyte Films for Solid-State Batteries,” *ACS Appl. Energy Mater.*, vol. 2, no. 12, pp. 8511–8524, 2019, doi: 10.1021/acsaem.9b01387.
- [21] A. Koçak, “MATERIALS SCIENCE AND ENGINEERING: Thin Film Preparation, Particle Size and Thickness Analysis Experimental Report,” no. February, p. 31, 2018.
- [22] I. Levin and D. Brandon, “Metastable alumina polymorphs: Crystal structures and transition sequences,” *J. Am. Ceram. Soc.*, vol. 81, no. 8, pp. 1995–2012, 1998, doi: 10.1111/j.1151-2916.1998.tb02581.x.
- [23] I. V. Roslyakov *et al.*, “Annealing induced structural and phase transitions in anodic aluminum oxide prepared in oxalic acid electrolyte,” *Surf. Coatings Technol.*, vol. 381, no. November 2019, p. 125159, 2020, doi: 10.1016/j.surfcoat.2019.125159.
- [24] I. V Roslyakov *et al.*, “Journal P,” *Surf. Coat. Technol.*, p. 125159, 2019, doi: 10.1016/j.surfcoat.2019.125159.
- [25] R. Prins, “On the structure of  $\gamma$ -Al<sub>2</sub>O<sub>3</sub>,” *J. Catal.*, vol. 392, pp. 336–346, 2020, doi: 10.1016/j.jcat.2020.10.010.

- [26] A. Jimenéz-González and D. Schmeisser, "Preparation and spectroscopic characterization of  $\gamma$ -Al<sub>2</sub>O<sub>3</sub> thin films," *Surf. Sci.*, vol. 250, no. 1–3, pp. 59–70, 1991, doi: 10.1016/0039-6028(91)90709-2.
- [27] P. F. Smet, J. Lauwaert, N. Avci, D. Poelman, and H. Vrielinck, "Optical and structural properties of aluminium oxide thin films prepared by a non-aqueous sol–gel technique," *J. Sol-Gel Sci. Technol.*, vol. 59, no. 2, pp. 327–333, 2011, doi: 10.1007/s10971-011-2505-9.
- [28] Z. Li, Y. Xin, Y. Liu, H. Liu, D. Yu, and J. Xiu, "Study of the annealing effect on the  $\gamma$ -phase aluminum oxide films prepared by the high-vacuum mpcvd system," *Coatings*, vol. 11, no. 4, 2021, doi: 10.3390/coatings11040389.
- [29] S. H. Tamboli, V. Puri, R. K. Puri, R. B. Patil, and M. F. Luo, "Comparative study of physical properties of vapor chopped and nonchopped Al<sub>2</sub>O<sub>3</sub> thin films," *Mater. Res. Bull.*, vol. 46, no. 6, pp. 815–819, 2011, doi: 10.1016/j.materresbull.2011.02.037.
- [30] L. Zhang, H. C. Jiang, C. Liu, J. W. Dong, and P. Chow, "Annealing of Al<sub>2</sub>O<sub>3</sub> thin films prepared by atomic layer deposition," *J. Phys. D. Appl. Phys.*, vol. 40, no. 12, pp. 3707–3713, 2007, doi: 10.1088/0022-3727/40/12/025.
- [31] Z. W. Zhao, B. K. Tay, and D. Sheeja, "Structural characteristics and mechanical properties of aluminium oxide thin films prepared by off-plane filtered cathodic vacuum arc system," *Surf. Coatings Technol.*, vol. 167, no. 2–3, pp. 234–239, 2003, doi: 10.1016/S0257-8972(02)00912-X.
- [32] C. Jeong, J. Lee, K. Sheppard, and C. H. Choi, "Air-Impregnated Nanoporous Anodic Aluminum Oxide Layers for Enhancing the Corrosion Resistance of Aluminum," *Langmuir*, vol. 31, no. 40, pp. 11040–11050, 2015, doi: 10.1021/acs.langmuir.5b02392.
- [33] E. Koushki, S. H. Mousavi, S. A. Jafari Mohammadi, M. H. Majles Ara, and P. W. De Oliveira, "Optical properties of aluminum oxide thin films and colloidal nanostructures," *Thin Solid Films*, vol. 592, pp. 81–87, 2015, doi: 10.1016/j.tsf.2015.09.003.
- [34] K. Srinivasan and A. Kottantharayil, "Aluminium oxide thin film deposited by spray coating for p-type silicon surface passivation," *Sol. Energy Mater. Sol. Cells*, vol. 197, no. March, pp. 93–98, 2019, doi: 10.1016/j.solmat.2019.03.048.

- [35] A. R. Sahoo, "Synthesis and Characterization of  $\alpha$ -Al<sub>2</sub>O<sub>3</sub> by Sol-Gel Process and Development of Zn-Al<sub>2</sub>O<sub>3</sub> Composites by Powder Metallurgy Route," *J. Porous Mater.*, vol. 9, no. 3, pp. 56–78, 2015.
- [36] M. Digne, P. Sautet, P. Raybaud, P. Euzen, and H. Toulhoat, "Use of DFT to achieve a rational understanding of acid-basic properties of  $\gamma$ -alumina surfaces," *J. Catal.*, vol. 226, no. 1, pp. 54–68, 2004, doi: 10.1016/j.jcat.2004.04.020.
- [37] R. Khosla, D. Schwarz, H. S. Funk, K. Guguieva, and J. Schulze, "High-quality remote plasma enhanced atomic layer deposition of aluminum oxide thin films for nanoelectronics applications," *Solid. State. Electron.*, vol. 185, p. 108027, 2021, doi: 10.1016/j.sse.2021.108027.
- [38] J. K. Vohs, A. Bentz, K. Eleamos, J. Poole, and B. D. Fahlman, "Chemical vapor deposition of aluminum oxide thin films," *J. Chem. Educ.*, vol. 87, no. 10, pp. 1102–1104, 2010, doi: 10.1021/ed100391p.
- [39] P. Katiyar, C. Jin, and R. J. Narayan, "Electrical properties of amorphous aluminum oxide thin films," *Acta Mater.*, vol. 53, no. 9, pp. 2617–2622, 2005, doi: 10.1016/j.actamat.2005.02.027.
- [40] G. Angarita, C. Palacio, M. Trujillo, and M. Arroyave, "Synthesis of Alumina Thin Films Using Reactive Magnetron Sputtering Method," *J. Phys. Conf. Ser.*, vol. 850, no. 1, 2017, doi: 10.1088/1742-6596/850/1/012022.
- [41] A. Bagheri Khatibani and S. M. Rozati, "Synthesis and characterization of amorphous aluminum oxide thin films prepared by spray pyrolysis: Effects of substrate temperature," *J. Non. Cryst. Solids*, vol. 363, no. 1, pp. 121–133, 2013, doi: 10.1016/j.jnoncrysol.2012.12.013.
- [42] M. Bouzbib, A. Pogonyi, T. Kolonits, Á. Vida, Z. Dankházi, and K. Sinkó, "Sol-gel alumina coating on quartz substrate for environmental protection," *J. Sol-Gel Sci. Technol.*, vol. 93, no. 2, pp. 262–272, 2020, doi: 10.1007/s10971-019-05193-y.
- [43] B. Hu, M. Yao, R. Xiao, J. Chen, and X. Yao, "Optical properties of amorphous Al<sub>2</sub>O<sub>3</sub> thin films prepared by a sol-gel process," *Ceram. Int.*, vol. 40, no. 9 PART A, pp. 14133–14139, 2014, doi: 10.1016/j.ceramint.2014.05.148.

- [44] C. Jing, X. Zhao, and Y. Zhang, "Sol-gel fabrication of compact, crack-free alumina film," *Mater. Res. Bull.*, vol. 42, no. 4, pp. 600–608, 2007, doi: 10.1016/j.materresbull.2006.08.005.
- [45] B. E. Yoldas, "Hydrolysis of aluminium alkoxides and bayerite conversion," *J. Appl. Chem. Biotechnol.*, vol. 23, no. 11, pp. 803–809, 1973, doi: 10.1002/jctb.5020231103.
- [46] M. I. F. Macêdo, C. C. Osawa, and C. A. Bertran, "Sol-gel synthesis of transparent alumina gel and pure gamma alumina by urea hydrolysis of aluminum nitrate," *J. Sol-Gel Sci. Technol.*, vol. 30, no. 3, pp. 135–140, 2004, doi: 10.1023/B:JSST.0000039497.46154.8f.
- [47] Y. Tokudome, K. Fujita, K. Nakanishi, K. Miura, and K. Hirao, "Synthesis of Monolithic Al<sub>2</sub>O<sub>3</sub> with Well-Defined Macropores and Mesoporous Skeletons via the Sol–Gel Process Accompanied by Phase Separation," *Chem. Mater.*, vol. 19, no. 14, pp. 3393–3398, 2007, doi: 10.1021/cm063051p.
- [48] Y. Kobayashi, T. Ishizaka, and Y. Kurokawa, "Preparation of alumina films by the sol-gel method," *J. Mater. Sci.*, vol. 40, no. 2, pp. 263–283, 2005, doi: 10.1007/s10853-005-6080-8.
- [49] Q. Fu, C.-B. Cao, and H.-S. Zhu, "Preparation of alumina films from a new sol–gel route," *Thin Solid Films*, vol. 348, no. 1–2, pp. 99–102, 1999, doi: 10.1016/S0040-6090(99)00023-1.
- [50] S. Alidoust, M. Zamani, and M. Jabbari, "IRANIAN JOURNAL OF CATALYSIS Sol-gel synthesis of nanoporous  $\gamma$ -alumina using TX-100 or gelatin/TX-100 mixture as effective catalysts for dehydration of alcohols."
- [51] J. Chandradass and M. Balasubramanian, "Sol-gel processing of alumina fibres," *J. Mater. Process. Technol.*, vol. 173, no. 3, pp. 275–280, 2006, doi: 10.1016/j.jmatprotec.2005.11.030.
- [52] T. Fernandez, G. Jose, S. Mathew, R. Pr, and U. Nv, "An ultra-low hydrolysis sol-gel route for titanosilicate xerogels and their characterization," *J. Sol-Gel Sci. Technol.*, vol. 41, no. 2, pp. 163–168, 2007, doi: 10.1007/s10971-006-0522-x.

- [53] Y. S. Rim, H. Chen, T. Bin Song, S. H. Bae, and Y. Yang, "Hexaaqua Metal Complexes for Low-Temperature Formation of Fully Metal Oxide Thin-Film Transistors," *Chem. Mater.*, vol. 27, no. 16, pp. 5808–5812, 2015, doi: 10.1021/acs.chemmater.5b02505.
- [54] J. Chandradass and D. S. Bae, "Synthesis and characterization of alumina nanoparticles by Igepal CO-520 stabilized reverse micelle and sol-gel processing," *Mater. Manuf. Process.*, vol. 23, no. 5, pp. 494–498, 2008, doi: 10.1080/10426910802104211.
- [55] B. Mirhadi and B. Mehdikhani, "Investigation of optical absorbance and crystallization of vanadium oxide in glasses," *J. Optoelectron. Adv. Mater.*, vol. 13, no. 6, pp. 679–683, 2011.
- [56] P. Guo, Z. Biegler, T. Back, and A. Sarangan, "Vanadium dioxide phase change thin films produced by thermal oxidation of metallic vanadium," *Thin Solid Films*, vol. 707, no. June 2019, p. 138117, 2020, doi: 10.1016/j.tsf.2020.138117.
- [57] C. Ko, Z. Yang, and S. Ramanathan, "Work function of vanadium dioxide thin films across the metal-insulator transition and the role of surface nonstoichiometry," *ACS Appl. Mater. Interfaces*, vol. 3, no. 9, pp. 3396–3401, 2011, doi: 10.1021/am2006299.
- [58] A. Sharoni, J. G. Ramírez, and I. K. Schuller, "Multiple avalanches across the metal-insulator transition of vanadium oxide nanoscaled junctions," *Phys. Rev. Lett.*, vol. 101, no. 2, pp. 2–5, 2008, doi: 10.1103/PhysRevLett.101.026404.
- [59] H. Jerominek, "Vanadium oxide films for optical switching and detection," *Opt. Eng.*, vol. 32, no. 9, p. 2092, 1993, doi: 10.1117/12.143951.
- [60] J. Livage, "Optical and electrical properties of vanadium oxides synthesized from alkoxides," 1999. [Online]. Available: [www.elsevier.com/locate/ccr](http://www.elsevier.com/locate/ccr).
- [61] X. Gao and J. Xu, "A new application of clay-supported vanadium oxide catalyst to selective hydroxylation of benzene to phenol," *Appl. Clay Sci.*, vol. 33, no. 1, pp. 1–6, 2006, doi: 10.1016/j.clay.2005.12.002.
- [62] E. Hryha, E. Rutqvist, and L. Nyborg, "Stoichiometric vanadium oxides studied by XPS," *Surf. Interface Anal.*, vol. 44, no. 8, pp. 1022–1025, Aug. 2012, doi: 10.1002/SIA.3844.

- [63] Z. S. El Mandouh and M. S. Selim, "Physical properties of vanadium pentoxide sol gel films," *Thin Solid Films*, vol. 371, no. 1, pp. 259–263, 2000, doi: 10.1016/S0040-6090(00)01003-8.
- [64] B. Samuneva, Y. Dimitriev, V. Dimitrov, E. Kashchieva, and G. Encheva, "Samuneva\_JSolGelSciTech13\_969\_1998.pdf," vol. 974, pp. 969–974, 1998.
- [65] A. Jin, W. Chen, Q. Zhu, Y. Yang, V. L. Volkov, and G. S. Zakharova, "Structural and electrochromic properties of molybdenum doped vanadium pentoxide thin films by sol-gel and hydrothermal synthesis," *Thin Solid Films*, vol. 517, no. 6, pp. 2023–2028, 2009, doi: 10.1016/j.tsf.2008.10.001.
- [66] J. Livage, "Vanadium Pentoxide Gels," *Chem. Mater.*, vol. 3, no. 4, pp. 578–593, 1991, doi: 10.1021/cm00016a006.
- [67] Y. H. Zhu *et al.*, "Reconstructed Orthorhombic V<sub>2</sub>O<sub>5</sub> Polyhedra for Fast Ion Diffusion in K-Ion Batteries," *Chem*, vol. 5, no. 1, pp. 168–179, 2019, doi: 10.1016/j.chempr.2018.10.004.
- [68] Q. Liu *et al.*, "Graphene-modified nanostructured vanadium pentoxide hybrids with extraordinary electrochemical performance for Li-ion batteries," *Nat. Commun.*, vol. 6, pp. 1–10, 2015, doi: 10.1038/ncomms7127.
- [69] E. A. A. Arbab and G. T. Mola, "V<sub>2</sub>O<sub>5</sub> thin film deposition for application in organic solar cells," *Appl. Phys. A Mater. Sci. Process.*, vol. 122, no. 4, pp. 25–28, 2016, doi: 10.1007/s00339-016-9966-1.
- [70] J. Liu, X. Wang, Q. Peng, and Y. Li, "Preparation and gas sensing properties of vanadium oxide nanobelts coated with semiconductor oxides," *Sensors Actuators, B Chem.*, vol. 115, no. 1, pp. 481–487, 2006, doi: 10.1016/j.snb.2005.10.012.
- [71] K. Schneider, M. Lubecka, and A. Czaplá, "V<sub>2</sub>O<sub>5</sub> thin films for gas sensor applications," *Sensors Actuators, B Chem.*, vol. 236, pp. 970–977, 2016, doi: 10.1016/j.snb.2016.04.059.
- [72] A. A. Bahgat, F. A. Ibrahim, and M. M. El-Desoky, "Electrical and optical properties of highly oriented nanocrystalline vanadium pentoxide," *Thin Solid Films*, vol. 489, no. 1–2, pp. 68–73, 2005, doi: 10.1016/j.tsf.2005.05.001.

- [73] O. Schilling and K. Colbow, "A mechanism for sensing reducing gases with vanadium pentoxide films," *Sensors Actuators B. Chem.*, vol. 21, no. 2, pp. 151–157, 1994, doi: 10.1016/0925-4005(94)80017-0.
- [74] X. Zhao *et al.*, "A relationship between the V<sup>4+</sup>/V<sup>5+</sup> ratio and the surface dispersion, surface acidity, and redox performance of V<sub>2</sub>O<sub>5</sub>-WO<sub>3</sub>/TiO<sub>2</sub> SCR catalysts," *RSC Adv.*, vol. 8, no. 54, pp. 31081–31093, 2018, doi: 10.1039/c8ra02857e.
- [75] S. Beke, "A review of the growth of V<sub>2</sub>O<sub>5</sub> films from 1885 to 2010," *Thin Solid Films*, vol. 519, no. 6, pp. 1761–1771, 2011, doi: 10.1016/j.tsf.2010.11.001.
- [76] Y. Yue and H. Liang, "Micro- and Nano-Structured Vanadium Pentoxide (V<sub>2</sub>O<sub>5</sub>) for Electrodes of Lithium-Ion Batteries," *Adv. Energy Mater.*, vol. 7, no. 17, pp. 1–32, 2017, doi: 10.1002/aenm.201602545.
- [77] F. Mattelaer, K. Geryl, G. Rampelberg, T. Dobbelaere, J. Dendooven, and C. Detavernier, "Atomic layer deposition of vanadium oxides for thin-film lithium-ion battery applications," *RSC Adv.*, vol. 6, no. 115, pp. 114658–114665, 2016, doi: 10.1039/C6RA25742A.
- [78] A. Sanger, A. Kumar, A. Kumar, J. Jaiswal, and R. Chandra, "A fast response/recovery of hydrophobic Pd/V<sub>2</sub>O<sub>5</sub> thin films for hydrogen gas sensing," *Sensors Actuators, B Chem.*, vol. 236, pp. 16–26, 2016, doi: 10.1016/j.snb.2016.05.141.
- [79] T. D. Manning, I. P. Parkin, C. Blackman, and U. Qureshi, "APCVD of thermochromic vanadium dioxide thin films-solid solutions v 2-xMxO<sub>2</sub> (M = Mo, Nb) or composites VO<sub>2</sub>: SnO<sub>2</sub>," *J. Mater. Chem.*, vol. 15, no. 42, pp. 4560–4566, 2005, doi: 10.1039/b510552h.
- [80] D. Vernardou *et al.*, "A study of the electrochemical performance of vanadium oxide thin films grown by atmospheric pressure chemical vapour deposition," *Sol. Energy Mater. Sol. Cells*, vol. 95, no. 10, pp. 2842–2847, 2011, doi: 10.1016/j.solmat.2011.05.046.
- [81] N. Darroudi and H. Eshghi, "Effects of nozzle-to-substrate distance and annealing atmospheres on V<sub>2</sub>O<sub>5</sub> thin films prepared by spray pyrolysis technique," *Mater. Sci. Eng. B Solid-State Mater. Adv. Technol.*, vol. 262, no. August, p. 114726, 2020, doi: 10.1016/j.mseb.2020.114726.

- [82] S. Gavalas *et al.*, “Vanadium oxide nanostructured thin films prepared by Aerosol Spray Pyrolysis for gas sensing and thermochromic applications,” *Mater. Sci. Semicond. Process.*, vol. 89, no. September 2018, pp. 116–120, 2019, doi: 10.1016/j.mssp.2018.09.008.
- [83] C. Drosos *et al.*, “Aerosol-assisted chemical vapor deposition of V<sub>2</sub>O<sub>5</sub> cathodes with high rate capabilities for magnesium-ion batteries,” *J. Power Sources*, vol. 384, no. December 2017, pp. 355–359, 2018, doi: 10.1016/j.jpowsour.2018.02.074.
- [84] A. Carolin Amala, R. Vignesh, G. V. Geetha, and R. Sivakumar, “Electrochromic Behavior of Vanadium Pentoxide Thin Films Prepared by a Sol–Gel Spin Coating Process,” *Phys. Status Solidi Appl. Mater. Sci.*, vol. 2100282, pp. 1–12, 2021, doi: 10.1002/pssa.202100282.
- [85] B. Rajeswaran and A. M. Umarji, “Defect engineering of VO<sub>2</sub> thin films synthesized by Chemical Vapor Deposition,” *Mater. Chem. Phys.*, vol. 245, p. 122230, 2020, doi: 10.1016/j.matchemphys.2019.122230.
- [86] M. S. B. De Castro, C. L. Ferreira, and R. R. De Avillez, “Vanadium oxide thin films produced by magnetron sputtering from a V<sub>2</sub>O<sub>5</sub> target at room temperature,” 2013, doi: 10.1016/j.infrared.2013.03.001.
- [87] C. O. Avellaneda, “Electrochromic performance of sol–gel deposited V<sub>2</sub>O<sub>5</sub>:Ta films,” *Mater. Sci. Eng. B*, vol. 138, no. 2, pp. 118–122, Mar. 2007, doi: 10.1016/J.MSEB.2006.06.007.
- [88] A. Rakshit, M. Mukherjee, and S. Chakraborty, “Effect of oxygen content on the electrical properties of sputter deposited vanadium oxide thin-films,” *Mater. Sci. Semicond. Process.*, vol. 88, no. July, pp. 127–131, 2018, doi: 10.1016/j.mssp.2018.07.040.
- [89] M. M. Margoni, S. Mathuri, K. Ramamurthi, R. R. Babu, and K. Sethuraman, “Sprayed vanadium pentoxide thin films: Influence of substrate temperature and role of HNO<sub>3</sub> on the structural, optical, morphological and electrical properties,” *Appl. Surf. Sci.*, vol. 418, pp. 280–290, 2017, doi: 10.1016/j.apsusc.2017.02.039.
- [90] J. Chu *et al.*, “Hydrothermal synthesis of vanadium oxide nanorods and their electrochromic performance,” *Mater. Lett.*, vol. 166, pp. 179–182, 2016, doi: 10.1016/j.matlet.2015.12.067.

- [91] A. George *et al.*, “Two step synthesis of vanadium pentoxide thin films for optoelectronic applications,” *Mater. Today Proc.*, vol. 36, no. xxxx, pp. 464–467, 2019, doi: 10.1016/j.matpr.2020.05.104.
- [92] A. E. Danks, S. R. Hall, and Z. Schnepp, “The evolution of ‘sol-gel’ chemistry as a technique for materials synthesis,” *Mater. Horizons*, vol. 3, no. 2, pp. 91–112, 2016, doi: 10.1039/c5mh00260e.
- [93] L. L. Hench and J. K. West, “The Sol-Gel Process,” *Chem. Rev.*, vol. 90, no. 1, pp. 33–72, 1990, doi: 10.1021/cr00099a003.
- [94] A. Mahmood and A. Naeem, “Sol-Gel-Derived Doped ZnO Thin Films: Processing, Properties, and Applications,” *Recent Appl. Sol-Gel Synth.*, no. August, 2017, doi: 10.5772/67857.
- [95] M. Parashar, V. K. Shukla, and R. Singh, “Metal oxides nanoparticles via sol–gel method: a review on synthesis, characterization and applications,” *J. Mater. Sci. Mater. Electron.*, vol. 31, no. 5, pp. 3729–3749, 2020, doi: 10.1007/s10854-020-02994-8.
- [96] C. J. Brinker, G. C. Frye, A. J. Hurd, and C. S. Ashley, “Fundamentals of sol-gel dip coating,” *Thin Solid Films*, vol. 201, no. 1, pp. 97–108, 1991, doi: 10.1016/0040-6090(91)90158-T.
- [97] T. Schneller, R. Waser, M. Kosec, and D. Payne, “Chemical solution deposition of functional oxide thin films,” *Chem. Solut. Depos. Funct. Oxide Thin Film.*, vol. 9783211993118, pp. 1–796, Dec. 2013, doi: 10.1007/978-3-211-99311-8/COVER.
- [98] “Sol-Gel Technologies for Glass Producers and Users,” *Sol-Gel Technol. Glas. Prod. Users*, 2004, doi: 10.1007/978-0-387-88953-5.
- [99] S. Obregón and V. Rodríguez-González, “Photocatalytic TiO<sub>2</sub> thin films and coatings prepared by sol–gel processing: a brief review,” *J. Sol-Gel Sci. Technol.*, vol. 102, no. 1, pp. 125–141, 2022, doi: 10.1007/s10971-021-05628-5.
- [100] J. Yuan, K. Zhao, T. Cai, Z. Gao, L. Yang, and D. He, “One-step dip-coating of uniform  $\gamma$ -Al<sub>2</sub>O<sub>3</sub> layers on cordierite honeycombs and its environmental applications,” *Ceram. Int.*, vol. 42, no. 13, pp. 14384–14390, 2016, doi: 10.1016/j.ceramint.2016.06.003.

- [101] D. Vasanth Raj, N. Ponpandian, D. Mangalaraj, and C. Viswanathan, “Effect of annealing and electrochemical properties of sol-gel dip coated nanocrystalline V2O5 thin films,” *Mater. Sci. Semicond. Process.*, vol. 16, no. 2, pp. 256–262, 2013, doi: 10.1016/j.mssp.2012.11.001.
- [102] K. B. V. P. M. D. Govindhan Dhanaraj, “Springer Handbook of Crystal Growth,” *Springer Handb. Cryst. Growth*, 2010, doi: 10.1007/978-3-540-74761-1/COVER.
- [103] S. M. Shang and W. Zeng, *Conductive nanofibres and nanocoatings for smart textiles*. 2013.
- [104] T. G. Carreño, A. Mifsud, C. J. Serna, and J. M. Palacios, “Preparation of homogeneous ZnCo mixed oxides by spray pyrolysis,” *Mater. Chem. Phys.*, vol. 27, no. 3, pp. 287–296, Mar. 1991, doi: 10.1016/0254-0584(91)90125-E.
- [105] C. Li *et al.*, “Ultrasonic spray pyrolysis for nanoparticles synthesis,” *J. Mater. Sci.*, vol. 9, pp. 3647–3657, 2004.
- [106] M. Bouzbib, A. Pogonyi, T. Kolonits, Á. Vida, Z. Dankházi, and K. Sinkó, “Sol – gel alumina coating on quartz substrate for environmental protection,” *J. Sol-Gel Sci. Technol.*, pp. 262–272, 2020, doi: 10.1007/s10971-019-05193-y.
- [107] A. A. Ismail and I. A. Ibrahim, “Impact of supercritical drying and heat treatment on physical properties of titania/silica aerogel monolithic and its applications,” *Appl. Catal. A Gen.*, vol. 346, no. 1–2, pp. 200–205, 2008, doi: 10.1016/j.apcata.2008.05.031.
- [108] M. Bouzbib, A. Pogonyi, T. Kolonits, Á. Vida, Z. Dankházi, and K. Sinkó, “Sol-gel alumina coating on quartz substrate for environmental protection,” *J. Sol-Gel Sci. Technol.*, vol. 93, pp. 262–272, 2020, doi: 10.1007/s10971-019-05193-y.
- [109] A. K. Gupta and M. Gupta, “Synthesis and surface engineering of iron oxide nanoparticles for biomedical applications,” *Biomaterials*, vol. 26, no. 18, pp. 3995–4021, Jun. 2005, doi: 10.1016/J.BIOMATERIALS.2004.10.012.
- [110] D. Ochs, J. Schroeder, B. Cord, and J. Scherer, “Glass substrate cleaning using a low energy ion source,” *Surf. Coatings Technol.*, vol. 142, no. 144, pp. 767–770, 2001, doi: 10.1016/S0257-8972(01)01210-5.

- [111] M. Bouzbib, J. Rohonczy, and K. Sinkó, “Effect of vanadium precursor on dip-coated vanadium oxide thin films,” *J. Sol-Gel Sci. Technol.*, vol. 105, no. 1, pp. 278–290, 2023, doi: 10.1007/s10971-022-05965-z.
- [112] Y. Ao, Y. Yang, S. Yuan, H. Hu, H. Gu, and G. Chen, “Nanosized  $\gamma$ -Al<sub>2</sub>O<sub>3</sub> protective film for fluorescent lamps,” *Ceram. Int.*, vol. 33, no. 8, pp. 1547–1550, 2007, doi: 10.1016/j.ceramint.2006.06.003.
- [113] C. Wu, F. Feng, and Y. Xie, “Design of vanadium oxide structures with controllable electrical properties for energy applications,” *Chem. Soc. Rev.*, vol. 42, no. 12, pp. 5157–5183, 2013, doi: 10.1039/c3cs35508j.
- [114] Y. Shi, S. L. Chou, J. Z. Wang, H. Z. Li, H. K. Liu, and Y. P. Wu, “In-situ hydrothermal synthesis of graphene woven VO<sub>2</sub> nanoribbons with improved cycling performance,” *J. Power Sources*, vol. 244, pp. 684–689, 2013, doi: 10.1016/j.jpowsour.2012.11.151.
- [115] R. N. Nenashev, N. E. Mordvinova, V. P. Zlomanov, and V. L. Kuznetsov, “Thermal decomposition of vanadyl acetylacetonate,” *Inorg. Mater.*, vol. 51, no. 9, pp. 891–896, 2015, doi: 10.1134/S0020168515090150.
- [116] C. Costa, “Application of vanadium oxide nanoparticles in smart surfaces,” 2018.
- [117] E. BICER, N. DEGE, E. COSKUN, E. BICER, N. DEGE, and E. COSKUN, “SYNTHESIS, CHARACTERIZATION AND CRYSTAL STRUCTURE OF A NOVEL DECAVANADATE SALT, [V<sub>0.50</sub>(H<sub>2</sub>O)<sub>5</sub>]<sub>2</sub>[H<sub>2</sub>(V<sub>10</sub>O<sub>28</sub>)]·4(H<sub>2</sub>O),” *J. Chil. Chem. Soc.*, vol. 62, no. 3, pp. 3610–3614, 2017, doi: 10.4067/S0717-97072017000303610.
- [118] H. T. Evans, “The Molecular Structure of the Isopoly Complex Ion, Decavanadate (V<sub>10</sub>O<sub>28</sub>–),” *Inorg. Chem.*, vol. 5, no. 6, pp. 967–977, 1966, doi: 10.1021/IC50040A004/ASSET/IC50040A004.FP.PNG\_V03.
- [119] J. Livage, M. Henry, and C. Sanchez, “Sol-gel chemistry of transition metal oxides,” *Prog. Solid State Chem.*, vol. 18, no. 4, pp. 259–341, 1988, doi: 10.1016/0079-6786(88)90005-2.
- [120] M. Liu, B. Su, Y. Tang, X. Jiang, and A. Yu, “Recent advances in nanostructured vanadium oxides and composites for energy conversion,” *Adv. Energy Mater.*, vol. 7,

- no. 23, pp. 1–34, 2017, doi: 10.1002/aenm.201700885.
- [121] L. Zhao *et al.*, “A low cost preparation of VO<sub>2</sub> thin films with improved thermochromic properties from a solution-based process,” *Thin Solid Films*, vol. 543, pp. 157–161, 2013, doi: 10.1016/j.tsf.2012.11.154.
- [122] D. Porwal *et al.*, “Study of the structural, thermal, optical, electrical and nanomechanical properties of sputtered vanadium oxide smart thin films,” *RSC Adv.*, vol. 5, no. 45, pp. 35737–35745, 2015, doi: 10.1039/c5ra02092a.
- [123] F. Liu *et al.*, “Characterization of chemical bath deposited CdS thin films at different deposition temperature,” *J. Alloys Compd.*, vol. 1–2, no. 493, pp. 305–308, Mar. 2010, doi: 10.1016/J.JALLCOM.2009.12.088.
- [124] M. A. Asiabar, Z. Mohaghegh, and F. E. Ghodsi, “Synthesis and characterization of nanocrystalline vanadium oxide thin films: electrochemical behavior by annealing in different atmosphere,” *Appl. Phys. A Mater. Sci. Process.*, vol. 124, no. 1, pp. 1–9, Jan. 2018, doi: 10.1007/S00339-017-1476-2/FIGURES/7.
- [125] E. S. P. B. V, J. M. Criado, J. Malek, and A. Ortega, “APPLICABILITY OF THE MASTER PLOTS IN KINETIC ANALYSIS,” *Thermochim. Acta*, vol. 147, no. 2, pp. 377–385, 1989.
- [126] M. Villanueva, “Thermogravimetric study of the decomposition process of the system,” *Polymer (Guildf.)*, vol. 41, no. 12, pp. 4635–4641, 2000.
- [127] C. F. Dickinson and G. R. Heal, “Thermochimica Acta A review of the ICTAC Kinetics Project , 2000 Part 1 . Isothermal results,” vol. 494, pp. 1–14, 2009, doi: 10.1016/j.tca.2009.05.003.
- [128] L. Bustamante, T. Rogaume, and E. Guillaume, “Analysis of Principal Gas Products During Combustion of Polyether Polyurethane Foam at Different Irradiance Levels,” pp. 933–940, 2009, doi: 10.1016/j.firesaf.2009.05.003f.
- [129] M. Avrami, “Kinetics of Phase Change. I General Theory,” vol. 1103, 1939, doi: 10.1063/1.1750380.
- [130] J. P. Redfern, “Thermogravimetric Analysis,” *Analyst*, vol. 88, no. 1053, pp. 906–924, 1963.

## Appendix

- ***Kinetic approach***

There are several approaches for estimating kinetic parameters from thermogravimetric data. It is therefore essential to specify the approach adopted in any kinetic exploitation of the experimental mass loss data. The kinetic parameters are determined by the Coats Redfern method. The expression to achieve these parameters is obtained from the reaction rate. Thus, in the kinetic analysis of thermal decomposition reactions, reaction rate is written according to the following form:

$$\frac{d\alpha}{dt} = kf(\alpha) \quad \text{Eq. 7}$$

Where  $\alpha$  is a characteristic variable of reaction progress, related to the mass of the sample  $m$  by the formula:

$$\alpha = \frac{m_0 - m_t}{m_0 - m_f} \quad \text{Eq. 8}$$

Where,  $m_0$  is the initial weight of the sample,  $m_t$  is the weight of the sample at the particular temperature  $T$ , and  $m_\infty$  is the weight at the end of degradation step,  $f(\alpha)$  represents the mode of degradation of the substance. The function  $f(\alpha)$  does not depend on the temperature but rather on degradation mode of the subjected matter.

The different modes proposed in the literature[125]–[127] are grouped in (Table 4). In this

same table, the function  $g(\alpha) = \int_0^\alpha \frac{d\alpha}{f(\alpha)}$  represents the integral form of the function  $f(\alpha)$

[128].

k is the reaction rate constant. It is accepted that k following the Arrhenius law:

$$k = A \exp\left(\frac{-E}{RT}\right) \quad \text{Eq. 9}$$

Where E is the apparent activation energy in kJ/mol, R is the perfect gases constant in Joules.  $\text{K}^{-1} \cdot \text{mol}^{-1}$ , A is the pre-exponential factor or frequency factor in  $\text{min}^{-1}$ , T is the absolute temperature in  $^{\circ}\text{K}$ ,

A, E and  $f(\alpha)$  are called the kinetic triplets of a reaction.

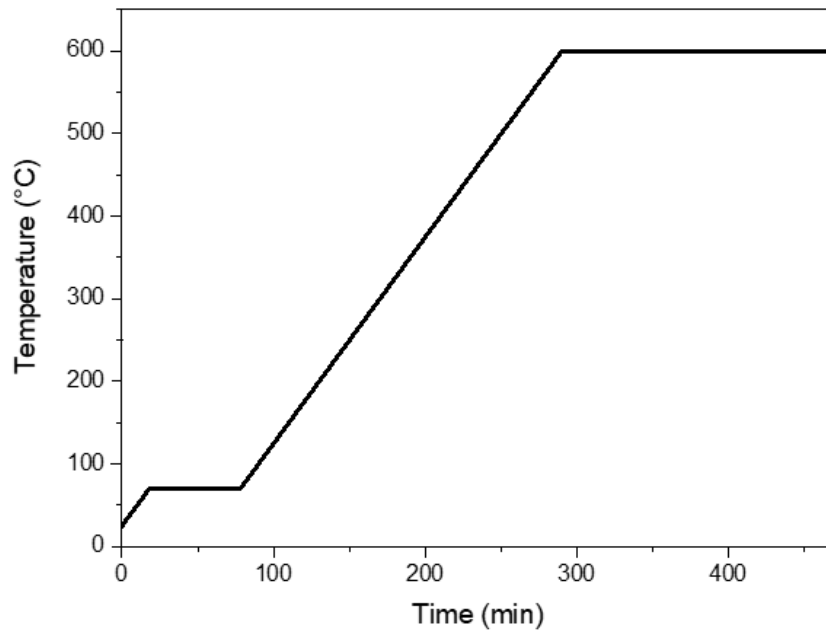


**Figure 44.** Schematically graph of heat treatment of gamma aluminum oxide thin films.

**Table 4.** Thermal degradation modes proposed for gas-solid reactions [125]–[127]

<i>Degradation mode</i>	<i>Code</i>	<i>Differential form : f(α)</i>	<i>Integral form : g(α)</i>
<b>Diffusion</b>			
One-way transport	<b>D1</b>	$1 / (2\alpha)$	$\alpha^2$
two-way transport , Valensi-Barrer	<b>D2</b>	$-1 / \text{Ln}(1-\alpha)$	$\alpha + (1-\alpha)\text{Ln}(1-\alpha)$
three-way transport, Jander	<b>D3</b>	$1,5(1-\alpha)^{2/3} / [1-(1-\alpha)^{1/3}]$	$[1-(1-\alpha)^{1/3}]^2$
Ginstling-Brounshtein	<b>D4</b>	$1,5 / [(1-\alpha)^{-1/3}-1]$	$1-2\alpha/3-(1-\alpha)^{2/3}$
Zhuravlev	<b>D5</b>	$1,5(1-\alpha)^{2/3} / [1 / (1-\alpha)^{1/3}-1]$	$[1 / (1-\alpha)^{1/3}-1]^2$
Anti-Jander	<b>D6</b>	$1,5(1+\alpha)^{2/3} / [(1+\alpha)^{1/3}-1]$	$[(1+\alpha)^{1/3}-1]^2$
Kroger-Ziegler	<b>D7</b>	$[1,5(1-\alpha)^{2/3} / [1-(1-\alpha)^{1/3}]] / t$	$[1-(1-\alpha)^{1/3}]^2 - \log(t)$
Two dimensions, Jander	<b>D8</b>	$(1-\alpha)^{1/2} / [1-(1-\alpha)^{1/2}]$	$[1-(1-\alpha)^{1/2}]^2$
Two dimensions, Anti-Jander	<b>D9</b>	$(1+\alpha)^{1/2} / [(1+\alpha)^{1/2}-1]$	$[(1+\alpha)^{1/2} - 1]^2$
Interfacial transfer	<b>D10</b>	$3(1-\alpha)^{4/3}$	$[1 / (1-\alpha)^{1/3} - 1]$
Transfer and diffusion	<b>D11</b>	$3 / [(1-\alpha)^{-4/3} - (1-\alpha)^{-1}]$	$1/(1-\alpha)^{1/3} - 1 + 1/3\text{Ln}(1-\alpha)$
Diffusion with two directions	<b>D12</b>	$3 / [(1-\alpha)^{-8/3} - (1-\alpha)^{-7/3}]$	$1/5(1-\alpha)^{-5/3} - 1/4(1-\alpha)^{-4/3} + 1/20$
<b>Random nucleation and nuclei growth</b>			
Avrami-Erofeev [129] n = 1, 2, 3, 4 et 5	<b>An</b>	$x(1-\alpha)[- \text{Ln}(1-\alpha)]^y$ x=4, 2, 3, 4/3 and 3/2 y=3/4, 1/2, 2/3, 1/4 and 1/3	$[- \text{Ln}(1-\alpha)]^z$ z=1/4, 1/2, 1/3, 3/4 and 2/3
<b>Chemical reactions</b>			
Zero order	<b>F0</b>	Constant	$\alpha$
First order	<b>F1</b>	$1-\alpha$	$-\text{Ln}(1-\alpha)$
Second order	<b>F2</b>	$(1-\alpha)^2$	$(1-\alpha)^{-1}-1$
Contraction (surface, volume and interface respectively for n = 2, 3 and 4)	<b>Rn</b>	$x(1-\alpha)^y$ x=2, 3 et 3/2. y=1/2, 2/3 and 1/3	$1-(1-\alpha)^z$ z = 1/2, 1/3 and 2/3
<b>Power / Exponential</b>			
Low power (half, third and quarter respectively for n = 2, 3 and 4)	<b>Pn</b>	$n\alpha^x$ x = 1/2, 2/3 and 3/4	$\alpha^y$ y = 1/2, 1/3 et 1/4
<b>Exponential</b>	<b>E1</b>	$\alpha$	$\text{Ln}(\alpha)$

**D<sub>1</sub>, D<sub>2</sub>,...**are symbols given to models

- ***Procedure for kinetic parameters determination***

In order to determine the kinetic parameters of our samples, the Coats–Redfern method [130], which is given Eq.10, is expressed as follows:

$$\text{Ln} \left( \frac{g(\alpha)}{T^2} \right) = \text{Ln} \frac{AR}{\beta E_a} - \frac{E_a}{RT} \quad \text{Eq. 10}$$

Where  $\alpha$  is a characteristic variable of reaction progress of the sample and T is the absolute temperature,  $g(\alpha)$  represents functions commonly used for description of thermal decomposition (Table 4). A is the frequency factor,  $E_a$  is the activation energy, R is the gas constant, and  $\beta$  is the heating rate.

A plot of  $\text{Ln} (g(\alpha)/T^2)$  against  $1/T$  will give a straight line of slope  $-E/R$  and an intercept of  $\text{Ln} (AR/ \beta E)$  for an appropriate form of  $g(\alpha)$ . Thus, based on the correct form of  $g(\alpha)$ , the activation energy and the pre-exponential factor could be respectively determined from the slope and intercept terms of the regression line.

(Table 4) lists the most common kinetic  $g(\alpha)$  functions, which were used in this study for the estimation of reaction mechanisms from dynamic TG curves by using the Coats–Redfern method.

- ***Thermal analyzes / Thermal profile under inert atmosphere.***

- ***Kinetic parameters estimation***

In order to calculate and understand the nature of the decomposition, kinetic exploitation is made on dynamic chemical regime assuming that the decomposition is a global reaction where physical limitation is neglected. The complete thermogram was divided into distinct sections according to their degradation steps. Curves indicating the solid-state mechanisms of alumina degradation under inert atmosphere are shown in (Fig. 45). Corresponding detailed curves for each degradation mode are given in appendix A.1. The values of activation energy  $E_a$ , pre-exponential factor A and correlation factors  $R^2$  for the first and second degradation step are listed in (Table 5). Moreover, the parameters A and E are moving in the same direction and their values depend on the mode of degradation. The relationship between A and  $E_a$ , called “apparent compensation effect” is often mentioned in literature. (Fig. 45) shows traces of the values of  $\text{Ln}A$  as a function of  $E_a$ . The effect of compensation is another way to further discrimination between degradation modes. Thus, for the first region (second weight loss step

in TGA thermogram), it was observed from (Table 5) that the best correlation coefficients were obtained for **F0, F1, F2, F3, R2, R3, P2, P3, D3, A2** and **A3**, with energy values running from **35.1 to 135.8 kJ/mol**. Regarding, second degradation step (third weight loss step), degradation mechanisms that gives the best mathematical fit for both samples were **F1, F2, F3, R2, R3, D3** and **A2**, with values of activation energy from **7.154 to 121,25 kJ/mol**. Likewise, results of the two regions show that the highest activation energies were found in the first thermal degradation regions where the main pyrolysis reaction took place and the largest weight loss occurred. The values of pre-exponential factor (Table 5) indicate that it depends on the degradation mode.

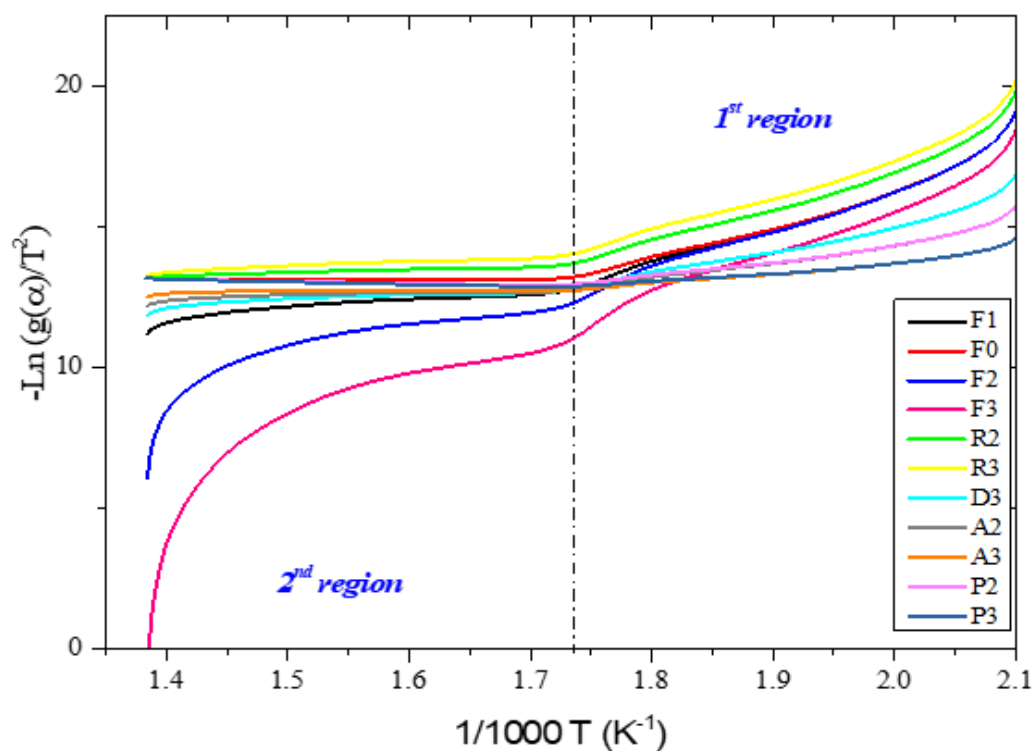


**Figure 45.** Curves indicate the solid-state mechanisms of bulk aluminum oxide degradation under inert atmosphere.

**Table 5.** Thermal kinetic results for bulk aluminum oxide pyrolysis

MD	1 <sup>st</sup> region			2 <sup>nd</sup> region		
	Ea (kJ.mol <sup>-1</sup> )	R <sup>2</sup>	Ln A (min <sup>-1</sup> )	Ea (kJ.mol <sup>-1</sup> )	R <sup>2</sup>	Ln A (min <sup>-1</sup> )
F1	122.537	<b>0.95148</b>	-8.323	9.262	<b>0.84556</b>	12.832
F0	116.238	<b>0.94047</b>	-6.845	0.259	0.00617	11.554
F2	126.387	<b>0.97401</b>	-9.275	71.801	<b>0.88681</b>	1.649
F3	135.861	<b>0.9674</b>	-12.151	121.250	<b>0.89997</b>	-9.252
R2	118.969	<b>0.94747</b>	-6.793	9.561	<b>0.96141</b>	13.728
R3	120.262	<b>0.94866</b>	-6.691	14.454	<b>0.94953</b>	13.479
P3	33.097	<b>0.91717</b>	9.164	-6.984	0.97796	-
D3	78.465	<b>0.9505</b>	0.470	12.347	<b>0.9151</b>	12.515
P2	53.789	<b>0.93044</b>	5.355	-5.219	0.94073	-
A2	56.764	<b>0.94564</b>	4.686	7.154	<b>0.837</b>	13.051
A3	35.1	<b>0.93365</b>	8.740	1.373	0.29837	12.596

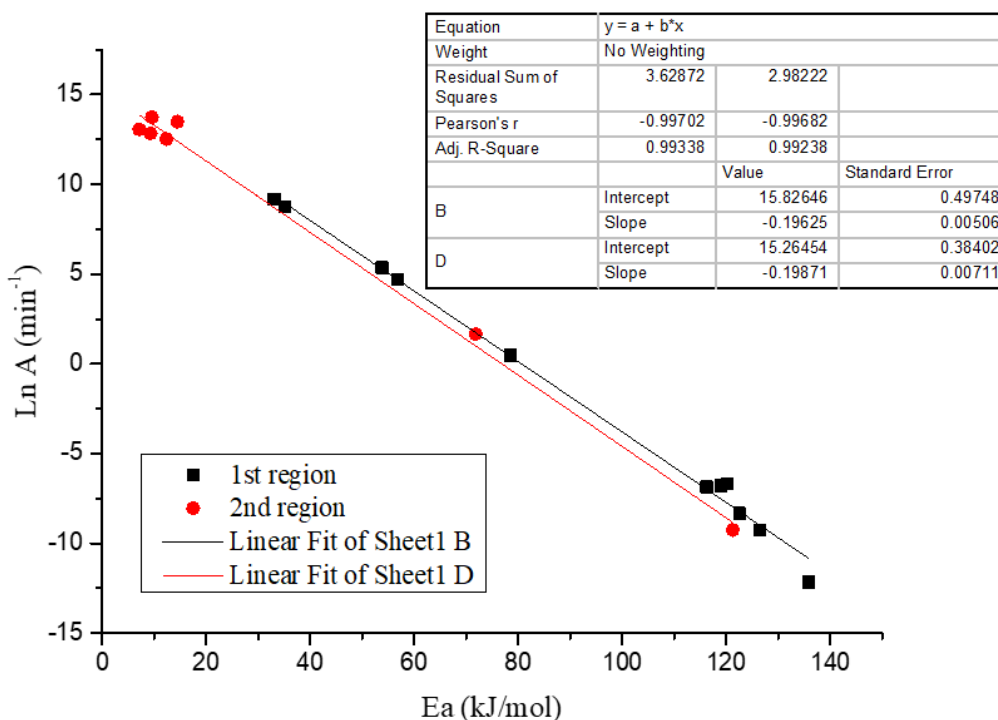


**Figure 46.** Compensation effect  $\text{Ln A} = f(E_a)$  for first and second regions of thermal degradation

**EÖTVÖS LORÁND UNIVERSITY**  
**DECLARATION FORM**  
**for disclosure of a doctoral dissertation**

**I. The data of the doctoral dissertation:**

Name of the author: **Bouzbib Mohammed**

MTMT-identifier: **10088457**

Title and subtitle of the doctoral dissertation: **Functional Inorganic Oxide Layers**

Keywords: **1. Thin films;2. Aluminum oxide;3. Vanadium oxide;4. Dip-coating;5. Sol gel;6. Optical and morphological properties**

DOI-identifier<sub>72</sub>: **10.15476/ELTE.2023.107**

Name of the doctoral school: **Environmental Sciences**

Name of the doctoral programme: **Environmental Chemistry**

Name and scientific degree of the supervisor: **Katalin Sinkó. Dr**

Workplace of the supervisor: **Eötvös Loránd University**

**II. Declarations**

1. As the author of the doctoral dissertation,<sup>73</sup>

a) I agree to public disclosure of my doctoral dissertation after obtaining a doctoral degree in the storage of ELTE Digital Institutional Repository. I authorize the administrator of the Department of Doctoral, Habilitational and International Affairs of the Dean's Office of the Faculty of Science to upload the dissertation and the abstract to ELTE Digital Institutional Repository, and I authorize the administrator to fill all the declarations that are required in this procedure.

b) I request to defer public disclosure to the University Library and the ELTE Digital Institutional Repository until the date of announcement of the patent or protection. For details, see the attached application form;<sup>74</sup>

c) I request in case the doctoral dissertation contains qualified data pertaining to national security, to disclose the doctoral dissertation publicly to the University Library and the ELTE Digital Institutional Repository ensuing the lapse of the period of the qualification process.;<sup>75</sup>

d) I request to defer public disclosure to the University Library and the ELTE Digital Institutional Repository, in case there is a publishing contract concluded during the doctoral procedure or up until the award of the degree. However, the bibliographical data of the work shall be accessible to the public. If the publication of the doctoral dissertation will not be carried out within a year from the award of the degree subject to the publishing contract, I agree to the public disclosure of the doctoral dissertation and abstract to the University Library and the ELTE Digital Institutional Repository.<sup>76</sup>

2. As the author of the doctoral dissertation, I declare that

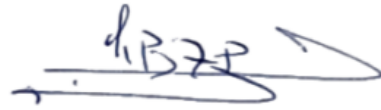
a) the doctoral dissertation and abstract uploaded to the ELTE Digital Institutional Repository are entirely the result of my own intellectual work and as far as I know, I did not infringe anyone's intellectual property rights.

b) the printed version of the doctoral dissertation and the abstract are identical with the doctoral dissertation files (texts and diagrams) submitted on electronic device.

3. As the author of the doctoral dissertation, I agree to the inspection of the dissertation and the abstract by uploading them to a plagiarism checker software.

Budapest 27.06.2023

Mohammed Bouzbib

A handwritten signature in blue ink, appearing to read 'M. Bouzbib', with a long horizontal stroke extending to the right.

*72 Filled by the administrator of the faculty offices.*

*73 The relevant part shall be underlined.*

*74 Submitting the doctoral dissertation to the Disciplinary Doctoral Council, the patent or protection application form and the request for deferment of public disclosure shall also be attached.*

*75 Submitting the doctoral dissertation, the notarial deed pertaining to the qualified data shall also be attached.*

*76 Submitting the doctoral dissertation, the publishing contract shall also be attached.*